nagra.

Technical Report 17-14

The development of a thermodynamic sorption data base for illite and the application to argillaceous rocks

November 2017

M.H. Bradbury, B. Baeyens

Paul Scherrer Institut, Villigen PSI

National Cooperative
for the Disposal of
Radioactive Waste

Hardstrasse 73
CH-5430 Wettingen
Switzerland
Tel. +41 56 437 11 11

www.nagra.ch

nagra.

Technical Report 17-14

The development of a thermodynamic sorption data base for illite and the application to argillaceous rocks

November 2017

M.H. Bradbury, B. Baeyens

Paul Scherrer Institut, Villigen PSI

National Cooperative
for the Disposal of
Radioactive Waste

Hardstrasse 73
CH-5430 Wettingen
Switzerland
Tel. +41 56 437 11 11

www.nagra.ch

ISSN 1015-2636

"Copyright © 2017 by Nagra, Wettingen (Switzerland) / All rights reserved.
All parts of this work are protected by copyright. Any utilisation outwith the remit of the copyright law is unlawful and liable to prosecution. This applies in particular to translations, storage and processing in electronic systems and programs, microfilms, reproductions etc."

Preface

The Laboratory for Waste Management of the Nuclear Energy and Safety Research Department at the Paul Scherrer Institute is performing work to develop and test models as well as to acquire specific data relevant to performance assessments of Swiss radioactive waste repositories. These investigations are undertaken in close co-operation with, and with the financial support of, the National Cooperative for the Disposal of Radioactive Waste (Nagra). The present report is issued simultaneously as a PSI Bericht and a Nagra Technical Report.

Abstract

A thermodynamic sorption database has been developed for application to argillaceous rocks based on radionuclide sorption experiments on illite. Sorption edges/isotherms have been measured on illite for Co(II), Ni(II), Zn(II), Eu(III), Am(III), Cm(III), Sn(IV), Th(IV), Np(V), Pa(V) and U(VI) and modelled using the two site protolysis non electrostatic surface complexation and cation exchange (2SPNE SC/CE) sorption model. A generalised sorption model for the uptake of caesium on illite is also given. All of these data are presented here together with the modelled curves, the corresponding surface complexation constants on the strong and weak sites, the selectivity coefficients and the hydrolysis constants used.

Linear free energy relationships (LFERs) between surface complexation constants and the appropriate corresponding aqueous hydrolysis constants have been derived separately for divalent transition metals, trivalent lanthanides/actinides and tetravalent actinides. These relationships allow surface site binding constants to be estimated for metals where the data are either very poor or absent, thus providing a means to calculate sorption values. In order to give an idea of how well such a procedure could work, test cases are presented in which sorption edges/isotherms were calculated using surface complexation constants taken from LFERs and compared with measured sorption values. A general methodology for using LFERs to calculate the sorption of metals for which no sorption data exist is suggested and applied to predict sorption edges/isotherms for Mn(II), Cu(II), Pu(III), U(IV), Np(IV) and Pu(IV) on illite.

The 2SPNE SC/CE sorption model, and the associated model parameters, were then used in blind predictions of sorption isotherms for Co(II), Ni(II), Eu(III), Th(IV) and U(VI) on Opalinus Clay for various groundwater compositions and were then compared with the measured values. The main assumption was that the sorption on Opalinus Clay is controlled by the illite content (where illite/smectite mixed layers were present they were assumed to have the same sorption characteristics as illite).

The main conclusion drawn from this work is that the tables of surface complexation constants and cation exchange selectivity coefficients compiled for illite and used in conjunction with the LFERs and the 2SPNE SC/CE sorption model, provide a powerful means of calculating the sorption of many radionuclides in complex porewater/argillaceous rock systems. Together they constitute a Thermodynamic Sorption Data Base (TSDB) for illite/argillaceous rock systems.

Zusammenfassung

Eine thermodynamische Sorptionsdatenbank wurde für die Anwendung an tonreichen Gesteinen entwickelt, basierend auf Sorptionsexperimenten an Illit. Sorptionskanten und -isothermen von Co(II), Ni(II), Zn(II), Eu(III), Am(III), Cm(III), Sn(IV), Th(IV), Np(V), Pa(V) und U(VI) wurden an Illit gemessen und mit dem "two site protolysis non electrostatic surface complexation cation exchange" (2SPNE SC/CE) Sorptionsmodell modelliert. Ebenfalls wird in dieser Arbeit ein generalisiertes Sorptionsmodell für die Aufnahme von Cäsium an Illit vorgestellt. Alle vorhandenen experimentellen Daten sind in diesem Bericht zusammengefasst, mit den berechneten Sorptionskurven, den entsprechenden Oberflächenkomplexierungskonstanten an starken und schwachen Sorptionsplätzen, den Selektivitätskoeffizienten und Hydrolysekonstanten.

Lineare Freie-Energie-Beziehungen ("linear free energy relationships", LFER) zwischen Oberflächenkomplexierungskonstanten und entsprechenden wässrigen Hydrolysekonstanten wurden separat für zweiwertige Übergangsmetalle, dreiwertige Lanthaniden/Actiniden und vierwertige Actiniden abgeleitet. Die LFER-Methode ermöglicht es, Oberflächenkomplexierungskonstanten abzuschätzen, falls experimentelle Daten von schlechter Qualität sind oder gänzlich fehlen, um so Sorptionswerte zu berechnen. Wie gut oder schlecht solch eine Schätzmethode funktioniert, wird an einem Beispiel erläutert, wo Oberflächenkomplexierungskonstanten für spezifische Metalle mittels LFER abgeschätzt wurden, um damit Sorptionskanten und -isothermen zu berechnen, die dann mit experimentellen Sorptionswerten verglichen wurden. Zudem wird eine generelle Methodik vorgeschlagen, um LFER zur Berechnung der Metallsorption in Fällen zu verwenden, wo keine Sorptionsdaten vorhanden sind. Sie wird auf die Voraussage von Sorptionskanten und -isothermen für Mn(II), Cu(II), Pu(III), U(IV), Np(IV) und Pu(IV) angewandt.

Schliesslich wird die Fähigkeit des 2SPNE SC/CE-Sorptionsmodells und der damit verbundenen Modellparameter geprüft, die Aufnahme von Radionukliden in komplexen Opalinuston/Porenwassersystemen quantitativ zu beschreiben. Dazu wurden Blindvoraussagen getroffen und mit gemessenen Sorptionsdaten verglichen. Die Hauptannahme dabei war, dass die Sorption an Opalinuston durch den Gehalt an Illit kontrolliert wird (bei Anwesenheit von Illit/Smektit-Mixed-Layers wird angenommen, dass sie das gleiche Sorptionsverhalten zeigen wie Illit).

Die Hauptschlussfolgerung der vorliegenden Arbeit lautet, dass die vorgestellten Tabellen mit Oberflächenkomplexierungskonstanten und Selektivitätskoeffizienten für Kationenaustausch in Verbindung mit der LFER-Methode und dem 2SPNE SC/CE-Sorptionsmodell ein leistungsfähiges Mittel sind, um die Sorption vieler Radionuklide in komplexen Porenwasser/Opalinuston-Systemen zu berechnen, und sie stellen eine eigentliche thermodynamische Sorptionsdatenbank für Illit/Opalinuston dar.

Résumé

Afin de prédire la rétention de radionucléides dans des roches argileuses, une base de données de sorption thermodynamique a été développée à partir de valeurs expérimentales obtenues pour l'illite. Pour le Co(II), Ni(II), Zn(II), Eu(III), Am(III), Cm(III), Sn(IV), Th(IV), Np(V), Pa(V) et U(VI) la sorption en fonction du pH et de la concentration en nucléides (isotherme) a été mesurée sur l'illite et modélisée avec le modèle de sorption « two site protolysis non electrostatic surface complexation cation exchange » (2SPNE SC/CE). Un modèle de sorption généralisé décrivant la rétention du Césium sur l'illite a également été mis au point. L'ensemble des données expérimentales avec les courbes de sorption obtenues, les constantes de complexation sur les sites de forte et faible affinité, les coefficients de sélectivité ainsi que les constantes d'hydrolyse sont compilés dans le présent rapport.

Des relations linéaires d'énergies libres (« linear free energy relationships », LFER) entre les constantes de complexation de surface et les constantes d'hydrolyse aqueuse correspondantes ont été dérivées séparément pour les métaux de transition divalents, les lanthanides/actinides trivalents et les actinides tétravalents. Ces relations permettent d'estimer des constantes de complexation de surface dans le cas de métaux pour lesquels les données expérimentales sont absentes ou de qualité insuffisante, et de calculer ainsi des valeurs de sorption. Cette approche d'estimation a été testée en calculant des valeurs de sorption (en fonction du pH et de la concentration) en utilisant les constantes de complexation de surface obtenue avec la LFER et en les comparant aux données expérimentales. Une méthodologie générale permettant de calculer la sorption de métaux pour lesquels aucune donnée n'existe est proposée. Cette méthodologie est en outre utilisée pour prédire la sorption (en fonction du pH et concentration) de Mn(II), Cu(II), Pu(III), U(IV), Np(IV) et Pu(IV) sur l'illite.

Finalement, le modèle de sorption « 2SPNE SC/CE », avec les paramètres qui lui sont associés, a été employé pour prédire en aveugle des isothermes de sorption pour le Co(II), Ni(II), Eu(III), Th(IV) et U(VI) sur l'Argile à Opalinus dans différentes eaux interstitielles, puis les valeurs calculées ont été comparées avec les données expérimentales. Ces calculs présupposent que la sorption sur l'Argile à Opalinus est principalement contrôlée par la teneur en illite de la roche argileuse (pour les interstratifiés illite/smectite, on suppose que leurs propriétés de sorption sont les mêmes que celles de l'illite)

La principale conclusion de cette étude est que les constantes de complexation de surface et les sélectivités d'échange cationique compilées pour l'illite, utilisées en combinaison avec la LFER et le model de sorption « 2SPNE SC/CE », constituent un outil performant pour prédire la sorption de nombreux radionucléides dans des systèmes des roches argileuses/eaux interstitielles complexes. L'ensemble constitue une base de données de sorption thermodynamique pour les systèmes illite/roches argileuses.

Table of Contents

List of Tables

List of Figures

1 Introduction

In many radioactive waste management programmes argillaceous rocks are the host formations of choice for deep geological disposal, *e.g.* Callovo-Oxfordian and Toarcian Clays, France (Andra 2001, Bonin 1998); Boom and Ypresian Clays, Belgium (Ondraf 2001); Opalinus Clay, Switzerland (Nagra 2002); Horonobe sediments, Japan (Aoki 2002); Boda Claystone, Hungary (Lázár & Máthé 2012). Two of their most important characteristics are low permeability and strong radionuclide retention. 2:1 type phyllosilicates such as illite, smectite, and illite/smectite mixed layers are mainly responsible for these properties and often make up 50 or more wt.-% of the total mass. The retardation of radionuclides in the far-field host rock is one of the main pillars of the multi-barrier safety concept (Nagra 2002, 2008).

It was recognised some years ago that a mechanistic understanding of sorption processes, and the development of corresponding predictive sorption models, would be of great advantage in justifying and defending the sorption values used in safety studies (NEA 1992, 2001, 2005). Further, it would be highly advantageous if it were possible to reliably calculate sorption values for the large range of conditions considered in the numerous scenario analyses carried out in safety analysis. The implication is that there is a need for a thermodynamic sorption data base (TSDB) which could be generally applied to argillaceous rock/groundwater systems.

In a recent publication (Baeyens & Bradbury 2017) the data and procedures for establishing a TSDB for montmorillonite was presented, described and discussed. The basis for this work was sorption edge and isotherm measurements carried out on purified homo-ionic Na-montmorillonite. In this work a TSDB for illite is developed based on sorption edge and isotherms measurements carried out on purified homo-ionic Na-illite (Illite du Puy, IdP).

Essentially the same methodology as given in Baeyens & Bradbury (2017) for montmorillonite/ bentonite is applied here for radionuclide sorption on argillaceous rocks based on sorption edge/ isotherm measurements on illite. Illite was chosen as the best representative for the sorption characteristics of the 2:1 type clay minerals in argillaceous rocks. The same compilations of hydrolysis (Appendix B) and other aqueous thermodynamic speciation constants (Appendix K) are used.

It is worthwhile to re-emphasise here that the sorption model, the assumptions in the model, the aqueous thermodynamic data used and the surface complexation constants and cation exchange selectivity coefficients in the TSDB are all linked and make up a complete package.

2 Sorption modelling

The two site protolysis non electrostatic surface complexation and cation exchange (2SPNE SC/CE) sorption model is used throughout to describe the sorption of dissolved metal species on 2:1 clay minerals by surface complexation and cation exchange. The uptake by both mechanisms is calculated simultaneously using the MINSORB code (Bradbury & Baeyens 1997). The model has been described in detail on a number of occasions (Bradbury & Baeyens 1997, 1999, 2002, 2006) and will not be discussed further here.

The main assumptions associated with the 2SPNE SC/CE sorption model are as follows:

1. The uptake of metals on 2:1 clay minerals is controlled by surface complexation and cation exchange reactions which take place simultaneously.
2. Sorption is assumed to be fast and reversible.
3. In illite, cation exchange takes place on the planar sites and the site capacity is given by the CEC in equivalents kg^{-1}.
4. Surface complexation reactions take place on amphoteric surface hydroxyl edge sites.
5. The protolysis behaviour of 2:1 clay minerals is governed by two site types called "weak-1 ($\equiv S^{W1}OH$)" and "weak-2 ($\equiv S^{W2}OH$)" sites, each having a site capacity of 40 mmol kg^{-1} and characterised by their own protonation and de-protonation constants.
6. Sorption by surface complexation occurs on so called "strong sites ($\equiv S^{S}OH$)" and "weak-1 ($\equiv S^{W1}OH$)" sites. Both have the same protolysis constants.
7. Sorption at trace concentrations occurs predominantly on the $\equiv S^{S}OH$ sites which have an average site capacity of 2 mmol kg^{-1}.
8. Surface activity coefficients for both cation exchange and surface complexation are taken to be unity.
9. Only cations and neutral and positively charged hydroxy species are sorbing. All other aqueous species are taken to be non-sorbing.
10. The selectivity coefficients (K_c values) given in Appendix E are valid in the ionic strength range from ~ 0.01 M to ~ 0.3 M (outside this range the K_c values are not assured).
11. The protolysis constants (Appendix A) and surface complexation constants (Appendices C and D) are only valid for ionic strengths < 0.5 M.

3 Measured sorption edges and isotherms and modelled curves

3.1 Preamble

Samples of illite were collected in the region of Le Puy-en-Velay (Haute-Loire), France; so-called Illite du Puy (Gabis 1958). Illite du Puy contains significant levels of background impurities which can influence the sorption properties of the clay suspensions and may lead to difficulties in the interpretation of data. A conditioning procedure was therefore applied to all of the illite used in the various sorption studies in order to remove these background metal impurities, soluble salts and sparingly soluble minerals. Part of the conditioning process was designed to convert the purified clay into the homo-ionic Na-form (Na-IdP) which was then thoroughly physico-chemically characterised (Poinssot et al. 1999). Most of the sorption experiments were carried out in a background electrolyte of $NaClO_4$ which was also purified. (Further details of the purification processes and their potential influences on sorption are given in Appendix K.)

The majority of the data sets are "in house" data (published and unpublished) carried out in controlled N_2 atmosphere glove boxes where the partial pressure of CO_2 was $< 10^{-5.5}$ bar at temperatures between 22 °C and 26 °C. The reason for their selection is that these data sets have been carried out under well-defined conditions (*e.g.* pH, background electrolyte, background impurities, concentration range). There are some additional data sets taken from the open literature which have been carried under atmospheric conditions at room temperature. For completeness, the total radionuclide concentration (RN_{TOT} and the sorbent concentration (*S*) has been included in the figure caption of the sorption edges.

The sorption edge/isotherm measurements were modelled in terms of surface complexation and cation exchange mechanisms via a stepwise iterative fitting/modelling procedure using the computer code MINSORB (Bradbury & Baeyens 1997). This code allowed the uptake of radionuclides by both mechanisms to be calculated simultaneously. Aqueous activity coefficients were calculated using the Davies relation (Davies 1962). In all of the calculations the site types and site capacities and protonation/de-protonation constants for the amphoteric surface hydroxyl groups (≡SOH) were fixed (Appendix A). The metal hydrolysis constants used are summarised in Appendix B.

3.2 Sorption edges: Figures and modelled curves

This section contains all of the sorption edges measured "in house" together with some data taken from the literature. In the vast majority of cases sorption is expressed as a distribution ratio, R_d, defined as:

$$R_d = \frac{C_{init.} - C_{eq.}}{C_{eq.}} \cdot \frac{V}{m} \qquad (3.1)$$

where:

$C_{init.}$ = initial aqueous concentration of active and inactive metal [M]
$C_{eq.}$ = equilibrium aqueous concentration of active and inactive metal [M]
V = volume of liquid phase [L]
m = mass of solid phase [kg]

The experimental methodology has been described on numerous occasions and the details can be found in Baeyens & Bradbury (1995a and b, 1997), Bradbury & Baeyens (2009a and b), for example.

The errors on the "in house" log R_d values are generally less than 0.3 log units but can be up to 0.5 log units for sorption values greater than 10^5 L kg^{-1}.

A compilation of sorption edges for the elements Co(II), Ni(II), Zn(II), Eu(III), Am(III), Sn(IV), Th(IV), Np(V), Pa(V) and U(VI), together with the modelled curves, are presented in Figs. 3.1 to 3.11. The experimental data points are given mainly as filled circles and the modelled curves as continuous black lines. For completeness, the total metal concentration (Me_{TOT}) and the sorbent concentration (*S*) are included in the figure caption for each sorption edge. A summary of the surface complexation reactions and constants is given in Appendix C and the selectivity coefficients in Appendix E. Note that the uptake of Cs(I) on illite is a special case and a sorption model for Cs(I) is presented in Chapter 9.

3.2.1 Cobalt

A Co(II) sorption edge and modelling has been reported previously in Bradbury & Baeyens (2009a). This data is reproduced here in Fig. 3.1a and the model parameters are given in Appendix C, Tab. C1. This experiment was carried out with a ^{60}Co tracer which had a high carrier concentration.

A new Co sorption edge (Montoya et al. 2018) was measured using a carrier free ^{57}Co tracer, but 7.5×10^{-8} M stable Co was added in the experiments. The results are shown in Fig. 3.1b. The Co edges are clearly different and the reason for this discrepancy is unclear. However, the shift to the right for the edge at high Co concentration (Fig. 3.1a) compared to the edge at lower Co concentration (Fig. 3.1b) is not due to strong site saturation.

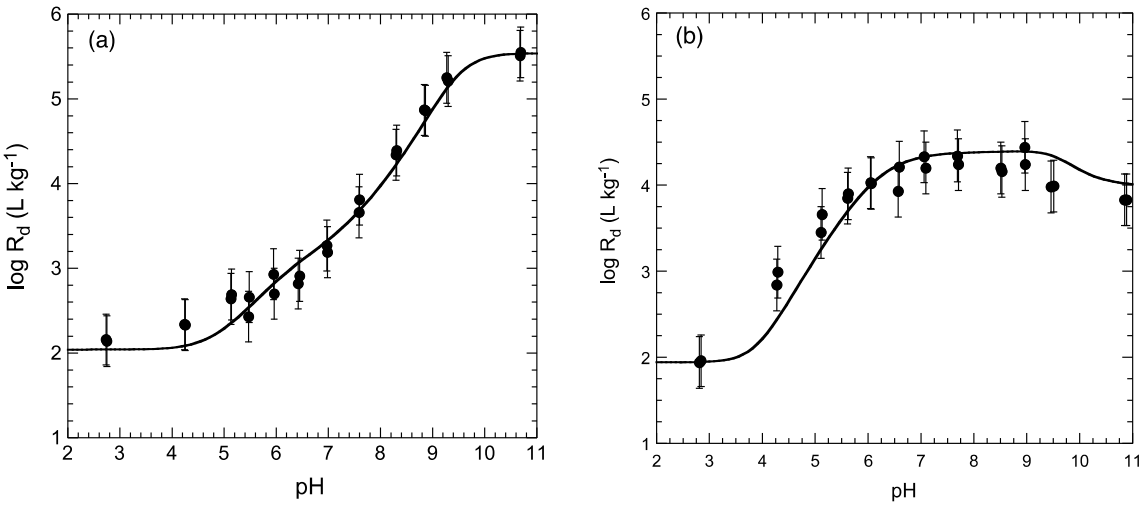

Fig. 3.1: Sorption edge for Co(II) on Na-IdP in 0.1 M $NaClO_4$, $Co_{TOT} = 2 \times 10^{-6}$ M, S = 1.56 g L^{-1} (a) and $Co_{TOT} = 7.5 \times 10^{-8}$ M, S = 3.46 g L^{-1} (b).

(a): experimental data (●) and modelled curve (—) (Bradbury & Baeyens 2009a) and (b): experimental data (●) (Montoya et al. 2018) and modelled curve (—) (*this study*).

3.2.2 Nickel

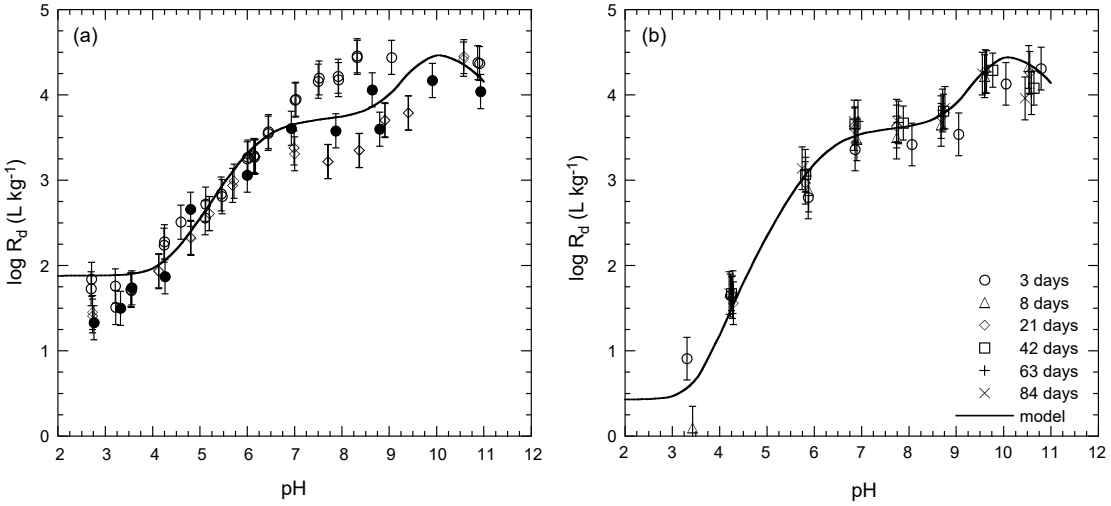

Fig. 3.2: Sorption edges for Ni(II) on Na-IdP in 0.1 M $NaClO_4$, $Ni_{TOT} = 2 \times 10^{-9}$ M, $S = 1.8 – 2.3$ g L^{-1}(a) and (b).

Experimental data (symbols) (Bradbury & Baeyens 2009a) and modelled curves (—) (*this study*).

3.2.3 Zinc

Note that the trace Zn sorption data given below at pH < 5 is anomalously high. An independent cation exchange experiment at higher Zn loadings yielded a Zn-Na selectivity coefficient of 4. The solid lines in Fig. 3.3 have been calculated using this selectivity coefficient.

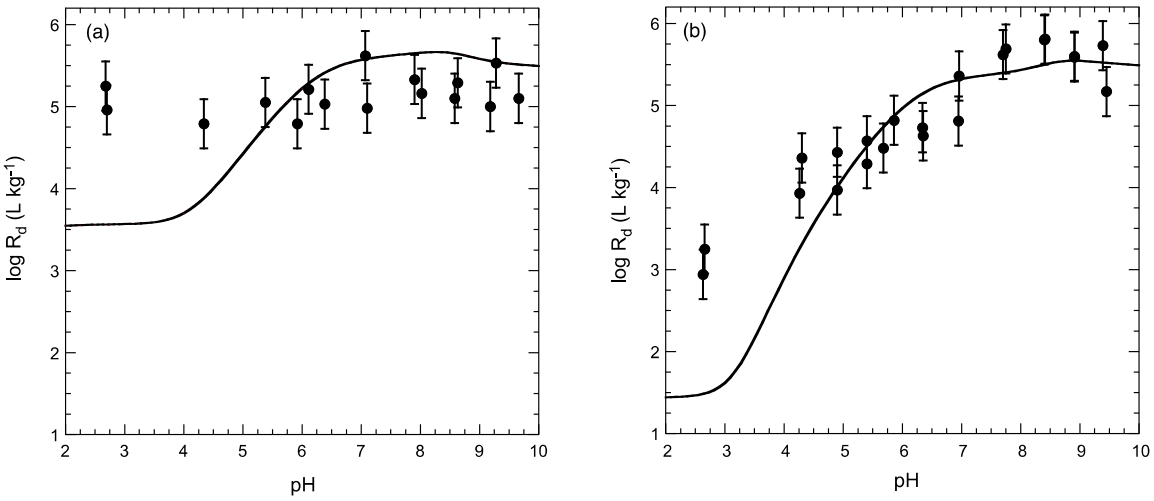

Fig. 3.3: Sorption edges for Zn(II) on Na-IdP in (a) 0.01 M $NaClO_4$, $Zn_{TOT} = 2.9 \times 10^{-7}$ M, $S = 0.4 – 2.1$ g L^{-1} and (b) 0.1 $NaClO_4$ M, $Zn_{TOT} = 2.9 \times 10^{-7}$ M; $S = 1.3 – 2.5$ g L^{-1}.

Experimental data (●) (Montoya et al. 2018) and modelled curves (—) (*this study*).

3.2.4 Europium

Poinssot et al. (1999) measured Eu edges at 2 different $NaClO_4$ background concentrations and one isotherm at pH 7.0. These measurements were extended to include an edge at 0.5 M $NaClO_4$ and an isotherm at pH 5.5 by Bradbury & Baeyens (2005a). At a later stage an additional sorption edge (Bradbury & Baeyens 2009a) and isotherm at pH 7.2 (*this study*) on a differently treated IdP (more sever acid treatment, see Appendix K) were carried out. These data sets were not fully consistent with the data from Poinssot et al. (1999) and Bradbury & Baeyens (2005a) and the modelling yielded slightly different surface complexation constants (also given in Appendix C). The reason for this discrepancy is not clear.

The question of trivalent metals forming aqueous silicate complexes with the low concentrations of Si present in solutions in equilibrium with 2:1 clay minerals (between 10^{-5} and ~ 8×10^{-5} M), and their influence on sorption and modelling was fully discussed in Baeyens & Bradbury (2017) for the case of montmorillonite. The Eu-silicate formation reaction and stability constant are given in Hummel et al. (2002), i.e.:

$$Eu^{3+} + Si(OH)_{4(aq)} \Leftrightarrow EuSiO(OH)_3^{2+} + H^+ \qquad \log K = -1.71 \qquad (3.1)$$

(This constant is by no means well-established.)

The main finding of Baeyens & Bradbury (2017) for montmorillonite was that the exclusion or inclusion of the $EuSiO(OH)_3^{2+}$ species in the modelling made no difference to the conclusion that the Eu mono-hydroxy complex was the main sorbing species in the pH range 5 to 9. The sorption data could equally well be modelled excluding or including the Eu-silicate complex. The preferred modelling approach was to exclude the aqueous silicate species. This interpretation of the sorption data for montmorillonite is taken over here for illite and applied to the modelling of the sorption of Eu, Am and Cm shown in Figs. 3.4 to 3.6, i.e. aqueous trivalent metal complexation with Si was not included for the surface complexation values given in Appendix C. For completeness, the surface stability constants and the modelling results for the sorption edges obtained for Eu, Am and Cm with the inclusion of silicate complexes are given in Appendix F.

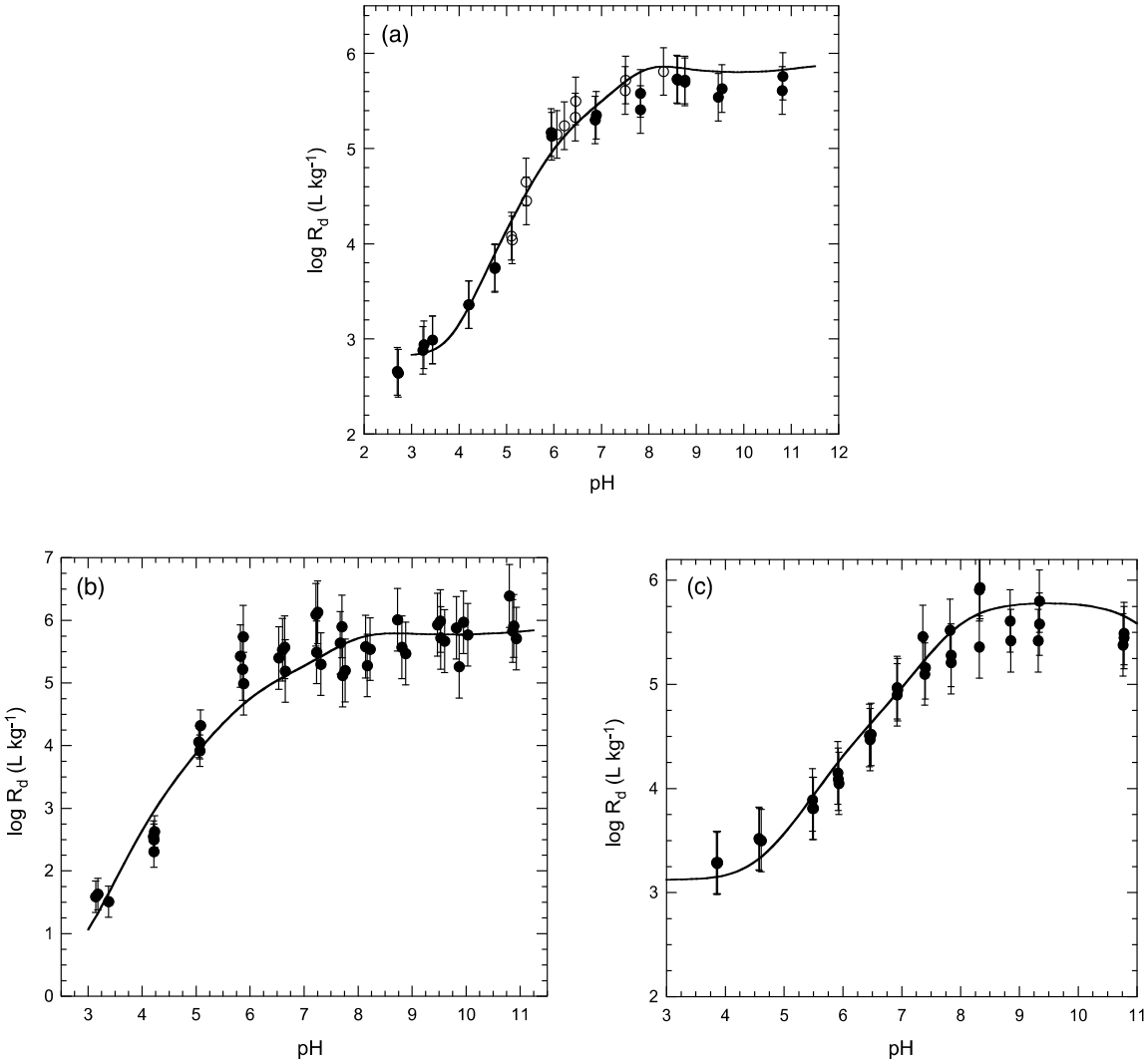

Fig. 3.4: Sorption edges for Eu(III) on Na-IdP in 0.1 M $NaClO_4$ (a), in 0.5 M $NaClO_4$ (b) and in 0.1 M $NaClO_4$ (c).

Experimental data (●): (a) $Eu_{TOT} = 3 \times 10^{-9}$ M, $S = 1.8$ g L^{-1}, from Poinssot et al. (1999) and (b) $Eu_{TOT} = 5 \times 10^{-10}$ M, $S = 1.4$ g L^{-1} (from Bradbury & Baeyens 2005a) and (c); $Eu_{TOT} = 3.9 \times 10^{-9}$ M; $S = 0.6 – 1.6$ g L^{-1} (from Bradbury & Baeyens 2009a) and modelled curves (—) *this study* and Bradbury & Baeyens (2009a). Excluding Eu-silicate aqueous species.

3.2.5 Americium

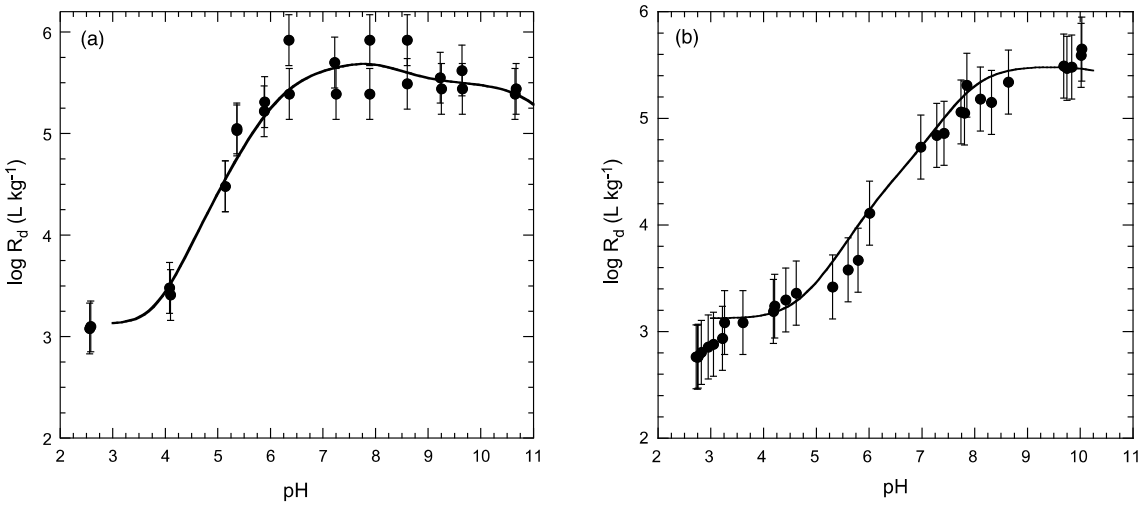

Fig. 3.5: Sorption edges for Am(III) in 0.1 M $NaClO_4$ on Na-IdP (a) and Illite du Puy (b).

Experimental data (●): (a) $Am_{TOT} = 4 \times 10^{-11}$ M, $S = 0.58$ g L^{-1} (Bradbury & Baeyens 2009b) and (b) $Am_{TOT} = 5 \times 10^{-8}$ M, $S = 4.9$ g L^{-1} (Gorgeon 1994) and modelled curves (—) (*this study*). Excluding Am-silicate aqueous species.

3.2.6 Curium

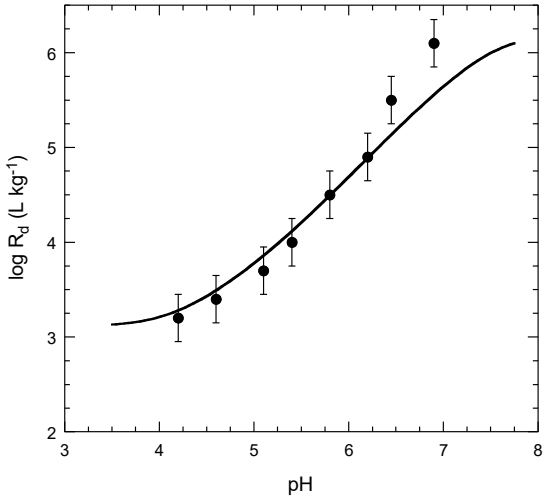

Fig. 3.6: Sorption edge for Cm(III) on Na-IdP in 0.1 M $NaClO_4$.

$Cm_{TOT} = 2.5 \times 10^{-7}$ M; $S = 0.25$ g L^{-1}. Experimental data (●) (Rabung et al. 2005) and modelled curve (—) (*this study*). Excluding Cm-silicate aqueous species.

3.2.7 Tin

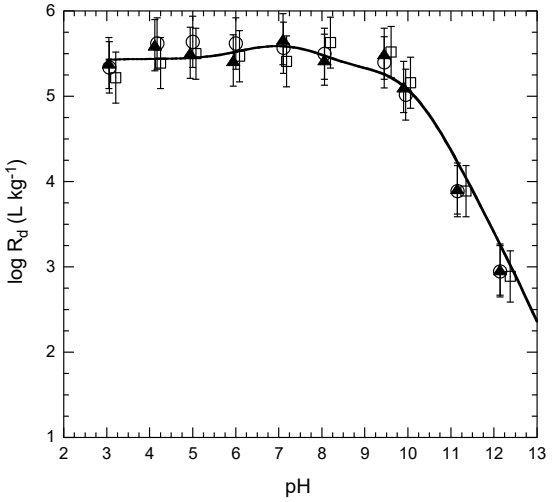

Fig. 3.7: Sorption edge for Sn(IV) on Na-IdP in 0.1 M $NaClO_4$.

Sn_{TOT} = 5 × 10^{-9} M, S = 1.1 g L^{-1}. Experimental data (○: 7 days; ▲: 21 days; □: 60 days) and modelled curve (—) (Bradbury & Baeyens 2009a).

3.2.8 Thorium

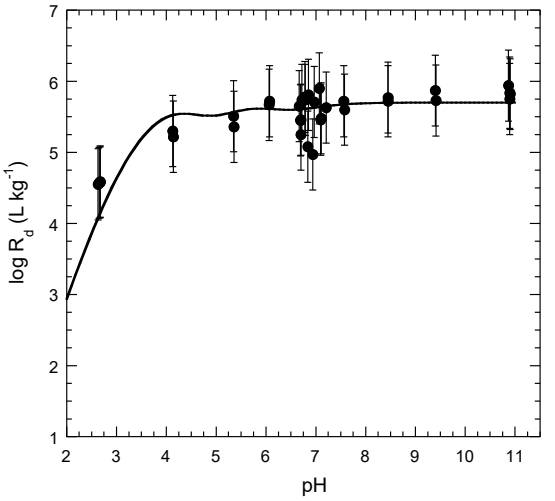

Fig. 3.8: Sorption edge for Th(IV) on Na-IdP in 0.1 M $NaClO_4$.

Th_{TOT} ~ 10^{-11} M, S = 0.67 g L^{-1}. Experimental data (●) and modelled curve (—) (Bradbury & Baeyens 2009b).

3.2.9 Neptunium

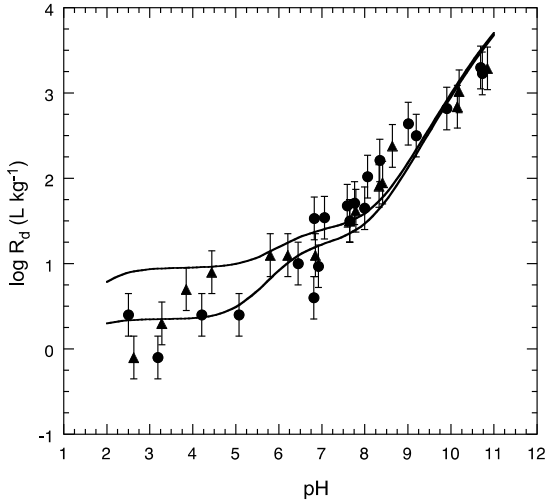

Fig. 3.9: Sorption edge for Np(V) on Na-illite.

$Np_{TOT} \sim 1.2 \times 10^{-6}$ M, $S = 8.8$ g L^{-1}. Experimental data on Na-IdP in (▲) 0.025 M $NaClO_4$ and (●) 0.1 M $NaClO_4$ (Gorgeon 1994) and modelled curves (—) (Bradbury & Baeyens 2009b).

3.2.10 Protactinium

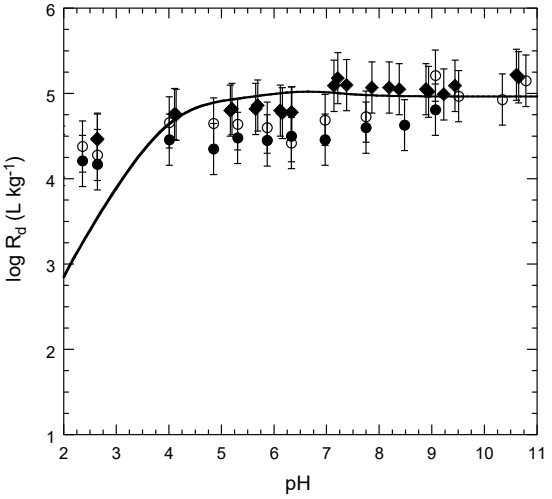

Fig. 3.10: Sorption edge for Pa(V) on Na-IdP in 0.1 M $NaClO_4$.

$Pa_{TOT} < 10^{-13}$ M; $S = 0.67$ g L^{-1}. Experimental data (○, ◆: 1 day equilibrium, ●: 7 days equilibrium) and modelled curve (—) (Bradbury & Baeyens 2009b).

3.2.11 Uranium

Because of the relatively complex hydrolysis behaviour of U(VI), four surface complexation reactions were needed to model the sorption edge from pH 3 to 11. In addition, the modelling of the three U(VI) isotherms given in section 3.3.6 revealed that the uptake on the weak sites was contributing to the sorption edge. Consequently, the modelling was more complicated than normal and involved an iterative procedure requiring that all of the edge and isotherm data were optimised together.

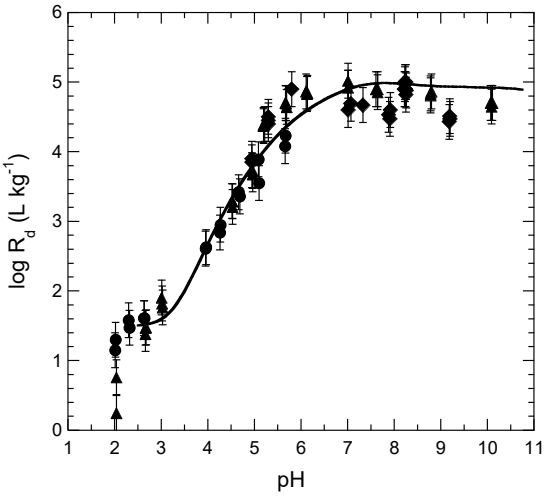

Fig. 3.11: Sorption edges for U(VI) on Na-IdP in 0.1 M $NaClO_4$.

$U_{TOT} \sim 10^{-7}$ M, $S = 2.6$ g L^{-1}: Experimental data (symbols) (Bradbury & Baeyens 2009b and modelled curve (—) (*this study*).

3.3 Sorption isotherms: Figures and modelled curves

A compilation of sorption isotherms for the elements Co(II), Ni(II), Zn(II), Eu(III), and U(VI) measured in the pH range 5 to 9 together with the modelled curves are presented in the Figs. 3.12 to 3.16. (The experimental data points are given as triangles and the modelled curves as continuous black lines.) A summary of the surface complexation reactions and constants on the weak sites are given in Appendix D.

The sorption isotherms in this report are presented as sorbed radionuclide concentrations (C_{sorb}) vs. the equilibrium aqueous concentrations of active and inactive metal (C_{eq}) in a plot of log C_{sorb} vs. log C_{eq} (for more details see Baeyens & Bradbury 1995b).

3.3.1 Cobalt

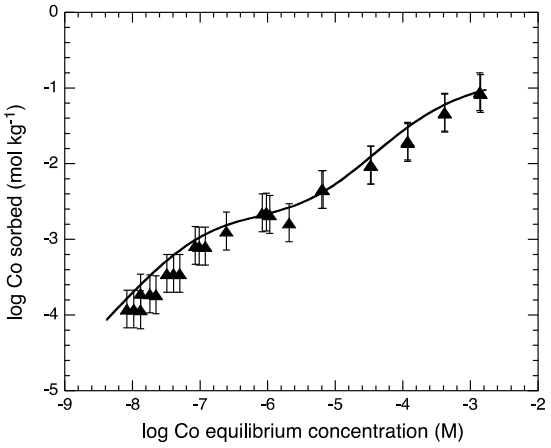

Fig. 3.12: Sorption isotherm for Co(II) on Na-IdP at pH 7.1 in 0.1 M $NaClO_4$.
Experimental data (▲) (Marques Fernandes et al. 2015) and modelled curve (—) (*this study*).

3.3.2 Nickel

The surface complexation constants on the strong sites modelled in this study are slightly different from those published in Bradbury & Baeyens (2009a). The reason is that in this study the weak sites have been included in the modelling of the edges. The 6 data sets presented here (2 edges, 4 isotherms) have been modelled with the Ni parameter set given in Appendix C and D.

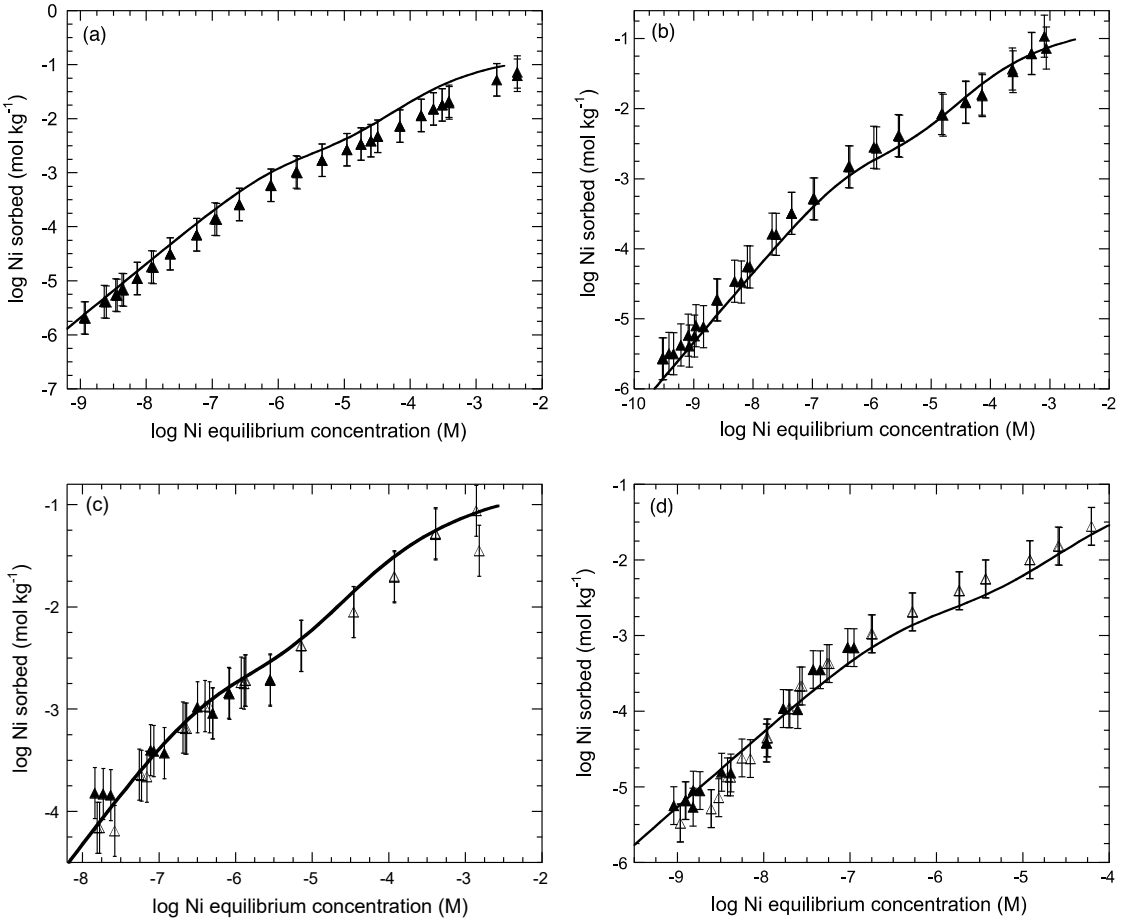

Fig. 3.13: Sorption isotherms for Ni(II) on Na-IdP in 0.1 M $NaClO_4$.

Experimental data (▲, △) at (a) pH 6.0, (b) pH 7.0, (c) pH 7.2 and (d) pH 7.8 (Poinssot et al. 1999) and pH = 7.2 (Marques Fernandes et al. 2015) and modelled curves (—) (*this study*).

3.3.3 Zinc

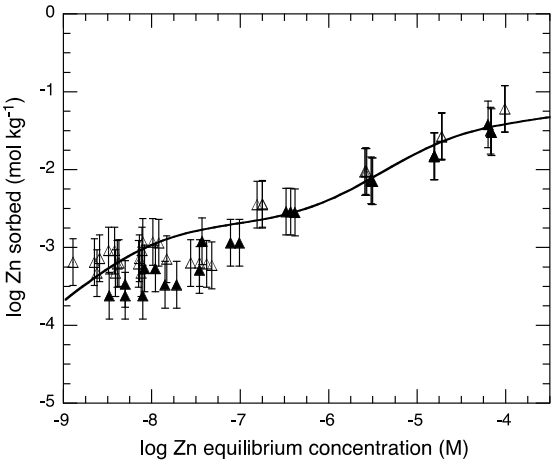

Fig. 3.14: Sorption isotherm for Zn(II) on Na-IdP at pH 7.2 in 0.1 M NaClO4.

Experimental data (▲, △) (Montoya et al. 2018) and modelled curve (—) (*this study*).

3.3.4 Europium

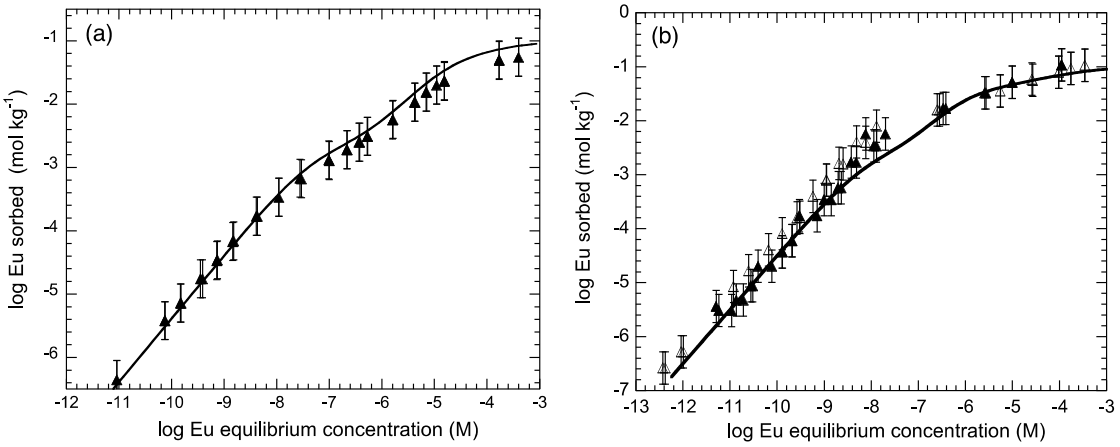

Fig. 3.15: Sorption isotherms for Eu on Na-IdP in 0.1 M $NaClO_4$ at pH= 5.5 (a) and pH = 7.0 (b).

Experimental data (▲, △) (Poinssot et al. 1999) and modelled curves (—) (*this study*). Excluding Eu-silicate aqueous species.

3.3.5 Uranium

The fits to the isotherm data (see also section 3.2.12) at pH 4.8 and 5.8 lie mainly within the error bars. For the two data sets measured at pH 7.3, the modelled curve agrees well with the measured data at equilibrium concentrations $< 5 \times 10^{-7}$ M. At higher equilibrium concentrations the measured values lie above the modelled curve. Although there is no corroborating EXAFS data available, there is a strong suspicion that at equilibrium concentrations $> 5 \times 10^{-7}$ M uranyl is undergoing surface precipitation at this pH.

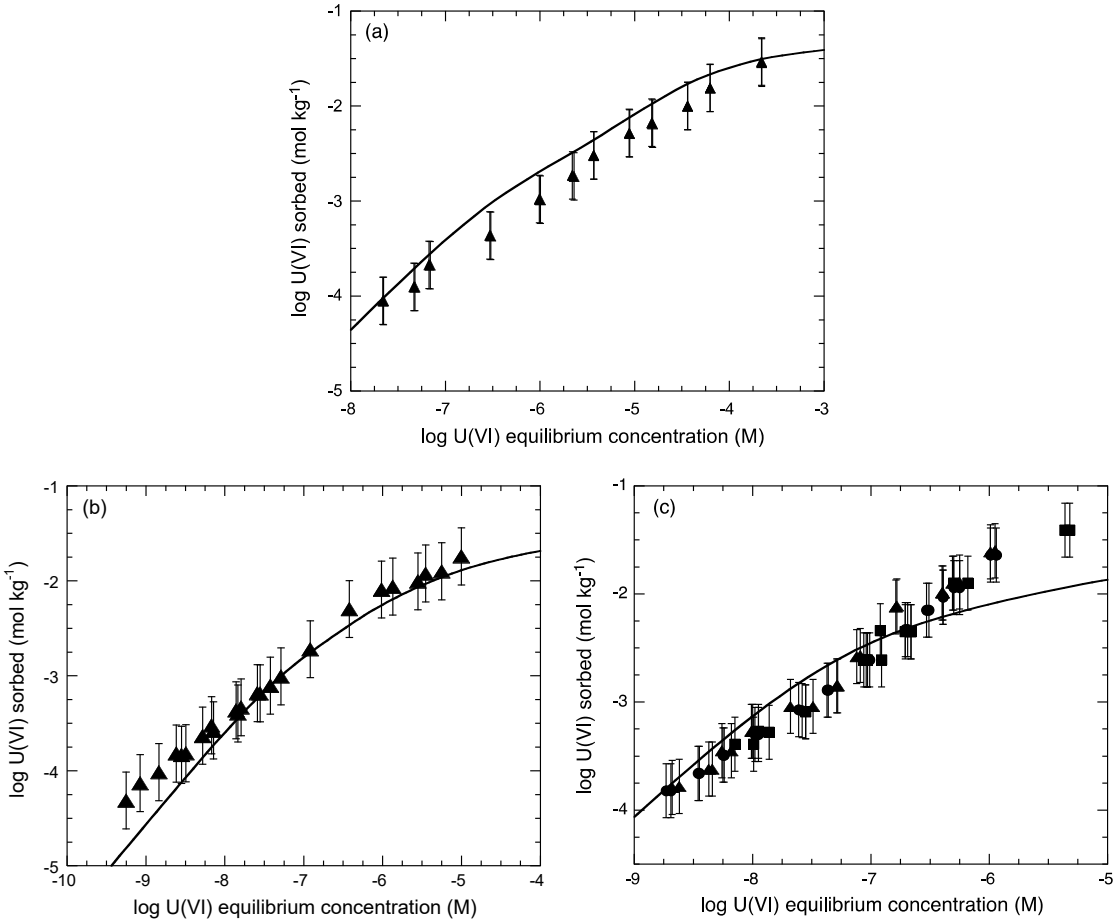

Fig. 3.16: Sorption isotherms for U(VI) on Na-IdP in 0.1 M $NaClO_4$ at pH 4.8 (a), pH 5.8 (b) and pH 7.3 (c).

Experimental data (▲) in (a), (b) (Bradbury & Baeyens 2005a) and (c) (●,▲, ■) (*this study*) and modelled curves and (—) (*this study*).

4 Linear free energy relationships for illite

4.1 General considerations for Linear Free Energy Relationships (LFER)

In solution thermodynamics it is common practice to seek relationships between the free energies of formation of aqueous complexes and the thermodynamic properties of the metal ions or ligands, such systematic dependencies are commonly termed linear free energy relationships, LFERs, (Larsson 1934, Hammett 1940, Chapman & Shorter 1972). It is extremely difficult to calculate surface complexation constants from theoretical considerations. Therefore, the motivation behind seeking LFERs for surface site binding constants was to provide a means to estimates constants for metals where the data are either very poor or non-existent which would then allow sorption values to be calculated.

The 2SPNE SC/CE sorption model has been used to quantitatively describe sorption edge and isotherm data sets measured on illite for radionuclides with valences between II and VI (see Chapter 3).

For a metal Me with valence z_{Me}, it may be stated in general terms that an aqueous species of the form:

$$Me(OH)_{(x-1)}^{z_{Me}-(x-1)} \tag{4.1}$$

sorbs to form a surface complex of the form:

$$\equiv S^{S}OMe(OH)_{y}^{z_{Me}-(y+1)} \tag{4.2}$$

which in turn correlates with the hydrolysed species:

$$Me(OH)_{x}^{z_{Me}-x} \tag{4.3}$$

where $x = y + 1$ and all three equations are valid when $x \geq 1$.

A good systematic linear correlation between the logarithms of the surface site binding constants on the strong and weak sites and the logarithm of the corresponding aqueous hydrolysis constants ${}^{OH}K_x$, according to the above, was found (Fig. 4.1) in some previous work (Bradbury & Baeyens 2005b, 2009b).

4.2 Further considerations to the LFER approach

Although the LFER correlation such as that shown in Fig. 4.1 for the strong sites on illite look very good i.e. extend over more than 30 orders of magnitude and has a correlation coefficient, R, near to unity, implying that the probability that the values are linearly correlated lies very close to 100 % (Taylor 1982), closer inspection shows that there are some difficulties associated with the LFER as shown.

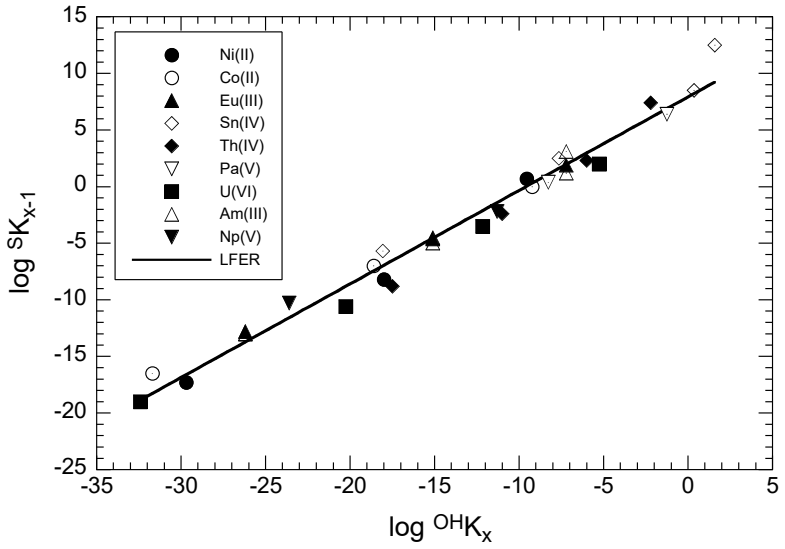

Fig. 4.1: Correlation of surface complexation constants of species sorbing on strong sites of illite with the corresponding hydrolysis constants.

See Eqs. 4.2 and 4.3 (taken from Bradbury & Baeyens 2009b); log $^{S}K_{x-1}$ = (8.0 ± 0.4) + (0.83 ± 0.02) log $^{OH}K_x$ (R = 0.99).

There may be significant errors associated with the hydrolysis constants given in Appendix B. Broadly speaking, the first hydrolysis constant values tend to be the most reliable because they can often be determined at high metal concentrations by potentiometric methods. An optimistic estimate for the uncertainty in log $^{OH}K_1$ values might be ± 0.1 but could be as high as ± 0.5. For the 1:2, 1:3 etc. hydrolysed species the constants are often obtained by fits to solubility measurements in which, for example, it is not always clear what the solid phase is, and solubility products and hydrolysis constants have to be fitted simultaneously. For these hydrolysis constants the values may be poorly defined.

At higher sorption values (> 10^4 L kg^{-1}), generally occurring at higher pH values (> 8.5), there is scatter in the sorption values which may be ± 0.5 log units or more. Therefore, the error in the surface complexation constants modelled in this region are also of this order.

The LFERs for ≡S^{S}OH sites presented for illite (Fig. 4.1) include surface complexation constants for all of the metals so far investigated, irrespective of their valence. In view of the discussions in section 2.3 and in Bradbury et al. (2017) on competition, in which it was concluded that metals in the same valence state have their own set of strong sites, it would now seem to be inconsistent to plot all metals together. Rather, only metals with the same valence should be included in LFER plots.

Further, the whole of the sorption edge data has been considered, most often in the pH range ~ 3 to over 10, and all modelled surface complexation constants have been included in the LFER plot. At low pH values (< 5) and high pH values (> 9) 2:1 clay minerals are unstable and tend to dissolve. Further, in real argillaceous rock systems the pH range of interest is ~ 7 to ~ 8.

The above considerations lead to the following proposals for modified LFER plots.

Separate LFER plots should be made for divalent transition metals, trivalent actinides and tetravalent metals. This condition arises from the results from sorption competition experiments. Only those surface complexation constants making major contributions to the sorption in the

range $5 \leq pH \geq 9$ should be considered in the LFER plots. This restriction takes into account the 2:1 clay mineral stability issue, reflects the pH range important in real systems, and in many cases (but not all) tends to result in the use of the first (and most reliable) hydrolysis constant values in the LFERs. The hydrolysis constants and corresponding surface complexation constants selected according to the above considerations are shown in bold type in Appendices B and C/D respectively and are used in the modified LFERs for illite (Figs. 4.5, 4.9, 4.11 and 4.16).

A number of comments need to be made concerning the LFERs for illite given here.

Firstly, the relationships between surface complexation constants and aqueous hydrolysis constants given in the following sections for illite are dependent on the sorption model itself, the model parameters used and the values of the stability constants for the hydrolysed species. Therefore, sorption model, surface parameters, hydrolysis constants and surface stability constants constitute an inseparable unit.

Secondly, in the case of tri- and tetravalent elements the number of elements for which there are data is limited, as is the number of data points in the LFERs. For trivalent metals, only data for Eu and Am are available, and both elements have essentially the same hydrolysis constants. For tetravalent metals, only data for Sn and Th are available. The chemistries of Sn and tetravalent actinides are so different that it was not considered justifiable to plot them together. Only the data for Th were plotted on a LFER. Unfortunately, the lack of data does not allow anything better at the present time. The above factors should be clearly held in mind if the LFERs for trivalent and tetravalent elements are used.

Thirdly, there is no information available on sorption competition on the weak sites. Because the site capacity of the weak sites is so large, no competitive sorption is assumed to take place on them. Also, it is not currently known whether there are different sorption site types for the different valence state of sorbing metals (*cf.* strong sites). The assumption is made here that metals of different valence can be included on the same LFER plot.

In section 4.3 the data sources and modelling are as referenced in Chapter 3.

4.3 Derivation of revised LFERs from speciation and modelling

4.3.1 Divalent transition metals: Co, Ni, Zn

In the following, plots of the aqueous speciation and surface speciation of each metal are shown. The aqueous sorbing species and the corresponding sorbed complexes are colour coded. Uptake by cation exchange is represented by broken black lines and surface complexation by continuous lines in the sorption edges.

From Figs. 4.2a to 4.4a it can be seen that the most prominent aqueous species in the pH range 5 to 9 are Co^{2+}, $Ni^{2+}$and Zn^{2+} respectively, which are also the dominant sorbing species (Figs. 4.2b to 4.4b) forming $\equiv^{S}SOCo^{+}$, $\equiv^{S}SONi^{+}$ and $\equiv^{S}SOZn^{+}$, respectively (the sorbing aqueous species has the same colour as the sorbed complex). According to section 4.1, the correlating hydrolysed species are $CoOH^{+}$, $NiOH^{+}$ and $ZnOH^{+}$, respectively.

Thus, a modified LFER for divalent transition metals for the pH range 5 to 9 (Fig. 4.5) can be constructed from the hydrolysis constants and surface complexation constants given in bold in Appendices B and C (Tab. C1), respectively.

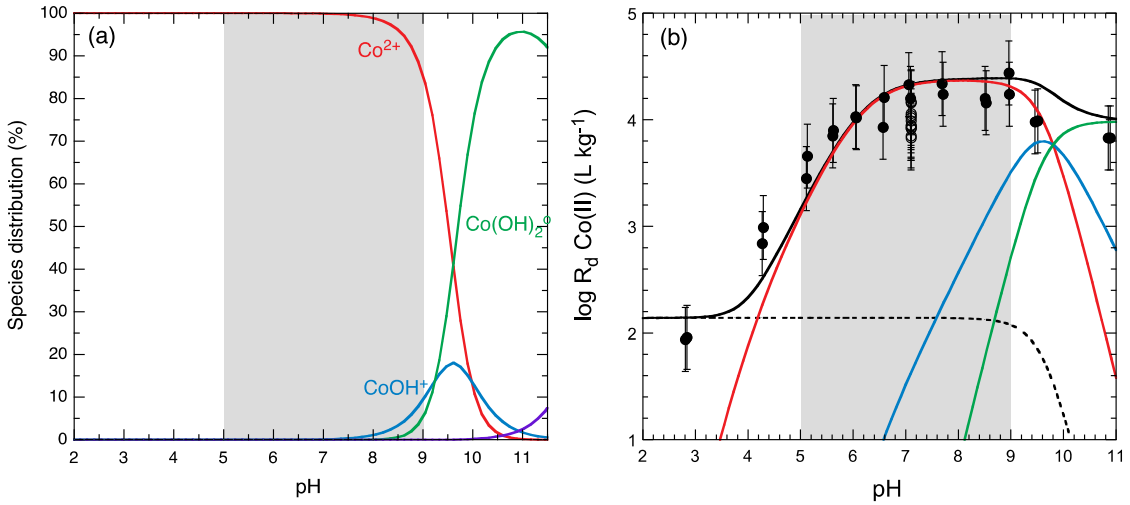

Fig. 4.2: (a) The aqueous speciation (Co_{TOT} = 10^{-8} M) and (b) sorption edge for Co(II) on Na-IdP in 0.1 M $NaClO_4$.

Corresponding to Fig. 3.1.

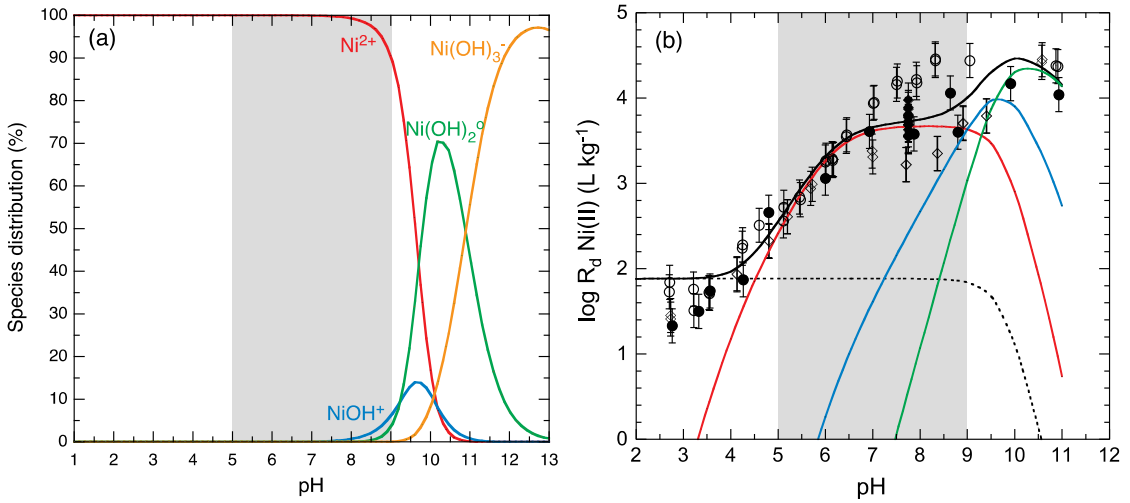

Fig. 4.3: (a) The aqueous speciation (Ni_{TOT} = 10^{-8} M) and (b) sorption edge for Ni(II) on Na-IdP in 0.1 M $NaClO_4$.

Corresponding to Fig. 3.2a.

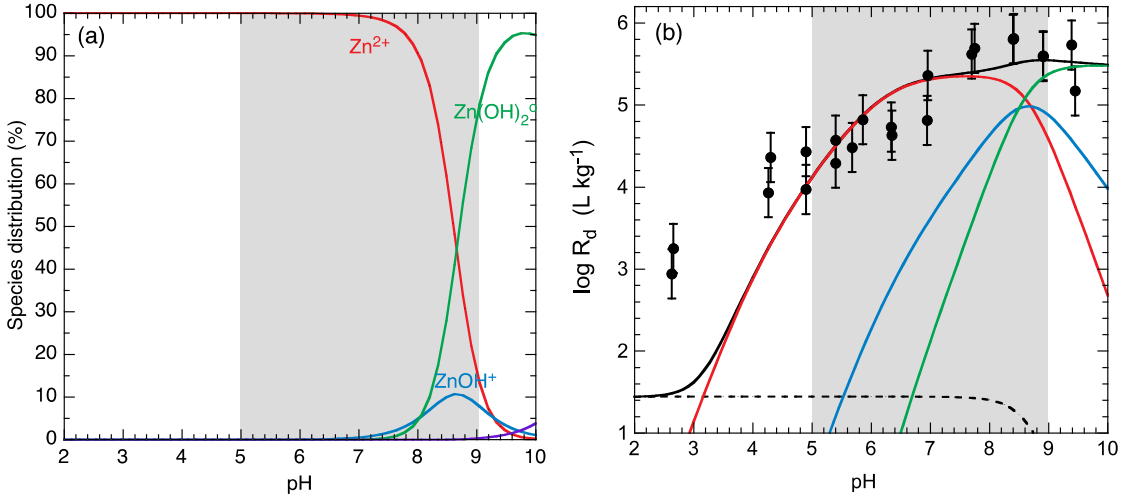

Fig. 4.4: (a) The aqueous speciation (Zn_{TOT} = 10^{-8} M) and (b) sorption edge for Zn(II) on Na-IdP in 0.1 M $NaClO_4$.

Corresponding to Fig. 3.3b.

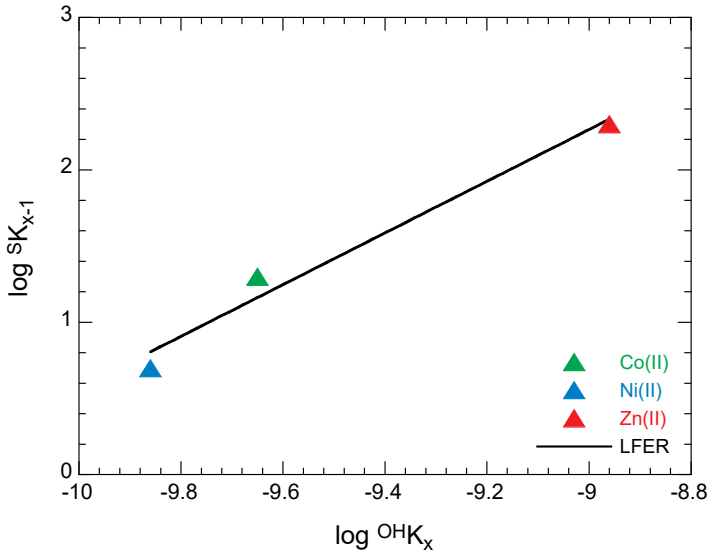

Fig. 4.5: LFER of divalent transition metals on strong sites using the hydrolysis constants from Appendix B and the surface complexation constants from Appendix C (Tab. C1) (values in bold type).

$\log {}^{S}K_{x-1} = (17.53 \pm 2.52) + (1.70 \pm 0.27) \log {}^{OH}K_x$ (R = 0.99).

4.3.2 Trivalent lanthanides and actinides metals: Eu, Am, Cm

Speciation and surface species plots for Eu, Am and Cm are illustrated below. It should be noted that the hydrolysis constants for Eu, Am and Cm are taken to be the same, Appendix B. (Again, the aqueous sorbing species and the corresponding sorbed complexes are colour coded.)

From Figs. 4.6a, 4.7a and 4.8a it can be seen that the most prominent aqueous species for Eu, Am and Cm in the pH range 5 to 9 are Eu^{3+}, $EuOH^{2+}$ and $Eu(OH)_2^+$, Am^{3+}, $AmOH^{2+}$ and $Am(OH)_2^+$ and Cm^{3+}, $CmOH^{2+}$ and $Cm(OH)_2^+$ respectively, which are also the dominant sorbing species (Figs. 4.6b, 4.7b and 4.8b). From this a modified LFER (Fig. 4.9) can be made taking the hydrolysis and surface complexation constants given in bold in Appendix B and Tab. C2, respectively.

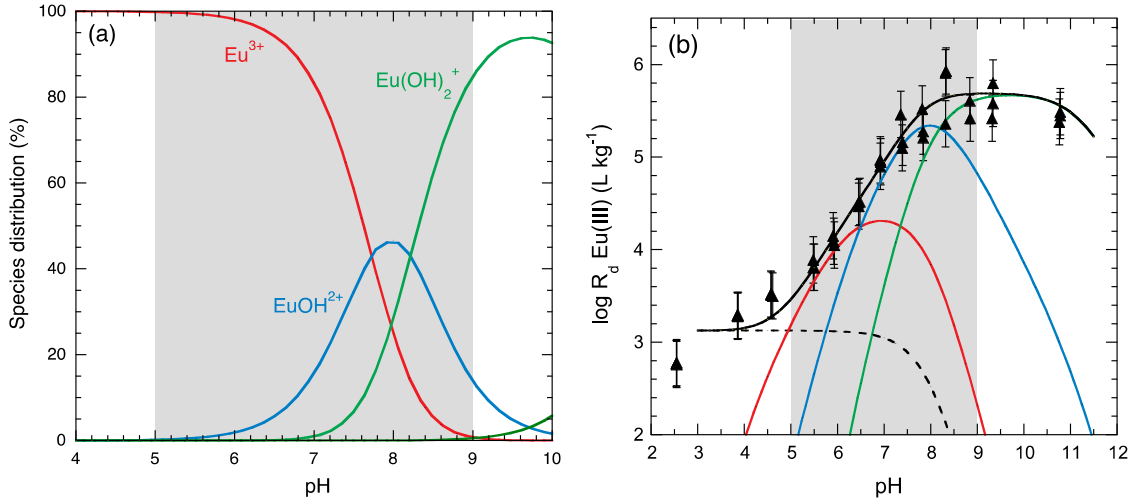

Fig. 4.6: (a) The aqueous speciation ($Eu_{TOT} = 10^{-8}$ M) and (b) sorption edge for Eu(III) on Na-IdP in 0.1 M $NaClO_4$.

Corresponding to Fig. 3.4c.

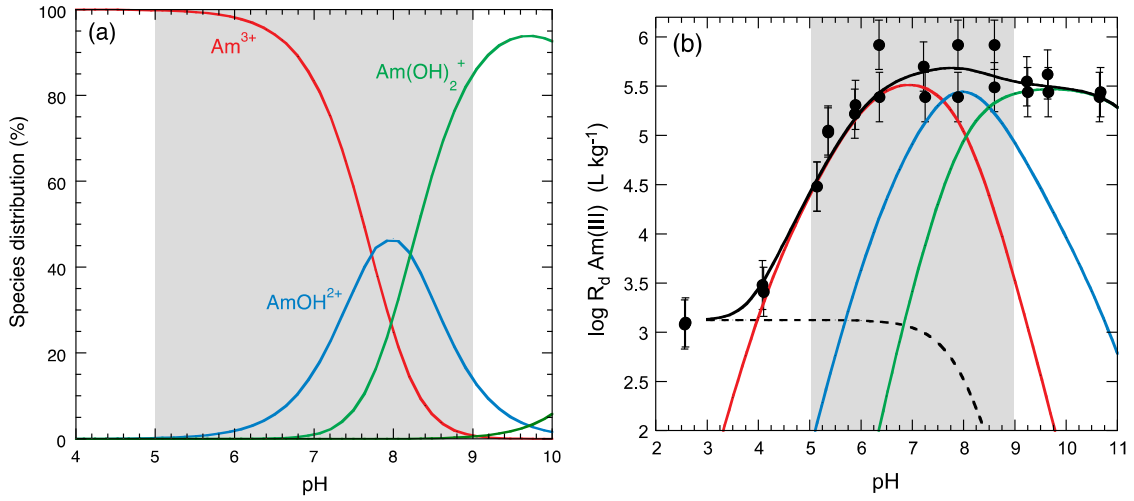

Fig. 4.7: (a) The aqueous speciation ($Am_{TOT} = 10^{-8}$ M) and (b) sorption edge for Am(III) on Na-IdP in 0.1 M $NaClO_4$.

Corresponding to Fig. 3.5a.

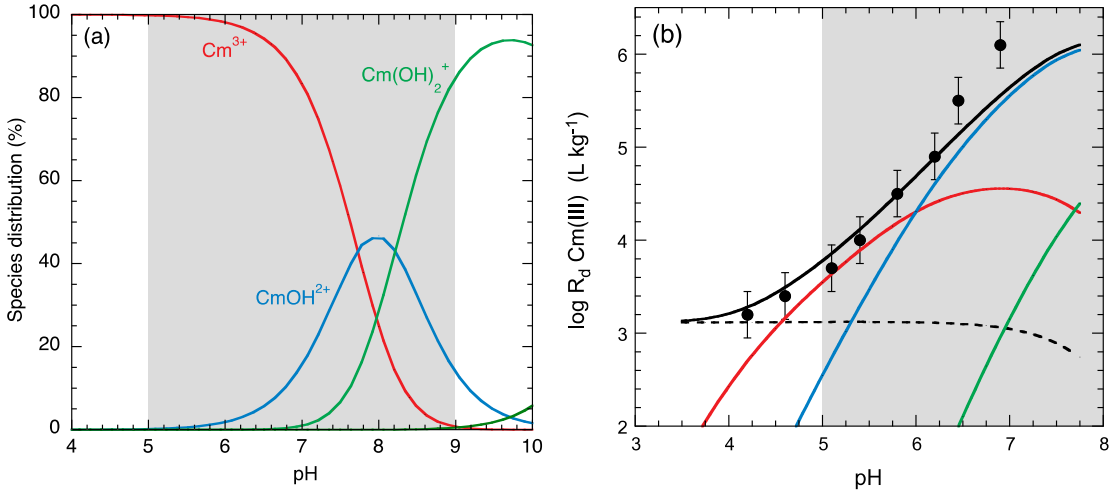

Fig. 4.8: (a) The aqueous speciation and (b) sorption edge for Cm(III) on Na-IdP in 0.1 M $NaClO_4$.

Corresponding to Fig. 3.6.

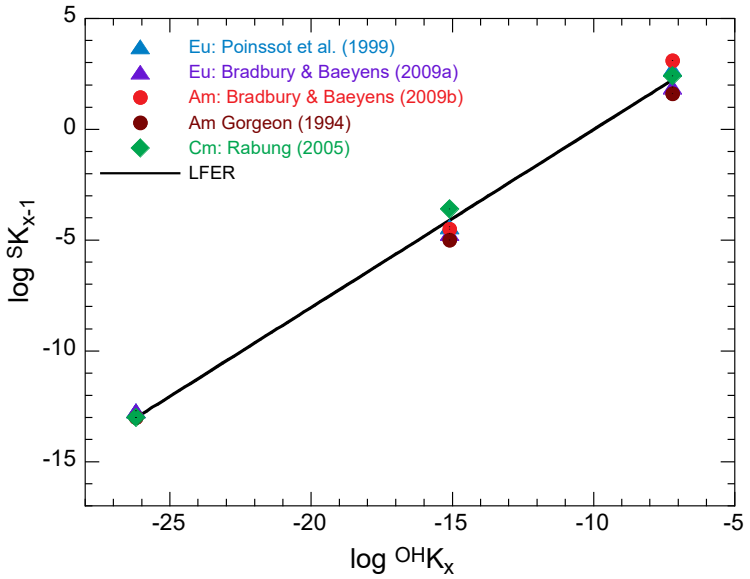

Fig. 4.9: LFER of trivalent elements on strong sites using the hydrolysis constants from Appendix B and the surface complexation constants from Appendix C, (Tab. C2) (values in bold type).

$\log {}^{S}K_{x-1} = (8.00 \pm 0.33) + (0.80 \pm 0.02) \log {}^{OH}K_x$ (R = 0.997).

4.3.3 Tetravalent actinides metals: Th(IV)

Th is the only tetravalent actinide for which sorption data exist. Speciation and surface complex plots for Th(IV) are illustrated in Fig. 4.10. From these plots it can be seen that the most prominent aqueous hydrolysed species in the pH range 5 to 9 are $Th(OH)^{3+}$, $Th(OH)_2^{2+}$, $Th(OH)_3^{+}$ and $Th(OH)_4^{0}$ which are also the dominant sorbing species (Fig. 4.10b). From this a modified LFER (Fig. 4.11) can be made taking the aqueous hydrolysis and surface complexation constants given

in bold in Appendices B and C (Tab. C3), respectively. Unfortunately, for the sorbed complex $\equiv SOTh(OH)_4^-$, which dominates the uptake of Th(IV) at pH =7 and higher, there is no corresponding aqueous hydrolysis species and therefore this (important) surface complex cannot be included in the LFER plot.

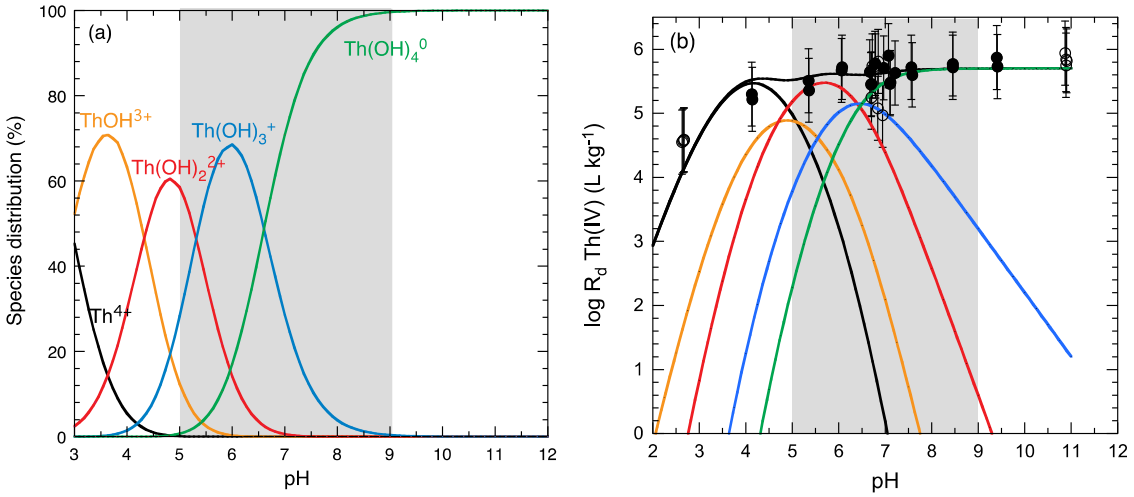

Fig. 4.10: (a) The aqueous speciation ($Th_{TOT} = 10^{-8}$ M) and (b) sorption edge for Th(IV) on Na-SWy-1 in 0.1 M $NaClO_4$.

Corresponding to Fig. 3.8.

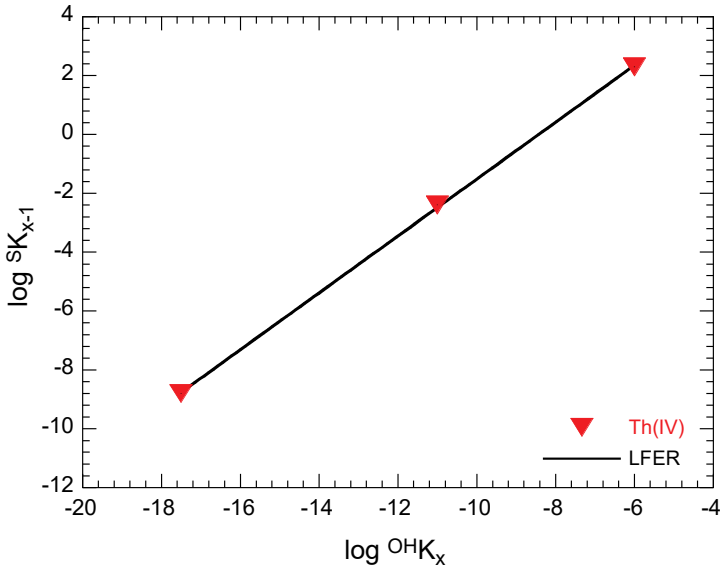

Fig. 4.11: LFER of tetravalent Th on strong sites using the hydrolysis constants from Appendix B and the surface complexation constants from Appendix C (Tab. C3) (values in bold type).

$\log {}^{S}K_{x-1} = (8.14 \pm 0.16) + (0.97 \pm 0.01) \log {}^{OH}K_x$ (R = 0.999).

4.3.4 Summary of the equations for the modified LFERs

The LFERs for strong sites on illite can be described by the following equations:

Divalent transition metals

$$\log {}^{S}K_{x-1} = (17.53 \pm 2.52) + (1.70 \pm 0.27) \log {}^{OH}K_{x} \quad (R = 0.99) \tag{4.4}$$

Trivalent lanthanides and actinides

$$\log {}^{S}K_{x-1} = (8.00 \pm 0.33) + (0.80 \pm 0.02) \log {}^{OH}K_{x} \quad (R = 0.997) \tag{4.5}$$

Tetravalent actinides

$$\log {}^{S}K_{x-1} = (8.14 \pm 0.16) + (0.97 \pm 0.01) \log {}^{OH}K_{x} \quad (R = 0.999) \tag{4.6}$$

where "x" is an integer in all of the above equations.

4.3.5 Metals for which sorption edge data are available, but are not included in the LFERs: Sn(IV), Np(V), Pa(V) and U(VI)

4.3.5.1 Sn(IV)

The results of the speciation and modelling calculations are shown in Fig. 4.12. The hydrolysis behaviour of Sn is very uncertain, especially in the acidic region. It was not possible to model the Sn sorption edge using the hydrolysis constants given in Hummel et al. (2002) alone. In some previous work Bradbury & Baeyens (2005b) used the first four conditional hydrolysis constants (log Q values) given in Baes & Mesmer (1976), converted to thermodynamic constants, and the Hummel et al. (2002) hydrolysis constants re-written with Sn^{4+} as the master species instead of $Sn(OH)_4^0$ (Appendix B) to calculate the Sn speciation (Fig. 4.12a), and model the Sn sorption edge. Although the modelling appeared to be successful (Fig. 4.12b), it has to be pointed out that there is considerable uncertainty concerning the log Q values given in Baes & Mesmer (1976), but there are, at present, no better hydrolysis data available in the open literature (Thoenen 2015, pers. comm.). In the pH range 5 to 9 the major aqueous species are $Sn(OH)_4^0$ and $Sn(OH)_5^-$, but the main sorbing species, according to the modelling, are $Sn(OH)_3^+$, $Sn(OH)_4^0$ and $Sn(OH)_5^-$, dominated by the uptake of the first two species. This behaviour is different from that observed in all previously described cases.

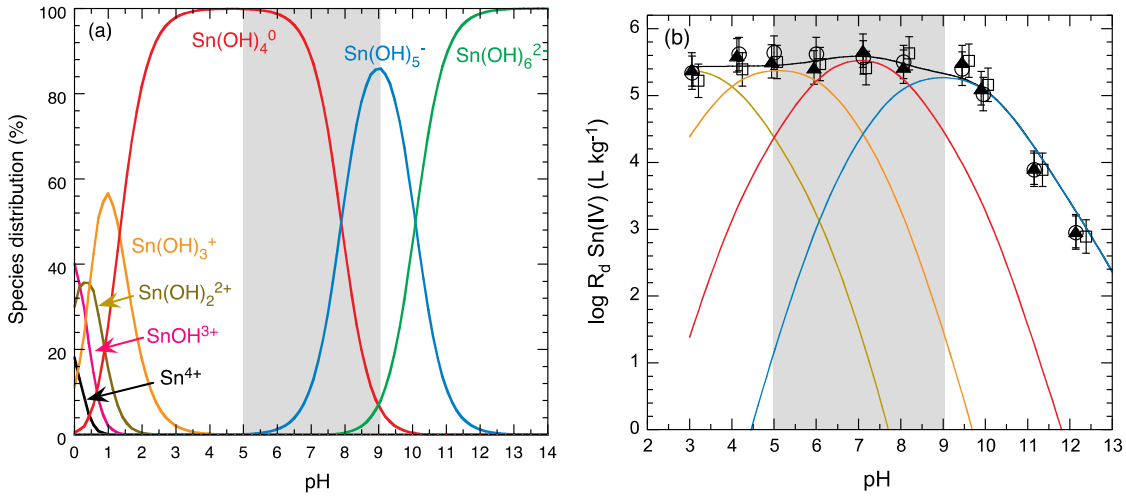

Fig. 4.12: (a) The aqueous speciation (Sn_{TOT} = 10^{-8} M) and (b) sorption edge for Sn(IV) on Na-IdP-1 in 0.1 M $NaClO_4$.

Corresponding to Fig. 3.7.

4.3.5.2 Np(V), Pa(V)

The results of the speciation and modelling calculations for Np(V) and Pa(V) are shown in Figs. 4.13 and 4.14, respectively.

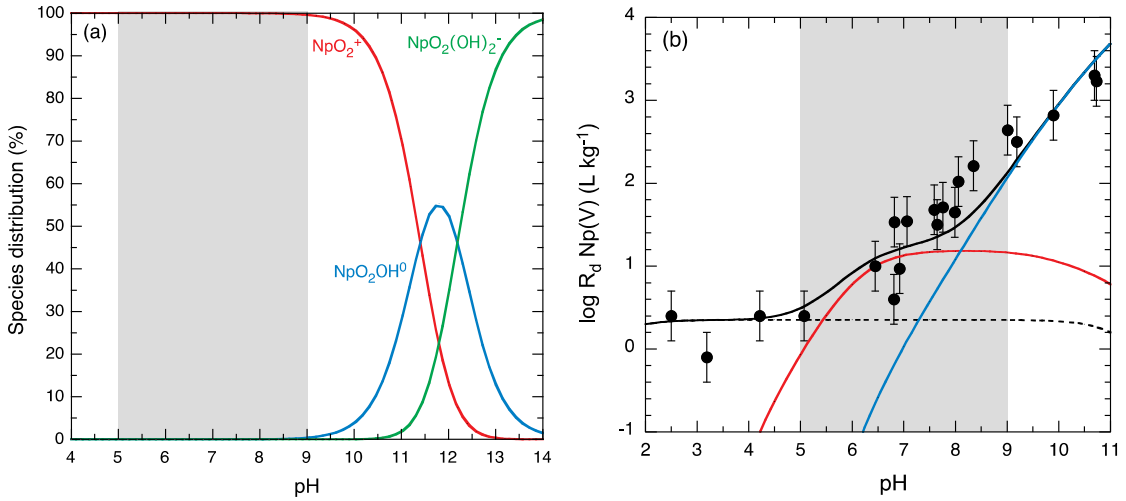

Fig. 4.13: (a) The aqueous speciation (Np_{TOT} = 10^{-8} M) and (b) sorption edge for Np(V) on Na-IdP in 0.1 M $NaClO_4$.

Corresponding to Fig. 3.9.

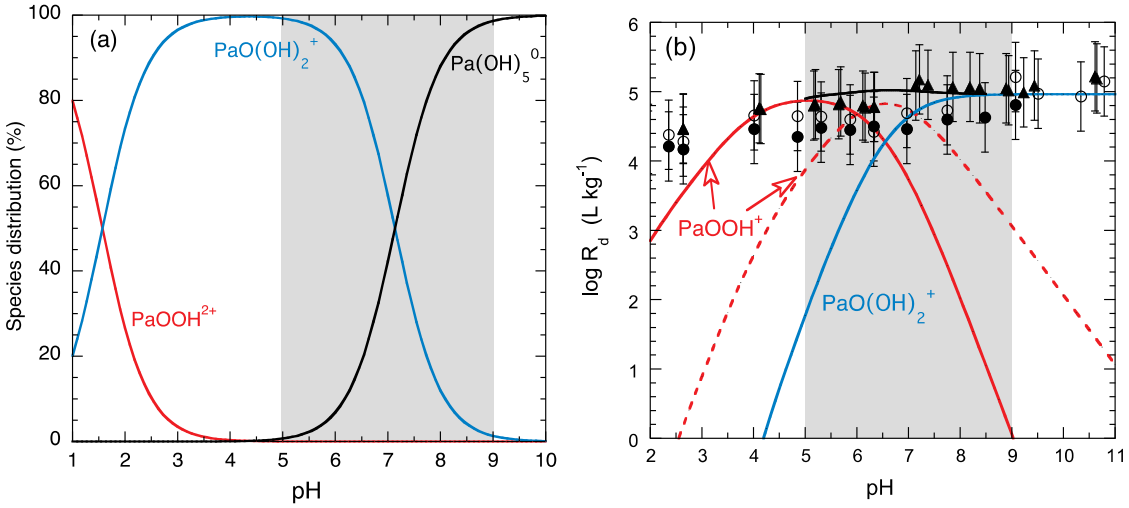

Fig. 4.14: (a) The aqueous speciation (Pa_{TOT} = 10^{-8} M) and (b) sorption edge for Pa(V) on Na-IdP-1 in 0.1 M $NaClO_4$.

Corresponding to Fig. 3.10.

The significant differences in the speciation behaviour of Np(V) and Pa(V) do not allow a LFER with these pentavalent elements to be made.

4.3.5.3 U(VI)

The results of the speciation and modelling calculations for U(V1) are shown in Fig. 4.15.

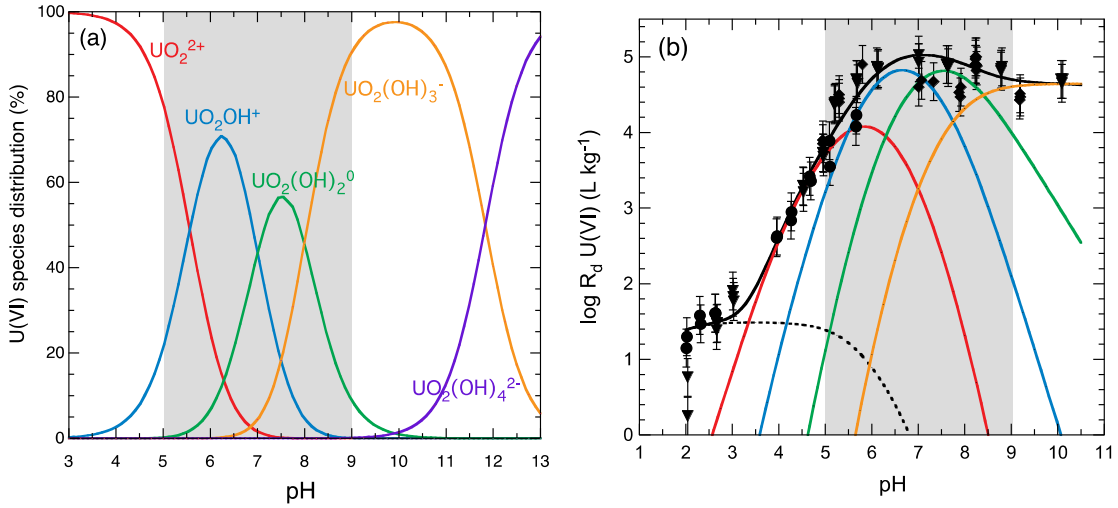

Fig. 4.15: (a) The aqueous speciation (U_{TOT} = 10^{-8} M) and (b) sorption edge for U(VI) on Na-IdP in 0.1 M $NaClO_4$.

Corresponding to Fig. 3.11.

A LFER for the hexavalent uranyl can be made for the monomeric U species. However, there are no other hexavalent elements for which sorption data needs to be derived, hence there is no need for a LFER.

4.4 LFERs for weak sites

For the elements Ni(II), Co(II), Zn(II), Eu(III) and U(VI) isotherms in the pH range from 5 to 8 have been measured and surface complexation constants for weak sites derived. The LFER for the weak sites (Fig. 4.16) was constructed for the above metals from the hydrolysis constants given in Appendix B (bold type) and the surface complexation constants given in Appendix D (Tab. D1). Contrary to montmorillonite, the U(VI) data for illite did not fit on the LFER for weak sites. The reason is not clear. U(VI) was not considered in the regression equation.

As mentioned previously in section 4.2, it is assumed that there is no sorption competition on the weak sites and all metals can be included in the LFER plot in Fig. 4.16.

For the tetravalent elements Sn and Th, and the pentavalent Pa, no isotherms are available due to solubility limits.

The LFER for weak sites can be described by the following equation:

$$\log {}^{W1}K_{x-1} = (6.23 \pm 0.34) + (0.82 \pm 0.03) \log {}^{OH}K_x \qquad (R = 0.998) \qquad (4.7)$$

where "x" is an integer equal to or greater than unity.

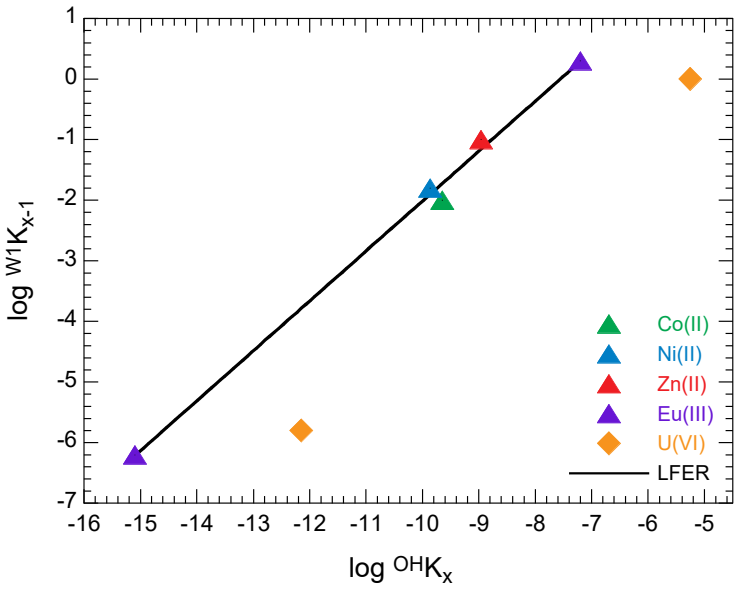

Fig. 4.16: LFER of elements on weak sites using the hydrolysis constants from Appendix B and the surface complexation constants from Appendix D (Tab. D1) (values in bold type).

$\log {}^{W1}K_{x-1} = (6.23 \pm 0.34) + (0.82 \pm 0.03) \log {}^{OH}K_x$ (R = 0.998).

5 Comparison of the sorption predicted from LFERs with measured values

The inevitable result arising from the restrictions given above in section 4.2 is that there are only a few data points in each of the LFERs, which may give rise to questions regarding their general applicability. Also, the LFERs average out the surface complexation constants derived from the experimental measurements in which the errors at higher sorption values may be as high as ± 0.5 log units. (Note: a general uncertainty value for all of the sorption measurements has been taken to be ± 0.3 log units.) Consequently, the sorption values calculated for a particular radionuclide from the appropriate LFER equation might not necessarily be expected to exactly reproduce the measured sorption data because of this averaging process occurring over many data sets.

Balanced against this is that the LFERs provide a chemically consistent, plausible and internally consistent relation between metal hydrolysis constants and surface complexation constants resulting from the application of a sorption model in which all of the basic parameters are fixed (Appendix A) for a particular clay mineral, irrespective of the metal under consideration. It may be argued that averaging over the data from many separate measurements performed at different times on samples of clay minerals sometimes obtained from different sources and subjected to different treatments may provide a more realistic representation of "sorption in general" than just relying on individual measurements.

The exercise illustrated in the following is intended to try to put the use of data from LFERs into some kind of perspective. The idea is to take the surface complexation constants for specific metals from the appropriate LFERs and compare the sorption edges/isotherms calculated with these values with the measured ones.

In the following, the measured sorption edge/isotherm data for Co(II), Ni(II), Zn(II) and Eu(III), and sorption edges for Am(III), Cm(III) and Th(IV) and modelled curves (black continuous lines) are compared with curves calculated with surface complexation constants taken from the appropriate LFERs (red continuous lines). The calculations were only performed in the pH range 5 to 9. All comparisons are grouped element by element.

The surface complexation constants derived from the LFERs (Eqs. 4.4 to 4.7) and used in the calculations are summarised in Tab. 5.1. The K_c values used are taken from Appendix E. The predicted sorption edge and/or isotherm curves are shown in Figs. 5.1 to 5.7 element by element.

Tab. 5.1: Surface complexation constants for the elements Co(II), Ni(II), Zn(II), Eu(III), Am(III), Cm(III) and Th(IV) taken from LFER for strong and weak sites and the corresponding hydrolysis constants.

Element	**Hydrolysis constants**	**Surface complexation constants**		**LFER equation**
	log ^{OH}K	log ^{S}K	log ^{W1}K	
Co(II)	-9.65	1.13	-1.69	Eq. 4.4 & 4.7
Ni(II)	-9.86	0.77	-1.87	Eq. 4.4 & 4.7
Zn(II)	-8.96	2.30	-1.11	Eq. 4.4 & 4.7
Eu(III)/	-7.2	2.24	0.39	Eq. 4.5 & 4.7
Am(III)/Cm(III)	-15.1	-4.08	-6.33	
	-26.2	-12.96	-	
Th(IV) *	-6.0	2.32	-	Eq. 4.6
	-11.0	-2.53	-	
	-17.5	-8.84	-	

* There is no measured isotherm for Th.

5.1 Cobalt

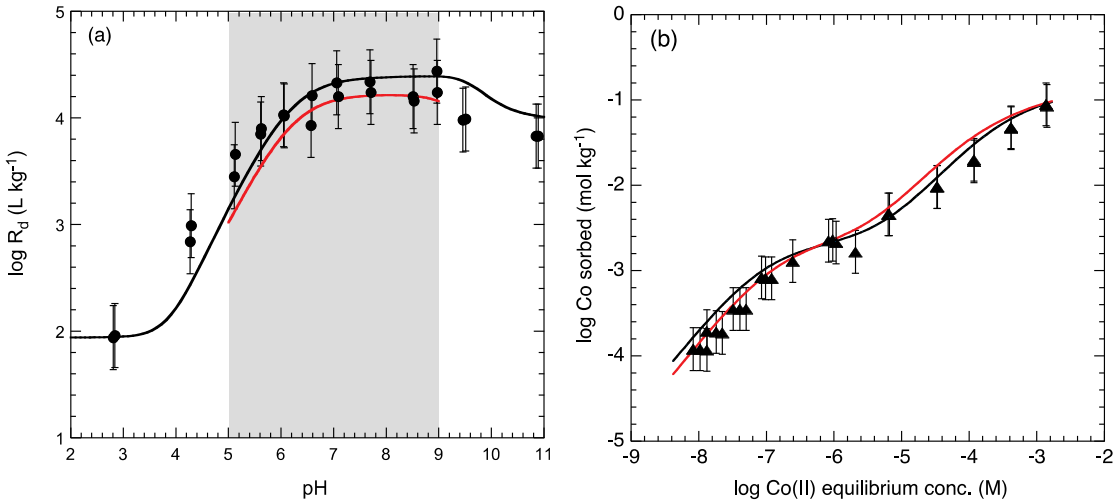

Fig. 5.1: Comparison of LFER calculations with model predictions for Co(II): (a) Measured sorption edge (Fig. 3.1) and (b) isotherm at pH = 7.1 (Fig. 3.12).

Experimental data (●, ▲) and modelled curves (—). Predicted curves in the pH range 5 to 9 (—) using the surface complexation constants given in Tab. 5.1.

5.2 Nickel

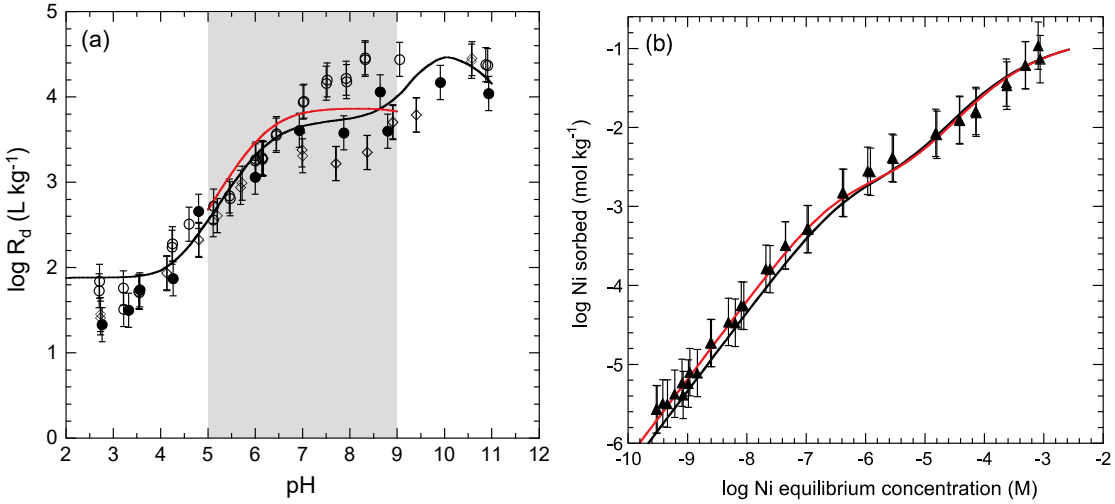

Fig. 5.2: Comparison of LFER calculations with model predictions for Ni(II): (a) Measured sorption edge (Fig. 3.2a) and (b) isotherm at pH = 7.0 (Fig. 3.13b).

Experimental data (●, ○, ▲) and modelled curves (—). Predicted curves in the pH range 5 to 9 (—) using the surface complexation constants given in Tab. 5.1.

5.3 Zinc

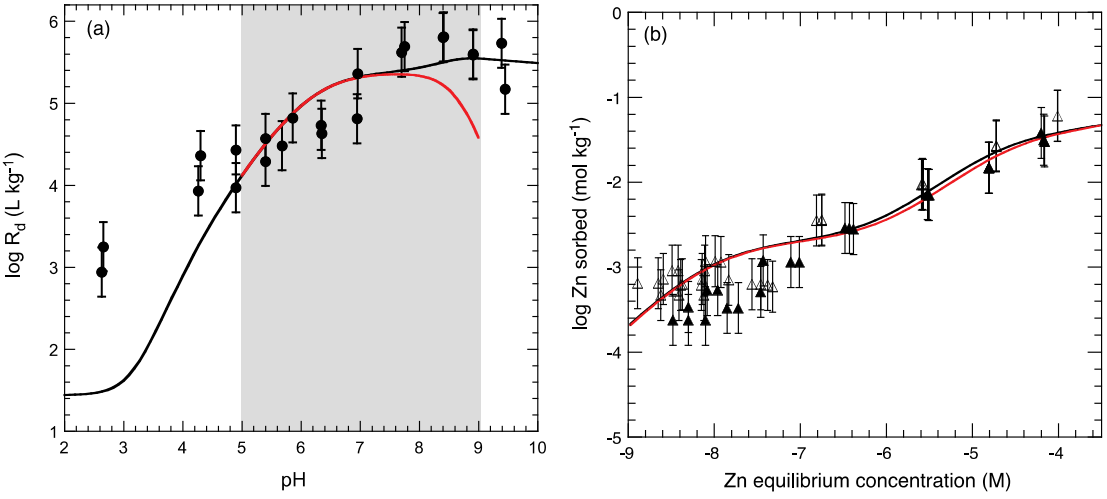

Fig. 5.3: Comparison of LFER calculations with model predictions for Zn(II): (a) Measured sorption edge (Fig. 3.3b) and (b) isotherm at pH = 7.2 (Fig. 3.14).

Experimental data (●, ▲, △) and modelled curves (—). Predicted curves in the pH range 5 to 9 (—) using the surface complexation constants given in Tab. 5.1.

5.4 Europium

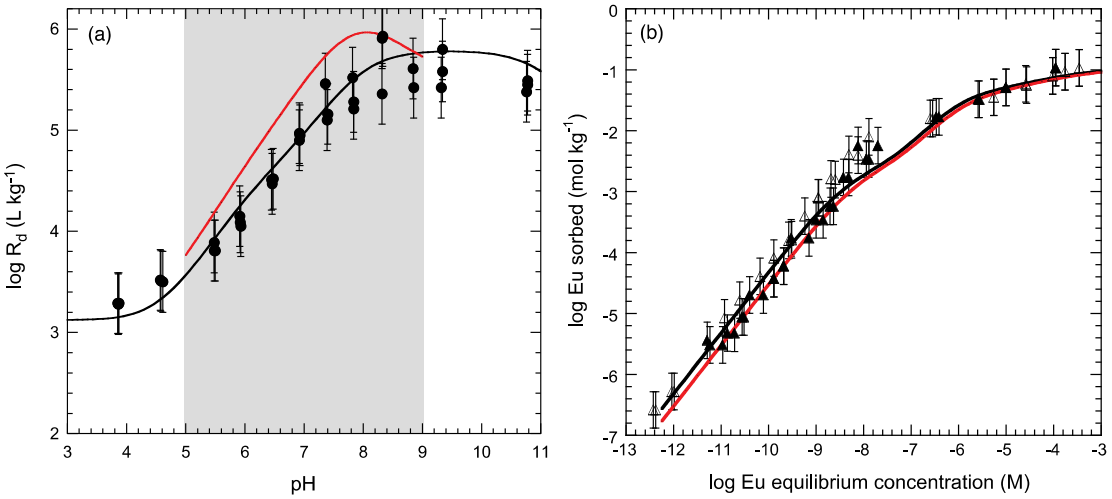

Fig. 5.4: Comparison of LFER calculations with model predictions for Eu(III): (a) Measured sorption edge (Fig. 3.4c) and (b) isotherm at pH 7.0 (Fig. 3.15b).

Experimental data (●, ▲, △) and modelled curves (—). Predicted curves in the pH range 5 to 9 (—) using the surface complexation constants given in Tab. 5.1.

5.5 Americium

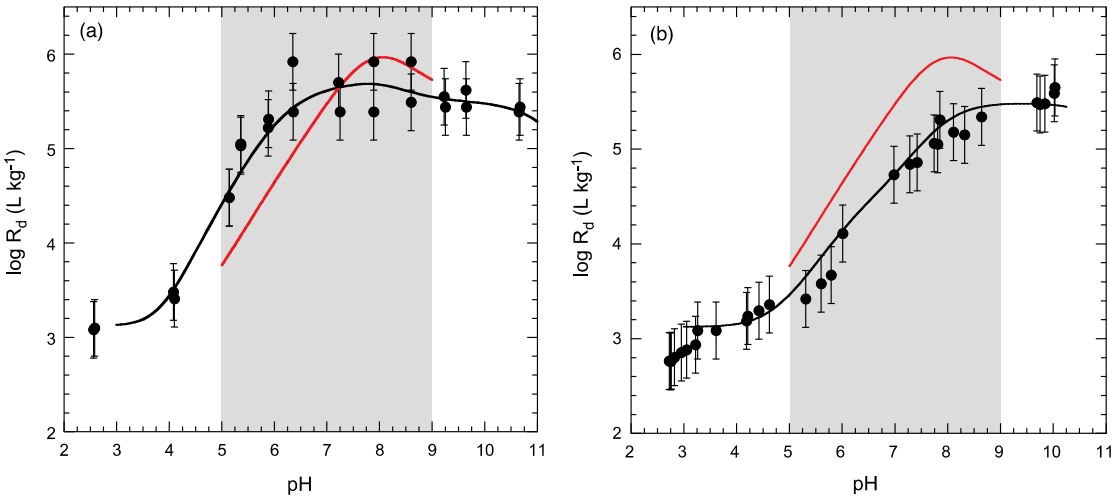

Fig. 5.5: Comparison of LFER calculations with model predictions for Am(III): Measured sorption edges (Fig. 3.5) from (a) Bradbury & Baeyens (2009b) and (b) Gorgeon (1994).

Experimental data (●) and modelled curves (—). Predicted curves in the pH range 5 to 9 (—) using the surface complexation constants given in Tab. 5.1.

5.6 Curium

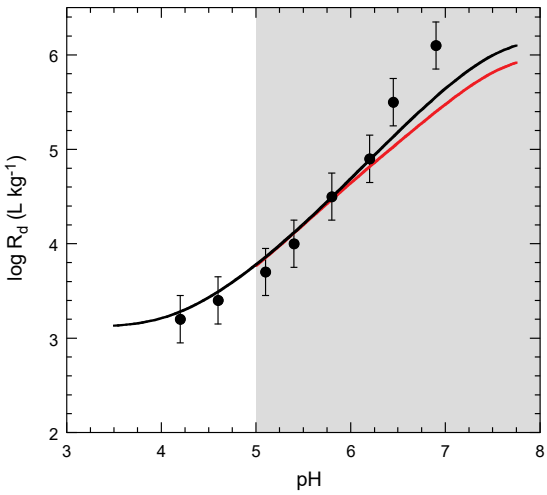

Fig. 5.6: Comparison of LFER calculations with model predictions for Cm(III).

Measured sorption edge (Fig. 3.6) (●) and modelled curve (—). Predicted curves in the pH range 5 to 9 (—) using the surface complexation constants given in Tab. 5.1.

5.7 Thorium

The prediction for Th(IV) using the LFER approach underestimates the sorption above pH 7. The dominating sorbing species here is $Th(OH)_4^0$ which, as stated previously, cannot be correlated with an aqueous hydrolysis Th(IV) complex because the $Th(OH)_5^-$ species apparently does not exist. Thus, it is not possible to read off a complexation constant for $\equiv SOTh(OH)_4^-$ from the LFER plot which means that its (important) contribution to the overall sorption cannot be included.

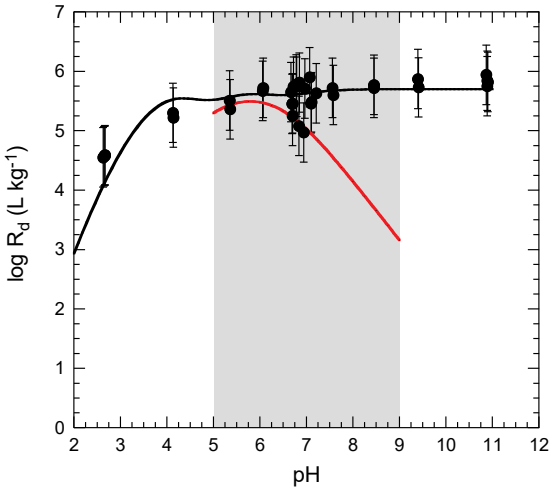

Fig. 5.7: Comparison of LFER calculations with model prediction for Th(IV).

Measured sorption edge (Fig. 3.8) (●) and modelled curve (—). Predicted curve in the pH range 5 to 9 (—) using the surface complexation constants given in Tab. 5.1.

These comparisons give an idea of the quality of the sorption values which would be predicted just using the surface complexation constants taken from LFERs. From all the graphs shown, it can be seen that all predictions based on the LFERs are within about ± 0.5 log units of the experimental data except Th(IV) where no correlating hydrolysis constant for the $\equiv S^sOTh(OH)_4^-$ surface complex is available.

The results of this exercise give an idea of the quality of the predictions of sorption values that might be predicted from LFERs in the case of metals for which no measurements are available and for which the appropriate LFERs exists (see Chapter 6).

6 Examples of modelling predictions of sorption edges and isotherms for metals for which no sorption data are available

6.1 General application of the thermodynamic sorption data base (TSDB)

The surface complexation reactions and constants derived from experimental measurements using the aqueous metal hydrolysis constants in Appendix B (bold type) are given in Appendix C (strong sites, bold type) and Appendix D (weak sites). The reactions and constants in bold type are those which essentially describe the sorption in the pH range 5 – 9 and are considered to be the values of choice for modelling. The reasons behind the preference for the data given in bold type were explained in section 4.2 (stability of the clay, the reliability of the hydrolysis constants and the pH range in natural systems).

Surface complexation constants should only be taken from LFERs in those cases where no other reliable data are available.

The suggested general methodology for using LFERs to calculate the sorption of metals for which no sorption data exist is to first select the best available aqueous hydrolysis data and calculate the speciation in a simple 1:1 background electrolyte at 0.1 M. The dominant aqueous hydroxyl species occurring in the pH window from 5 to 9 are considered to be the sorbing species. The surface complexation constants and their corresponding hydrolysis constants (for the appropriate LFER) can then be deduced using Eqs. 4.1 to 4.3 given in section 4.1.

6.2 Modelling predictions of sorption edges/isotherms for Mn(II), Fe(II), Cu(II), Pu(III), U(IV), Np(IV) and Pu(IV) from LFERs

The surface complexation constants derived from the LFERs (Eqs. 4.4 to 4.7) and used in the predictive calculations of edges/isotherms on illite in the pH range 5 to 9 are summarised in Tab. 6.1. For each element the dominant aqueous species in the pH range 5 to 9 are given together with the corresponding surface complex and the correlating hydrolysed species. The K_c values used are taken from Appendix E.

In the cases of the tetravalent actinides U, Np and Pu, only sorption edges are predicted because of solubility constraints.

In Fig. 6.1 the positions of the elements listed in Tab. 6.1 are illustrated on the LFER plots obtained for the di-, tri- and tetravalent elements in Chapter 5. In the case of Mn and Cu the estimated hydrolysis and surface complexation constants fall outside the range of the transition elements for which experimental data was available. For Pu(III) and the tetravalent actinides the surface complexations constants are lying on the LFERs.

The predicted sorption edge/isotherm curves are shown in Figs. 6.2 to 6.8, metal by metal.

Tab. 6.1: Surface complexation constants for the elements Mn(II), Fe(II), Cu(II), Pu(III), U(IV), Np(IV) and Pu(IV) taken from appropriate LFERs for strong and weak sites and the corresponding hydrolysis constants.

Element	**Aqueous species:** 5 < pH > 9	**Surface complex**	**Correlating aqueous species**	**log ^{OH}K**	**log ^{S}K**	**log ^{W1}K**	**LFER**
Mn(II)	Mn^{2+}	$\equiv SOMn^{+}$	$MnOH^{+}$	-10.59	-0.47	-2.5	Eqs. 4.4 & 4.7
Fe(II)	Fe^{2+}	$\equiv SOFe^{+}$	$FeOH^{+}$	-9.1	2.06	-1.23	Eqs. 4.4 & 4.7
	$FeOH^{+}$	$\equiv SOFeOH^{0}$	$Fe(OH)_2^{0}$	-20.6	-		No LFER
Cu(II)	Cu^{2+}	$\equiv SOCu^{+}$	$CuOH^{+}$	< -8	< 4.02	< -0.29	Eqs. 4.4 & 4.7
	$CuOH^{+}$	$\equiv SOCuOH^{0}$	$Cu(OH)_2^{0}$	(< -17.3)	-		No LFER
	$Cu(OH)_2^{0}$	$\equiv SOCu(OH)_2^{-}$	$Cu(OH)_3^{-}$	(< -27.8)	-		No LFER
Pu(III)	Pu^{3+}	$\equiv S^{S}OPu^{2+}$	$PuOH^{2+}$	-6.9	2.48	0.65	Eqs. 4.5 & 4.7
	$PuOH^{2+}$	$\equiv S^{S}OPuOH^{+}$	$Pu(OH)_2^{+}$	-14.8	-3.84	-6.07	Eqs. 4.5 & 4.7
	$Pu(OH)_2^{+}$	$\equiv S^{S}OPu(OH)_2^{0}$	$Pu(OH)_3^{0}$	-25.9	-12.72		Eq. 4.5
U(IV) *	$U(OH)_3^{+}$	$\equiv SOU(OH)_3^{0}$	$U(OH)_4^{0}$	-10	-1.56	-	Eq. 4.6
	$U(OH)_4^{0}$	$\equiv SOU(OH)_4^{-}$	$U(OH)_5^{-}$	no ^{OH}K	no ^{S}K		-
Np(IV) *	$Np(OH)_3^{+}$	$\equiv SONp(OH)_3^{0}$	$Np(OH)_4^{0}$	-8.3	0.09	-	Eq. 4.6
	$Np(OH)_4^{0}$	$\equiv SONp(OH)_4^{-}$	$Np(OH)_5^{-}$	no ^{OH}K	no ^{S}K		-
Pu(IV) *	$Pu(OH)_3^{+}$	$\equiv SOPu(OH)_3^{0}$	$Pu(OH)_4^{0}$	-9.3	-0.88	-	Eq. 4.6
	$Pu(OH)_4^{0}$	$\equiv SOPu(OH)_4^{-}$	$Pu(OH)_5^{-}$	no ^{OH}K	no ^{S}K		-

* Because of solubility limits in the pH range 5 to 9, isotherms for these metals are inappropriate.

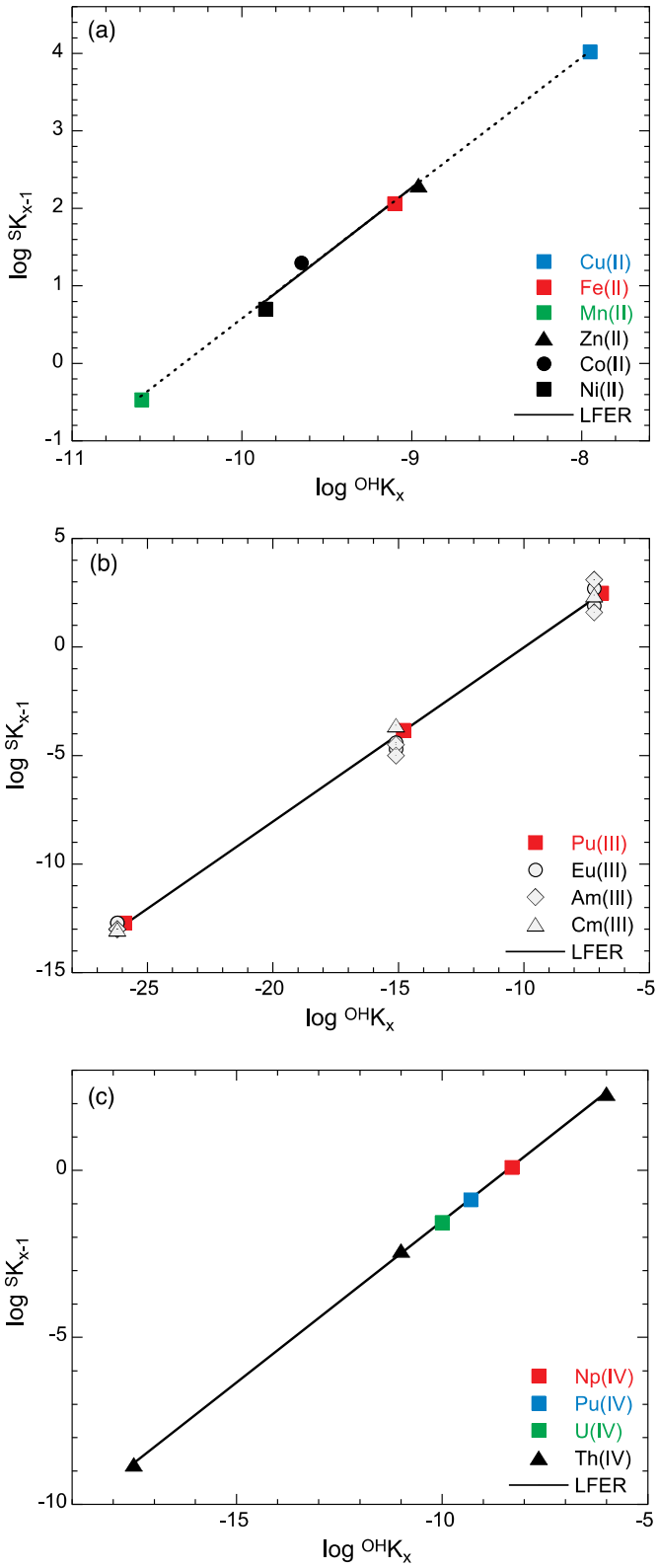

Fig. 6.1: Estimates of the surface complexation constants for (a) Mn(II), Fe(II) and Cu(II), (b) Pu(III) and (c) U(IV), Np(IV) and Pu(IV) on the strong sites of Na-IdP.

6.2.1 Mn(II)

Mn(II) is omnipresent in the porewater of natural systems and may, depending on the system, be of some importance as a metal which might compete for the available sorption sites with other transition metals. In view of this, it is recommended that for modelling purposes the surface complexation constants for Mn(II) are taken from the LFERs in Figs. 4.5 and 4.16 and which are given in Tab. 6.1. In the pH range from 5 to 9 the main sorbing species is taken to be Mn^{2+}, and the predicted sorption edge in this pH range and the isotherm at pH = 7, are given in Fig. 6.2.

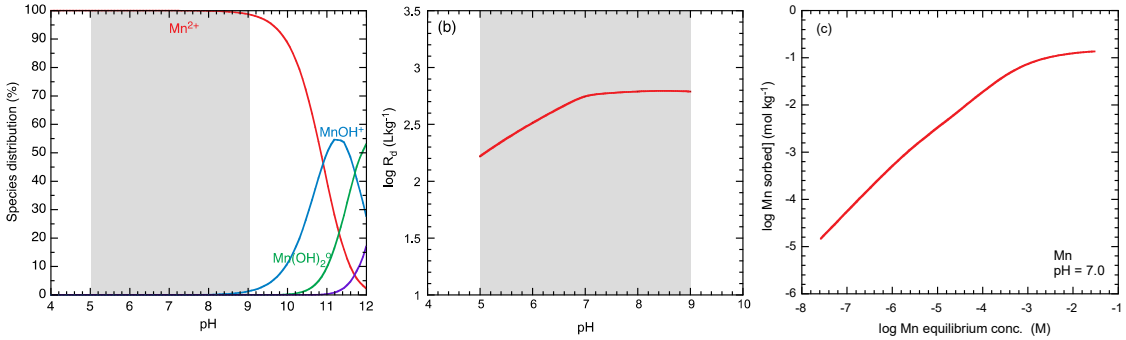

Fig. 6.2: (a) The aqueous speciation of Mn(II), (b) the sorption edge in the pH range 5 to 9 and (c) the sorption isotherm at pH = 7 on illite in 0.1 M $NaClO_4$ calculated using the surface complexation constants given in Tab. 6.1.

6.2.2 Fe(II)

Fe(II) is ubiquitous in almost all reducing argillaceous rock porewaters. Its importance lies in the fact that it is competitive for the sorption sites favoured by divalent transition metals.

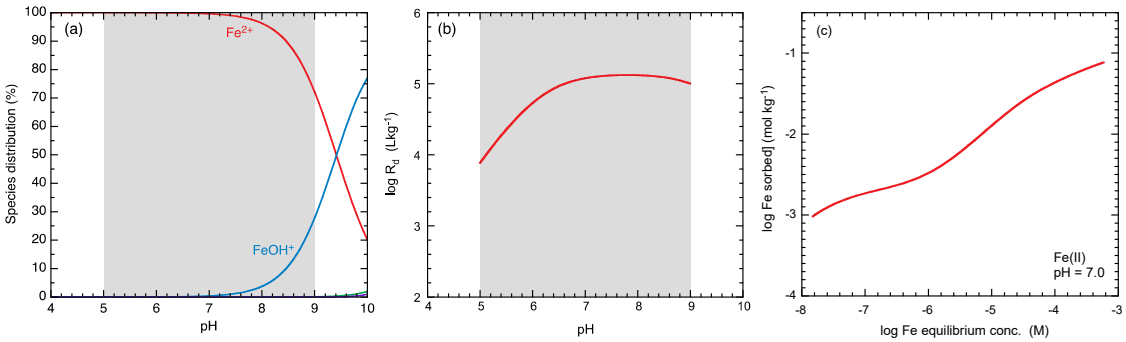

Fig. 6.3: (a) The aqueous speciation of Fe(II), (b) the sorption edge in the pH range 5 to 9 and (c) the sorption isotherm at pH = 7 on illite in 0.1 M $NaClO_4$ calculated using the surface complexation constants given in Tab. 6.1.

6.2.3 Cu(II)

According to the thermodynamic data given in Appendix B (Powell et al. 2007), Cu(II) is the most strongly hydrolysed of all the first and second row transition metals in the Periodic Table. In addition to Cu^{2+}, $CuOH^{+}$ and $Cu(OH)_2^0$ are also present as major, potentially sorbing species in the pH range 5 to 9. However, there is no appropriate LFER from which surface complexation

constants for these hydrolysed species can be obtained. Thus, on the basis of the information available, any predictions of the sorption of Cu(II) are restricted to the uptake of Cu^{2+}. Because of the very strong hydrolysis behaviour of Cu(II), the predicted surface complexation constant is very high, and lies well outside the range of the other transition metals (see Fig. 6.3). This in turn leads to exceedingly high predicted sorption values (Fig. 6.4b) and implies that the strong sites reach saturation already at Cu(II) equilibrium concentrations of ~ 10^{-9} M at pH = 7 (see Fig. 6.4c). Such predictions for the sorption behaviour of Cu(II), which are significantly at variance with the other transition metals, may well imply that they should be treated with some misgivings.

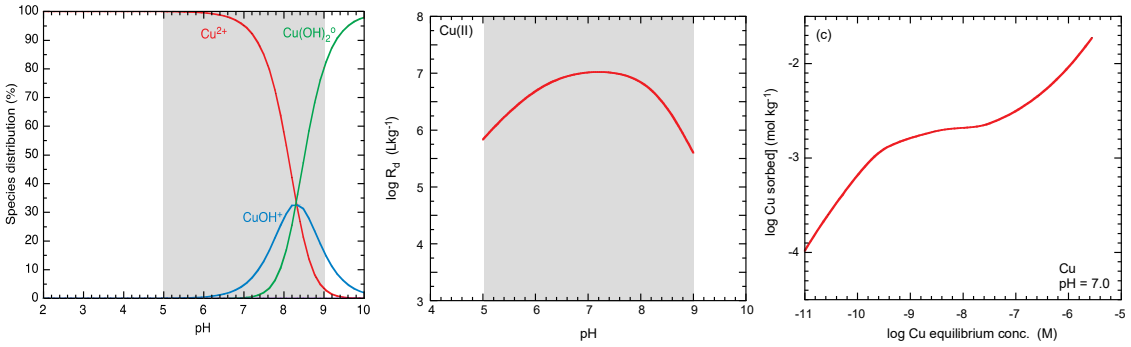

Fig. 6.4: (a) The aqueous speciation of Cu(II), (b) the sorption edge in the pH range 5 to 9 and (c) the sorption isotherm at pH = 7 on illite in 0.1 M $NaClO_4$ calculated using the surface complexation constants given in Tab. 6.1.

6.2.4 Pu(III)

According to Fig. 6.5a, the main sorbing species for Pu(III) in the pH range 5 to 9 are taken to be Pu^{3+}, $PuOH^{2+}$ and $Pu(OH)_2^{+}$. The predicted sorption edge and isotherm at pH = 7 are given in Fig. 6.5b and c.

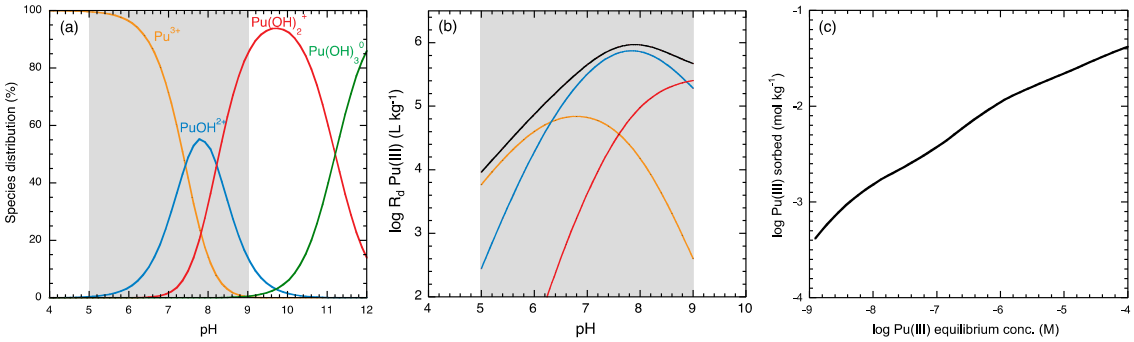

Fig. 6.5: (a) The aqueous speciation of Pu(III), (b) the sorption edge in the pH range 5 to 9 and (c) the sorption isotherm at pH = 7 on illite in 0.1 M $NaClO_4$ calculated using the surface complexation constants given in Tab. 6.1.

For lanthanides and the trivalent actinides (Ac, Cm) the same approach can be used to predict sorption edges and isotherms in the pH range 5 to 9.

6.2.5 Tetravalent actinides: U(IV), Np(IV) and Pu(IV)

For the approach described previously, it would be anticipated that the potentially dominant aqueous sorbing species for U(IV) in the pH range 5 to 9 are $U(OH)_3^+$ and $U(OH)_4^0$, and likewise for Np(IV), $Np(OH)_3^+$ and $Np(OH)_4^0$, and for Pu(IV); $Pu(OH)_3^+$ and $Pu(OH)_4^0$. The hydrolysis behaviours of U(IV), Np(IV) and Pu(IV) are somewhat stronger than for Th(IV), and the aqueous speciation profiles are also shifted. Because of this, the sorption of the neutral hydroxy species in the pH range 5 to 9 do not seem to play such an important role for these three tetravalent actinides as for Th(IV). The sorption is dominated by the uptake of the $An(OH)_3^+$ actinide aqueous species.

The predicted sorption edges are given in Figs. 6.6b, 6.7b and 6.8b for U(IV), Np(IV) and Pu(IV) respectively.

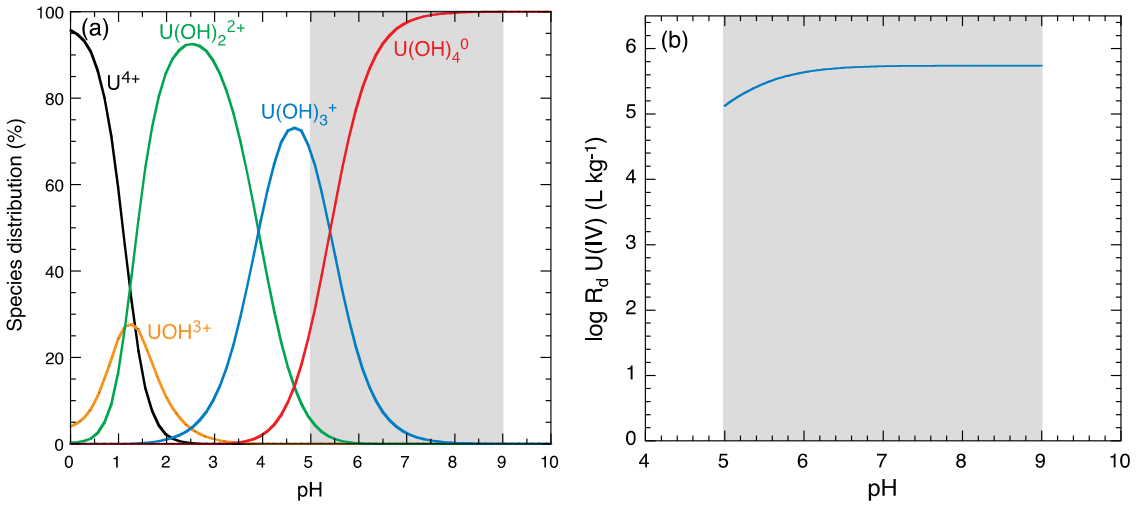

Fig. 6.6: (a) The aqueous speciation of U(IV), (b) the sorption edge in the pH range 5 to 9 on illite in 0.1 M $NaClO_4$ calculated using the surface complexation constants given in Tab. 6.1.

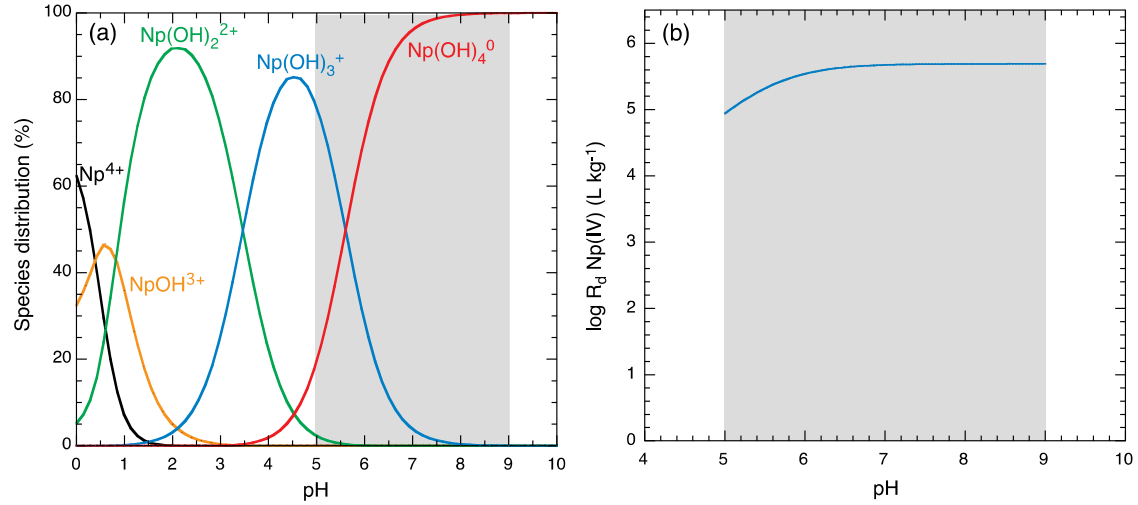

Fig. 6.7: (a) The aqueous speciation of Np(IV) and (b) the sorption edge in the pH range 5 to 9 on illite in 0.1 M $NaClO_4$ calculated using the surface complexation constants given in Tab. 6.1.

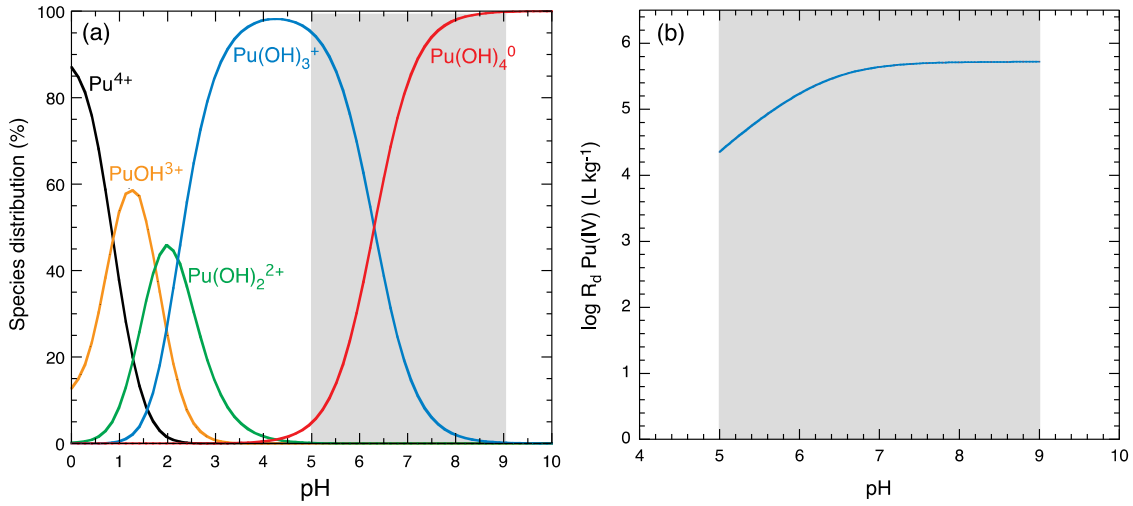

Fig. 6.8: (a) The aqueous speciation of Pu(IV) and (b) the sorption edge in the pH range 5 to 9 on illite in 0.1 M $NaClO_4$ calculated using the surface complexation constants given in Tab. 6.1.

6.3 Metals for which the LFER approach is not applicable

With reference to the list of safety relevant radionuclides (Nagra 2008) sorption parameters for the following metals Ag(I), Be(II), Pd(II), Tc(IV), Po(IV), Zr(IV), Nb(V) cannot be deduced from LFERs.

6.3.1 Ag(I)

Silver is a monovalent transition metal for which no LFER exists.

6.3.2 Be(II)

Beryllium is an alkaline earth metal. The speciation given in Fig. 6.9 shows that it hydrolyses more strongly than the metals included in the LFER given in Fig. 4.5. According to the approach described in section 4.1, $BeOH^+$ would be expected to be the main sorbing species in the pH range 5 to 9 and the corresponding surface complexation constant would be correlated with the hydrolysis constant for $Be(OH)_2^0$. An appropriate LFER is not available.

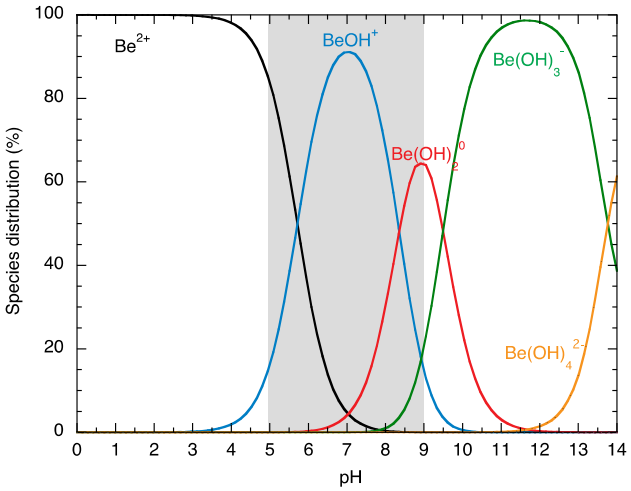

Fig. 6.9: The aqueous speciation of Be(II) in 0.1 M $NaClO_4$ at trace concentration.

6.3.3 Pd(II)

Although palladium is a divalent transition metal, the speciation plot given in Fig. 6.10 shows that it hydrolyses much more strongly than the metals included in the LFER given in Fig. 4.5. According to the approach described in section 4.1, $Pd(OH)_2^0$ would be expected to be the main sorbing species in the pH range 5 to 9 and the corresponding surface complexation constant would be correlated with the hydrolysis constant for $Pd(OH)_3^-$. Again, an appropriate LFER is not available.

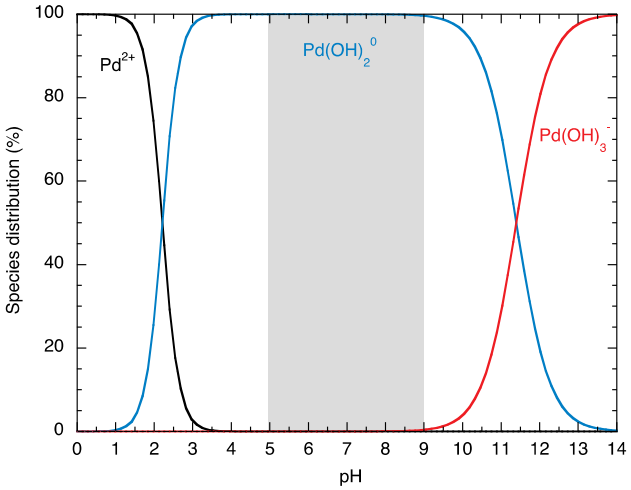

Fig. 6.10: The aqueous speciation of Pd(II) in 0.1 M $NaClO_4$ at trace concentration.

6.3.4 Tc(IV), Po(IV), Zr(IV)

For Tc(IV), Po(IV) and Zr(IV) the hydrolysis data are somewhat uncertain, or absent (Po(IV)), and, in any case, appropriate LFERs do not exist.

6.3.5 Nb(V)

Nb(V) forms predominantly oxy anions in solution and does not therefore fit into the LFER structure.

7 Comparisons between sorption values measured in complex Opalinus Clay/groundwater systems and sorption model predictions

It is clearly important to test the predictive capabilities of the 2SPNE SC/CE sorption model and the associated model parameters against experimental sorption measurements carried out under a variety of realistic chemical conditions. Sorption isotherms were determined for Co(II) and Ni(II), Eu(III), Th(IV), and U(VI) on Opalinus Clay (Figs. 7.1 to 7.5) in a variety of porewater compositions (see Appendix H, Tab. H2). These metals were chosen to be representative for divalent transition metals, lanthanides and trivalent metals, tetravalent actinides and hexavalent metals respectively. The main assumption was that the sorption on Opalinus Clay is controlled by the illite plus illite/smectite content. Illite/smectite was assumed to have the same sorption properties as illite. Any contributions due to other clay minerals present such as kaolinite (20 wt.-%) and chlorite (10 wt.-%), were not included.

The Opalinus Clay/ porewater systems studied are characterised by the data given in Appendix H and the parameters used in the 2SPNE SC/CE sorption model calculations can be found in Appendices A, C, D and E. The hydrolysis constants, Appendix B, the thermodynamic constants, Appendix J, and the PSI/Nagra 12/07 thermodynamic data base (Thoenen et al. 2014) were used in the predictive modelling. Aqueous activity coefficients were calculated using the Davies relation with a value of 0.3 for the C_D constant (Davies 1962).

The sorption isotherms for Co(II), Ni(II), Eu(III), Th(IV) and U(VI) for Opalinus Clay were calculated for illite and then scaled by the weight fraction of illite plus illite/smectite. In most cases the measurements and predictions cover over 4 orders of magnitude of the metal aqueous equilibrium concentration. There were no adjustable parameters in the sorption calculations.

For Co(II), only that part of the isotherm measured on Opalinus Clay above an equilibrium concentration of $> 10^{-6}$ M was available. The Co(II) isotherm shown in Fig. 7.1 is the re-interpreted data, presented in Figure 6 in Bradbury & Baeyens (2009a), taking into account the Co carrier concentration in the ^{60}Co tracer source (see section 3.2). The blind predicted curve, which includes contributions from both strong and weak sites, represents the measured data very well.

The sorption isotherm for Ni(II) on Opalinus Clay was measured under reducing conditions in the presence of 2.4×10^{-5} M Fe(II). The blind predictions, with and without Fe(II) competition, are shown in Fig. 7.2. The surface complexation constants for Fe(II) were taken from the LFERs in Figs. 4.5 and 4.16 (see Tab. 6.1). The sorption model (including Fe(II) competition) under-predicts the measured data at equilibrium concentrations $< 10^{-6}$ M by a factor of ~ 3, otherwise the agreement between model and measurements lies within the experimental error.

In the cases of Eu(III), Th(IV) and U(VI) shown in Figs. 7.3 to 7.5, respectively, the agreement between experiment (solid circles) and the blind predictive modelling (black curves) can be seen to be good to very good; the calculated values lie within the experimental error bars given.

On the basis of the modelling results presented here, the "bottom up" approach, used in conjunction with some simplifying assumptions, and the straightforward procedures described, may be regarded as a reliable method for quantitatively calculating radionuclide uptake in complex geochemical systems.

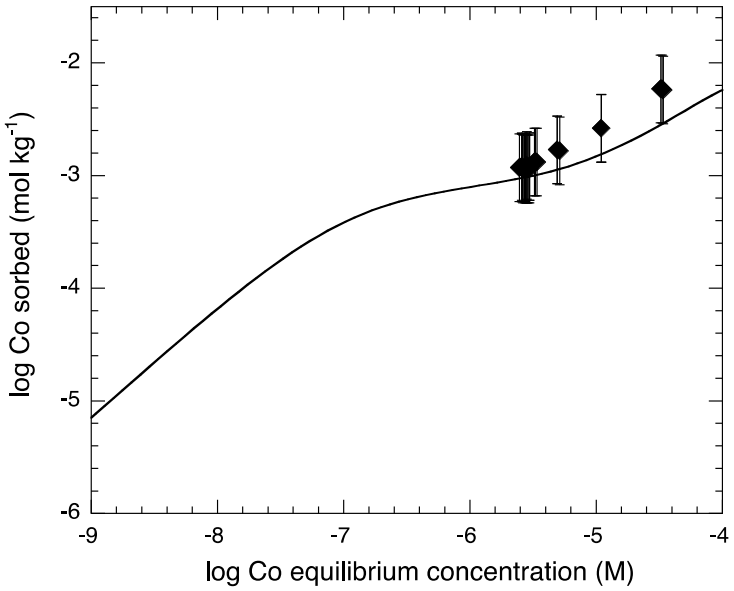

Fig. 7.1: Co(II) sorption isotherm on Opalinus Clay carried out under oxidising conditions: Appendix H2, Tab. H2, porewater c).

Experimental data (◆) (Bradbury & Baeyens 2011). The continuous line is the blind model prediction (*this study*).

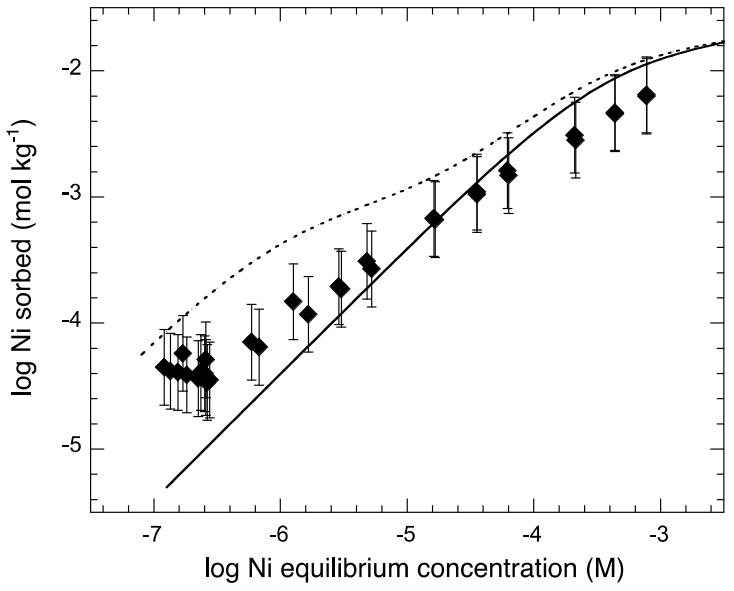

Fig. 7.2: Ni(II) sorption isotherm on Opalinus Clay carried out under reducing conditions (Appendix H2, Tab. H2, porewater (a)).

Experimental data (◆) (Bradbury & Baeyens 2011). The dotted line is the blind model prediction excluding sorption competition from Fe(II). The continuous line is the blind model prediction including sorption competition from Fe(II) at a concentration of 2.4×10^{-5} M (*this study*).

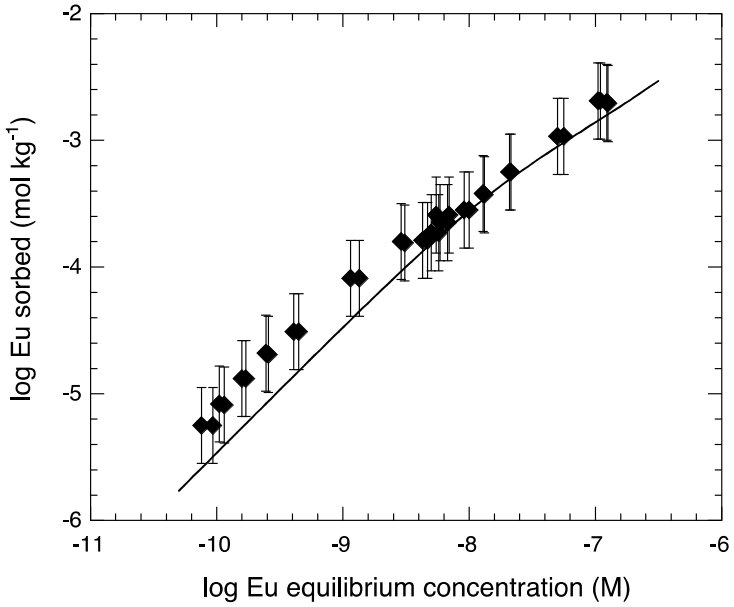

Fig. 7.3: Eu(III) sorption isotherm on Opalinus Clay carried out under reducing conditions (Appendix H2, Tab. H2, porewater (b)).

Experimental data (◆). The continuous line is the blind model prediction (Bradbury & Baeyens 2011).

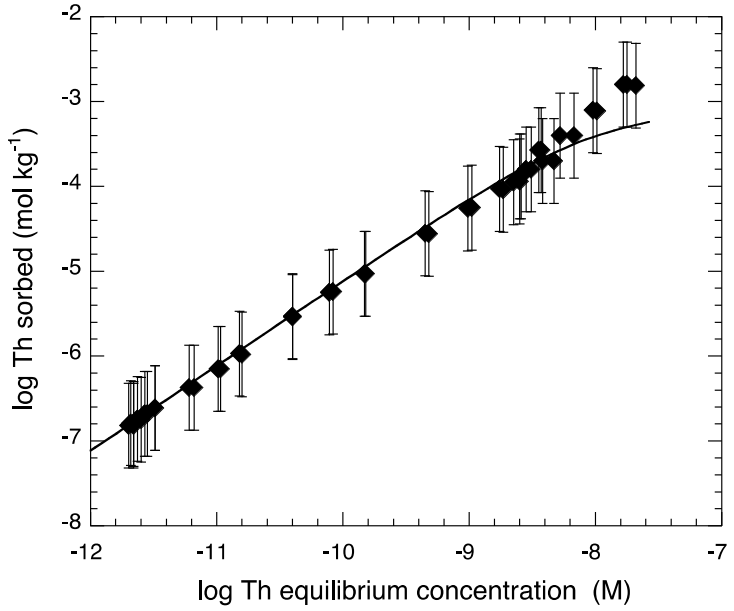

Fig. 7.4: Th(IV) sorption isotherm on Opalinus Clay carried out under reducing conditions; Appendix H2, Tab. H2, porewater b).

Experimental data (◆). The continuous line is the blind model prediction (Bradbury & Baeyens 2011).

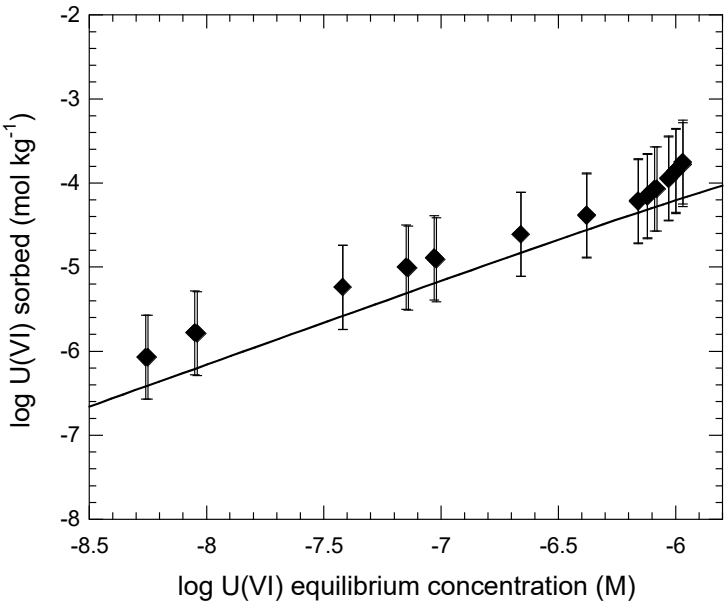

Fig. 7.5: U(VI) sorption isotherm on Opalinus Clay carried out under reducing conditions (Appendix H2, Tab. H2, porewater (b)).

Experimental data (◆) (Bradbury & Baeyens 2011). The continuous line is the blind model prediction using the U(VI) aqueous speciation data in Appendix J (Tab. J1) (*this study*).

8 Generalised Cs sorption model and modelling the uptake of Cs in complex argillaceous rock/groundwater systems

8.1 Generalised Cs sorption model

The 'Generalised Caesium Sorption' (GCS) model, summarised here, is taken from the work of Bradbury & Baeyens (2000) where a much more detailed description can be found. The uptake of Cs on Na-illite is envisaged as taking place on three site types each having different site capacities and affinities. These are denoted as frayed edge sites (FES), type II and planar sites (PS). The relations between these site capacities are expressed in Appendix G (Tab. G1) as fixed percentages of the illite CEC. An integral assumption in the model concept is that the relationships between the three different sites are valid for all illites irrespective of their origin.

Selectivity coefficients for Cs and the main competing cations (K, Rb and NH_4) were deduced from literature sorption measurements on illites from different sources according to their measured CEC values, background electrolyte concentrations and the site type distributions. A set of "reference selectivity coefficients" are presented in Appendix G (Tab. G2) which are considered to be generally valid for all illite clay minerals and are accordingly non-adjustable model parameters. CEC values, site capacities and measured sorption data may be illite type dependent, but the K_c values are not.

In illite and argillaceous rock systems at Cs equilibrium concentrations $< 10^{-3}$ M, only the Cs uptake on FES and type II sites is important. The nature of these sites is such that they are predominantly accessible only to cations with low hydration energies (K, Rb, NH_4) and these cations compete the most effectively with Cs. Na may also compete, but only when the concentration is many orders of magnitude greater than that of Cs and/or K, Rb, or NH_4. Divalent cations such as Mg, Ca and Sr, with relatively large hydration energies, are effectively non-competitive for steric reasons.

FES exhibit the strongest affinity for Cs and are the main sorbing sites at concentrations $< 10^{-9}$ M where the sorption is linear. In the concentration range up to ~ 10^{-4} M, type II sites dominate, and the sorption is non-linear. Non-linear sorption behaviour extends to even higher concentrations due to contributions from the planar sites and site saturation effects.

8.2 Modelling Cs sorption in argillaceous rock systems

In order to apply the GCS model to argillaceous rock systems, the CEC of the illite (illite/ smectite is assumed to be the same) fraction must be known, since one of the main model concepts is that the illite (plus illite/smectite) component is solely responsible for the uptake of Cs. To achieve this in a consistent manner, a "reference illite" with a CEC of 0.20 eq. kg^{-1} was defined (Grim 1953) and was used together with the illite (plus illite/smectite) content of any argillaceous rock to yield the CEC due to the illite (plus illite/smectite) fraction.

Calculations of Cs sorption in argillaceous rock systems require the water chemistry to be known, especially the concentrations of Cs itself and the competing cations K, Rb and NH_4. The concentrations of the major cations should also be known but, for the reasons given above, they are not particularly competitive with Cs on the FES and type II sites. Also, the mineralogy of the rock is required, or, more specifically, the illite (plus illite/smectite mixed layer) clay mineral content.

With all model parameters fixed (e.g. Appendix G), the computer code MINSORB (Bradbury & Baeyens 1997) was used to calculate the Cs sorption in a given argillaceous rock system for the derived CEC of the illite plus illite/smectite mixed layer fraction.

The Cs isotherms calculated for Opalinus Clay (see Appendices G and I), Boom Clay, Oxfordian Clay and Palfris Marl (details given in Bradbury & Baeyens 2000) are shown below (Figs. 8.1 to 8.4).

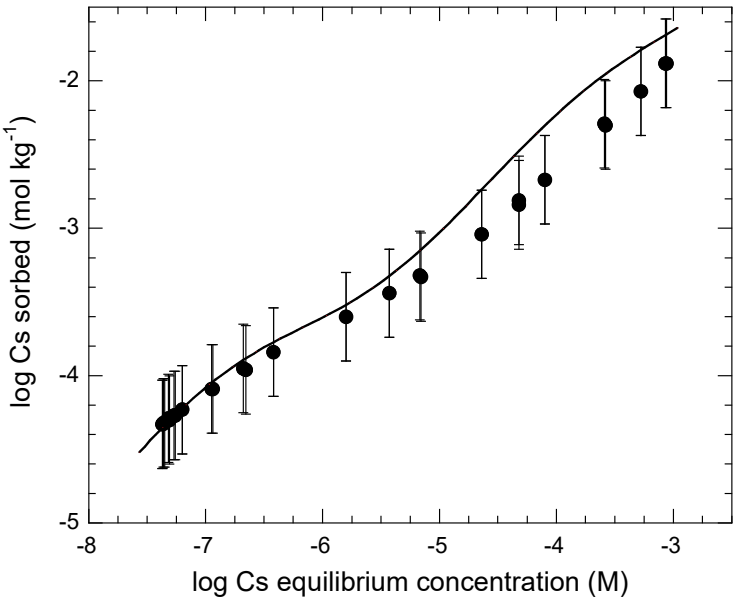

Fig. 8.1: Cs sorption isotherm measured on Opalinus Clay samples (Lauber et al. 2000).

The continuous lines were calculated using parameters for illite (see Tabs. G1 and G2), and the mineralogical and water compositions for Opalinus Clay are given in Tabs. J1 and J2, respectively.

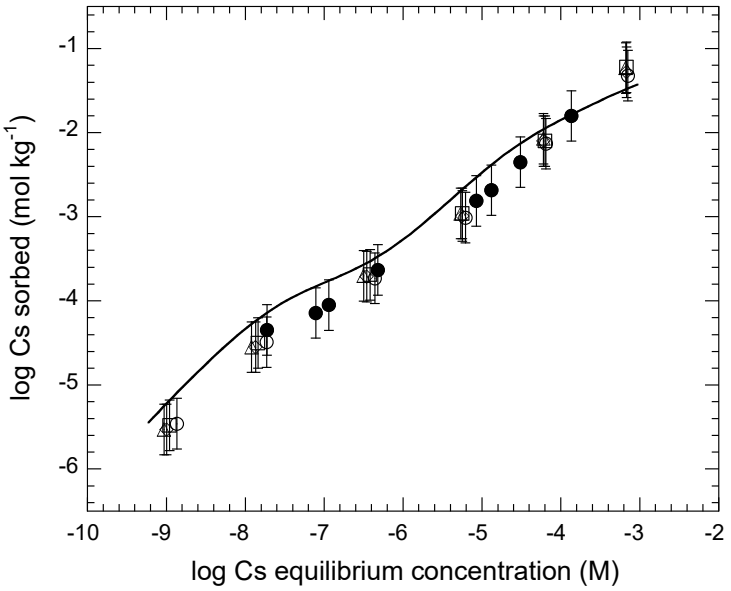

Fig. 8.2: Cs sorption isotherm measured on Boom Clay samples.

Filled circles: De Preter et al. (1991). The different sets of open symbols represent sorption data measured on different samples (Baeyens 1982). The continuous line was calculated using parameters for illite (see Tabs. G1 and G2), and the mineralogical and water compositions for Boom Clay are given in Tabs. J1 and J2, respectively.

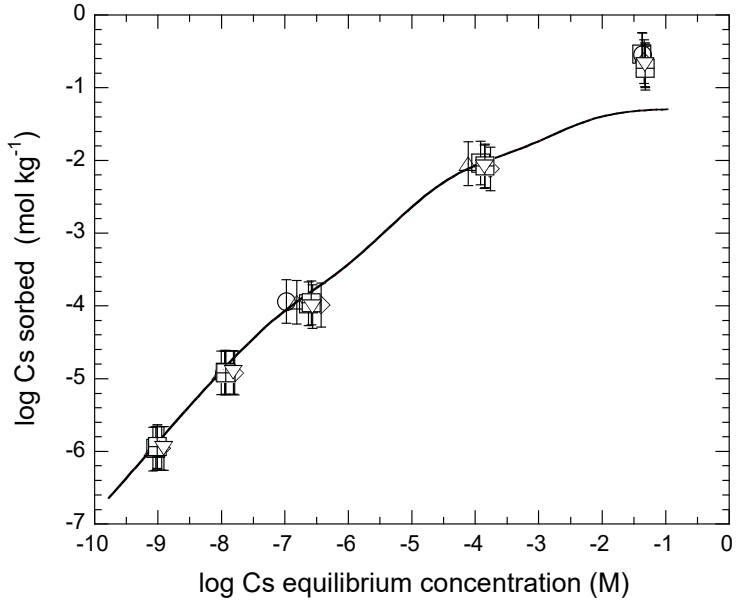

Fig. 8.3: Cs sorption isotherm measured on Oxford Clay samples (McKinley & West 1982).

The different sets of symbols represent sorption data measured on different samples The continuous line was calculated using parameters for illite (see Tab. G1 and G2), and the mineralogical and water compositions for Opalinus Clay are given in Tabs. J1 and J2, respectively.

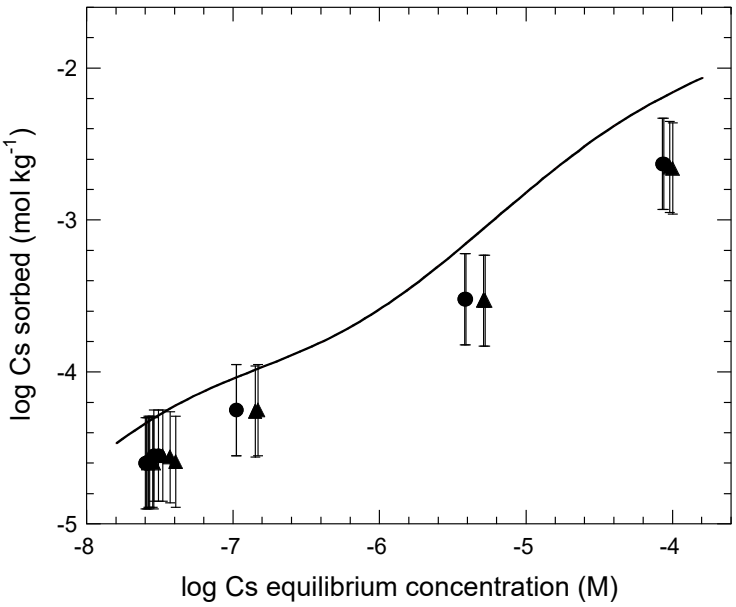

Fig. 8.4: Cs sorption isotherm measured on Palfris Marl samples (Aksoyoglu et al. 1991).

The continuous line was calculated using parameters for illite (see Tabs. G1 and G2), and the mineralogical and water compositions for Opalinus Clay are given in Tabs. J1 and J2, respectively.

9 Summary

The compiled data sets constitute the core of a Thermodynamic Sorption Data Base (TSDB) for illite which can be used to calculate sorption values in argillaceous rocks in which illite plus illite/smectite clay minerals constitute the major sorbing phases. Sorption edge/isotherm measurements on illite for Co(II), Ni(II), Zn(II), Eu(III), Am(III), Cm(III), Sn(IV), Th(IV), Np(V), Pa(V), U(VI), from predominantly "in house" investigations, have been summarised in Chapter 3. These data were modelled with the 2SPNE SC/CE sorption model using the fixed model parameters in Appendix A and the metal hydrolysis constants selected in Appendix B. The surface complexation reactions and derived constants for strong and weak sites are tabulated in Appendices C and D respectively. The cation exchange selectivity coefficients (K_c values) are listed separately in Appendix E.

Blind predictions of sorption values have been compared with the measured ones in a number of cases described in Chapter 6, for illite in simple 1:1 electrolytes, and in Chapter 8 for chemically realistic Opalinus Clay systems. In general, the correspondences have been good to very good. Within the framework given, this should provide confidence in using the data in the Thermodynamic Sorption Data Base for the predictive modelling of sorption.

Surface complexation constants can only be calculated from theoretical considerations with extreme difficulty. Therefore, a means was sought to allow estimates to be made for these constants for metals where the data are either very poor or non-existent and which would then allow sorption values to be calculated. Good systematic linear correlations between the logarithms of the surface site binding constants on the strong and weak sites and the logarithm of the corresponding aqueous hydrolysis constants were found, so called Linear Free Energy Relationships (LFERs). Separate LFERs have been constructed for bivalent transition metals, lanthanides and trivalent actinides for strong and weak sites and tetravalent actinides for strong sites valid in the pH range 5 to 9. However, the LFERs should be used judiciously. Sometimes they are based on (very) limited data sets and there are restrictions in their use. These issues are discussed fully in Chapter 4. LFERs are seen as being complimentary to the TSDB.

The suggested general methodology for estimating surface complexation constants from LFERs is to first select the best available aqueous hydrolysis data for the metal in question, and then to calculate the speciation in a simple 1:1 background electrolyte at 0.1 M. The dominant aqueous hydroxyl species occurring in the pH window from 5 to 9 are considered to be the main sorbing species. Surface complexation constants can then be deduced from the corresponding hydrolysis constants (for the appropriate LFER) using Eqs. 4.1 to 4.3 given in section 4.1. Surface complexation constants have been taken for specific metals from the appropriate LFERs and the sorption edges/isotherms calculated with these values compared with the measured ones. In general, all of the predictions based on the LFERs were within about ± 0.5 log units of the experimental data except Th(IV). The results of this exercise give an idea of the quality of the predictions of sorption values that might be predicted from LFERs.

Sorption edges/isotherms have been predicted for Mn(II), Fe(II), Cu(II), Pu(III), U(IV), Np(IV) and Pu(IV) in simple 1:1 electrolytes and are illustrated, together with the corresponding aqueous speciations, in Chapter 6 (Figs. 6.2, 6.3, 6.4, 6.5, 6.6, 6.7 and 6.8, respectively). Clearly, the quality of these predictions, and therefore the validity of the approach, can only be decided when experimental data are available.

With reference to the list of safety-relevant radionuclides (Nagra 2008), sorption data for the following metals Ag(I), Be(II), Pd(II), Tc(IV), Po(IV), Zr(IV), Nb(V) do not exist and the necessary sorption parameters cannot be derived mainly because the appropriate LFERs do not exist.

Finally, a separate cation exchange based Generalised Cs Sorption Model for argillaceous rocks based on Cs uptake on illite has been presented. Blind predictions with the model were very successful in reproducing Cs sorption isotherms measured on Boom Clay, Oxford Clay, Palfris Marl and Opalinus Clay.

The overall conclusion of this work is that a Thermodynamic Sorption Data Base has been developed which is justifiably capable of being used to calculate the sorption of many safety-relevant radionuclides in safety assessment studies for the disposal of radioactive waste in argillaceous host rock formations.

Acknowledgements

We would like to express our gratitude to Dr. V. Brendler (Helmholtz-Zentrum Dresden Rossendorf, Germany) and Dr. J. Mibus (Nagra) for reviewing the manuscript. The final layout of the report was carried out by B. Gschwend. Partial financial support was provided by Nagra.

10 References

Aksoyoglu, S., Cornell, R.M., Haselbeck, S., Mantovani, M., Bleidissel, K. & Dierickx, A. (1991): Marl programme progress report: Sorption of cesium. Paul Scherrer Institut, TM-43-90-53.

Andra (2001): Référentiel géologique du site de Meuse/Haute Marne. Andra Rapp. ADS 99-005. L'Agence nationale pour la gestion des déchets radioactifs Andra, Châtenay-Malabry, France.

Aoki, K. (2002): Recent activities at underground research laboratories in Japan. Proc. Internat. Symp. NUCEF 2001, Japan Atomic Energy Research Institute, JAERI-Conf. 2002-04, 361-362.

Baes, C.F. & Mesmer, R.E. (1976): The hydrolysis of cations. Wiley, New York.

Baeyens, B. (1982): Strontium, caesium and europium retention in Boom Clay: A potential repository site for nuclear waste. Ph.D. Thesis, Univ. Leuven, Belgium.

Baeyens, B. & Bradbury, M.H. (1995a): A quantitative mechanistic description of Ni, Zn and Ca sorption on Na-montmorillonite. Part I: Physico-chemical characterisation and titration measurements. PSI Bericht Nr. 95-10 and Nagra Tech. Report NTB 95-04.

Baeyens, B. & Bradbury, M.H. (1995b): A quantitative mechanistic description of Ni, Zn and Ca sorption on Na-montmorillonite. Part II: Sorption measurements. PSI Bericht Nr. 95-11 and Nagra Tech. Report NTB 95-05.

Baeyens, B. & Bradbury, M.H. (1997): A mechanistic description of Ni and Zn sorption on Na-montmorillonite. Part I: Titration and sorption measurements. J. Contam. Hydrol. 27, 199-222.

Baeyens, B. & Bradbury, M.H. (2004): Cation exchange capacity measurements on illite using the sodium and cesium isotope dilution technique: Effects of the index cation, electrolyte concentration and competition: Modelling. Clays and Clay Minerals 52/4, 421-431.

Baeyens, B. & Bradbury, M.H. (2017): The development of a Thermodynamic Sorption Data Base for montmorillonite and the application to bentonite. PSI Bericht Nr. 17-05 and Nagra Tech. Report NTB 17-13.

Bonin, J. (1998): Deep geological disposal in argillaceous formations: Studies at the Tournemire test site. J. Contam. Hydrol. 35, 315-330.

Bradbury, M.H. & Baeyens, B. (1997): A mechanistic description of Ni and Zn sorption on Na-montmorillonite. Part II: Modelling. J. Contam. Hydrol. 27, 223-248.

Bradbury, M.H. & Baeyens, B. (1999): Modelling the sorption of Zn and Ni on Ca-montmorillonite. Geochim. Cosmochim. Acta 63, 325-336.

Bradbury, M.H. & Baeyens, B. (2000): A generalised sorption model for the concentration dependent uptake of Cs by argillaceous rock. J. Contam. Hydrol. 42, 141-163.

Bradbury, M.H. & Baeyens, B. (2002): Sorption of Eu on Na- and Ca-montmorillonites: Experimental investigations and modelling with cation exchange and surface complexation. Geochim. Cosmochim. Acta 66, 2325-2334.

Bradbury, M.H. & Baeyens, B. (2005a): Experimental and modelling investigations on Na-illite: Acid base behaviour and the sorption of strontium, nickel, europium and uranyl. PSI Bericht Nr. 05-02 and Nagra Tech. Report NTB 04-02.

Bradbury, M.H. & Baeyens, B. (2005b): Modelling the sorption of Mn(II), Co(II), Ni(II), Cd(II), Eu(III), Am(III), Sn(IV), Th(IV), Np(V) and U(VI) on montmorillonite: Linear free energy relationships and predictions of surface binding constants for some selected heavy metals and actinides. Geochim. Cosmochim. Acta 69, 875-892.

Bradbury, M.H. & Baeyens, B. (2006): A quasi-mechanistic non-electrostatic modelling approach to metal sorption on clay minerals. *In:* Lützenkirchen, J. (ed.): Surface complexation modelling. Elsevier Ltd., 518-538.

Bradbury, M.H. & Baeyens, B. (2009a): Sorption modelling on illite. Part I: Titration measurements and the sorption of Ni, Co, Eu and Sn. Geochim. Cosmochim. Acta 73, 990-1003.

Bradbury, M.H. & Baeyens, B. (2009b). Sorption modelling on illite. Part II: Actinide sorption and linear free energy relationships. Geochim. Cosmochim. Acta 73, 1004-1013.

Bradbury, M.H. & Baeyens, B. (2011): Predictive sorption modelling of Ni(II), Co(II), Eu(III), Th(IV) and U(VI) on MX-80 bentonite and Opalinus Clay: A "bottom-up" approach. Appl. Clay Sci. 52, 27-33.

Bradbury, M.H., Marques Fernandes, M. & Baeyens, B. (2017): Estimates of the influence of radionuclide solubility limits and sorption competition on the sorption values in the SDBs of MX-80 bentonite and Opalinus Clay. PSI Bericht Nr. 17-04 and Nagra Tech. Report NTB 17-11.

Brown, P.L., Curti, E. & Grambow, B. (2005): Chemical thermodynamics of zirconium. Chemical Thermodynamics, Vol. 8. OECD Nuclear Energy Agency Data Bank, Eds., North Holland Elsevier Science Publishers B.V., Amsterdam, The Netherlands.

Chapman, N.B. & Shorter, J. (1972): Advances in linear free energy relationships. Plenum Press, London.

De Preter, P., Van Loon, L., Maes, A. & Cremers, A. (1991): Solid/liquid distribution of radiocesium in Boom clay. A quantitative interpretation. Radiochim. Acta 52/53, 299-302.

Davies, C.W. (1962): Ion association. Butterworths, London.

Gabis, V. (1958): Etude préliminaire des argiles oligocènes du Puy-en-Velay (Haute Loire). Bull. Soc. Mineral. Cristallog. 81, 183-185.

Gorgeon, L. (1994): Contribution à la modélisation physico-chimique de la retention de radioéléments à vie longue par des materiaux argileux. Unpubl. PhD Thesis. Université Paris 6.

Grenthe, I., Fuger, J., Konings, R.J., Lemire, R.J., Muller, A.B., Nguyen-Trung, C. & Wanner, H. (1992): Chemical thermodynamics of uranium. Chemical Thermodynamics 1. OECD Nuclear Energy Agency Data Bank, Eds., North Holland Elsevier Science Publishers B.V., Amsterdam, The Netherlands.

Griffault, L., Merceron, T., Mossman, J.R., Neerdael, B., De Canniere, P., Beaucaire, C., Daumas, S., Bianchi, A. & Christen, R. (1996): Acquisition et régulation de la chimie des eaux en milieu argileux pour le projet de stockage de déchets radioactifs en formation géologique. Projet Archimède argile. Rapport final EUR 17454.

Grim, R.E. (1953): Clay mineralogy. Mc Graw-Hill, New York.

Guillaumont, R., Fanghänel, T., Fuger, J., Grenthe, I., Neck, V., Palmer, D.A. & Rand, M.H. (2003): Update on the chemical thermodynamics of uranium, neptunium, plutonium, americium and technetium. Chemical Thermodynamics 5. OECD Nuclear Energy Agency Data Bank, Eds., North Holland Elsevier Science Publishers B.V., Amsterdam, The Netherlands.

Hammett, L.P. (1940): Physical organic chemistry. McGraw-Hill, New York.

Hummel, W., Berner, U., Curti, E., Pearson, F.J., & Thoenen, T. (2002): Nagra / PSI Chemical Thermodynamic Data Base 01/01. Nagra Tech. Report NTB 02-16 and Universal Publishers/uPublish.com, Parkland, Florida, USA.

Larsson, E. (1934): Die Dissoziationskonstanten von Aminium- und Silberdiaminionen und ein Zusammenhang zwischen ihnen. Z. Phys. Chem. A 169, 207-223.

Lauber, M., Baeyens, B. & Bradbury, M.H. (2000): Physico-chemical characterisation and sorption measurements of Cs, Sr, Ni, Eu, Th, Sn and Se on Opalinus Clay from Mont Terri. PSI Bericht Nr. 00-10 and Nagra Tech. Report NTB 00-11.

Lázár, K. & Máthé, Z. (2012): Claystone as a potential host rock for nuclear waste storage. *In*: Valaškova, M. & Martynkova, G.S. (eds.): Clay minerals in nature – Their characterization, modification and application. Rijeka, Croatia, INTECH Open Access Publisher, 55-80.

Lemire, R., Fuger, J., Nitsche, H., Potter, P., Rand, M., Rydberg, J., Spahiu, K., Sullivan, J., Ullman, W. & Vitorge, P. (2001): Chemical thermodynamics of neptunium and plutonium. Chemical Thermodynamics 4. OECD Nuclear Energy Agency Data Bank, Eds., North Holland Elsevier Science Publishers B.V., Amsterdam, The Netherlands.

Lemire, R., Berner, U., Musikas, C., Palmer, D., Taylor, P. & Tochiyama, O. (2013): Chemical thermodynamics of iron. Part 1. Chemical Thermodynamics 13a. OECD Nuclear Energy Agency Data Bank, Eds., OECD Publications, Paris, France.

Marques Fernandes, M., Baeyens, B., Dähn, R., Scheinost, A.C. & Bradbury, M.H. (2012): U(VI) sorption on montmorillonite in the absence and presence of carbonate: A macroscopic and microscopic study. Geochim. Cosmochim. Acta 93, 267-277.

Marques Fernandes, M., Ver, N. & Baeyens, B. (2015): Predicting the uptake of Cs, Co, Ni, Eu, Th and U on argillaceous rocks using sorption models for illite. Appl. Geochem. 59, 189-199.

Marques Fernandes, M., Scheinost, A. & Baeyens B. (2016): Sorption of trivalent lanthanides and actinides onto montmorillonite: Macroscopic, thermodynamic and structural evidence for ternary hydroxo and carbonato surface complexes on multiple sorption sites. Water Research 99, 74-82.

McKinley, I.G. & West, J.M. (1982): Sorption/desorption properties of argillaceous strata from boreholes at Harwell. Environmental Protection Unit. ENPU 82-6.

Montoya, V., Baeyens, B., Glaus, M.A., Kupcika, T., Marques Fernandes, M., Van Laer, L.M., Bruggeman, C., Maes, N. & Schäfer, T. (2018): Sorption of Sr, Co and Zn on illite: Batch experiments and modelling including Co in-diffusion measurements on compacted samples. Geochim. Cosmochim Acta 223, 1-20.

Nagra (2002): Project Opalinus Clay – Safety Report. Demonstration of disposal feasibility for spent fuel, vitrified high-level waste and long-lived intermediate-level waste (Entsorgungsnachweis). Nagra Tech. Report NTB 02-05.

Nagra (2008): Vorschlag geologischer Standortgebiete für das SMA- und das HAA-Lager: Begründung der Abfallzuteilung, der Barrierensysteme und der Anforderungen an die Geologie (Bericht zur Sicherheit und technischen Machbarkeit). Nagra Tech. Report NTB 08-05.

Neck, V. & Kim, J.I. (2001): Solubility and hydrolysis of tetravalent actinides. Radiochim. Acta 89, 1.

NEA (1992): Radionuclide sorption from the safety evaluation perspective. Proc. NEA workshop, October 16-18, 1991, Interlaken, Switzerland. OECD Publications, Paris, France.

NEA (2001): Using thermodynamic sorption models for guiding radioelement distribution coefficient (Kd) investigations. OECD Publications, Paris, France.

NEA (2005): NEA Sorption Project Phase II: Interpretation and prediction of radionuclide sorption onto substrates relevant for radioactive waste disposal using thermodynamic sorption models. OECD/NEA, Paris.

Ondraf (2001): SAFIR 2: Safety assessment and feasibility interim report 2. NIROND-2001-06 E. Ondraf, Brussels.

Poinssot, C., Baeyens, B. & Bradbury, M.H. (1999): Experimental studies of Cs, Sr, Ni and Eu sorption on Na-illite and the modelling of Cs sorption. PSI Bericht Nr. 99-06, Paul Scherrer Institut and Nagra Tech. Report NTB 99-04.

Powell, K.J., Brown, P.L., Byrne, R.H., Gajda, T., Hefter, G., Söberg, S. & Wanner, H. (2007): Chemical speciation of environmentally significant metals with inorganic ligands. Part 2: The Cu^{2+}- OH^{-}, Cl^{-}, CO_3^{2-}, SO_4^{2-} and PO_4^{3-} systems (IUPAC Technical Report). Pure Appl. Chem. 79/5, 895-950.

Rabung, T., Pierret, M C., Bauer, A., Geckeis, H., Bradbury, M.H. & Baeyens, B. (2005): Sorption of Eu(III)/Cm(III) on Ca-montmorillonite and Na-illite. Part 1: Batch sorption and time-resolved laser fluorescence spectroscopy experiments. Geochim. Cosmochim. Acta 69/23, 5393-5402.

Taylor, J.R. (1982): An introduction to error analysis. University Science Books, Mill Valey, USA.

Thoenen, T., Hummel, W., Berner, U. & Curti, E. (2014): The PSI/Nagra Chemical Thermodynamic Database 12/07. PSI Bericht Nr. 14-04. Paul Scherrer Insitut, Villigen PSI.

Trubert, D., Le Naour, C., Jaussaud, C., Mrad, O. (2003): Hydrolysis of protactinium(V): III. Determination of standard thermodynamic data. J. Solution Chem. 32, 505-517.

Yun, J.I., Cho, H.R., Neck, V., Altmaier, M., Seibert, A., Marquardt, C.M., Walther, C. & Fanghänel, T. (2007): Investigation of the hydrolysis of plutonium (IV) by a combination of spectroscopy and redox potential measurements: Radiochim. Acta 95, 89-95.

Appendix A: Surface complexation site types and capacities and protolysis constants

Summary of site types, site capacities and protolysis constants determined for Na-illite (Bradbury & Baeyens 2009a) and used as non-adjustable parameters in the model calculations of the sorption edges and isotherms.

Amphotheric edge sites		**Protolysis reactions**	**Protolysis constants (log K)**		
Type	Capacity [mol kg^{-1}]		$\equiv S^{S}OH$	$\equiv S^{W1}OH$	$\equiv S^{W2}OH$
$\equiv S^{S}OH$	2×10^{-3}	$\equiv SOH + H^{+} \Leftrightarrow \equiv SOH_2^{+}$	4.0	4.0	8.5
$\equiv S^{W1}OH$	4.0×10^{-2}	$\equiv SOH \Leftrightarrow \equiv SO^{-} + H^{+}$	-6.2	-6.2	-10.5
$\equiv S^{W2}OH$	4.0×10^{-2}				

Cation exchange capacity for Na-illite = 225 meq kg^{-1} (Baeyens & Bradbury 2004)

Appendix B: Metal hydrolysis constants used in the modelling of sorption edges and isotherms on montmorillonite

Metal	Hydrolysis reactions	log ^{OH}K	Reference
Mn(II)	$Mn^{2+} + H_2O \Leftrightarrow MnOH^+ + H^+$	-10.59	Baes & Mesmer (1976)
	$Mn^{2+} + 2H_2O \Leftrightarrow Mn(OH)_2^0 + 2H^+$	(-22.2)	
	$Mn^{2+} + 3H_2O \Leftrightarrow Mn(OH)_3^- + 3H^+$	(-34.8)	
Fe(II)	**$Fe^{2+} + H_2O \Leftrightarrow FeOH^+ + H^+$**	**-9.1**	Lemire et al. (2013)
	$Fe^{2+} + 2H_2O \Leftrightarrow Fe(OH)_2^0 + 2H^+$	-20.6	Baes & Mesmer (1976)
	$Fe^{2+} + 3H_2O \Leftrightarrow Fe(OH)_3^- + 3H^+$	-31	
Co(II)	**$Co^{2+} + H_2O \Leftrightarrow CoOH^+ + H^+$**	**-9.65**	Baes & Mesmer (1976)
	$Co^{2+} + 2H_2O \Leftrightarrow Co(OH)_2^0 + 2H^+$	-18.8	
	$Co^{2+} + 3H_2O \Leftrightarrow Co(OH)_3^- + 3H^+$	-31.5	
Ni(II)	**$Ni^{2+} + H_2O \Leftrightarrow NiOH^+ + H^+$**	**-9.86**	Baes & Mesmer (1976)
	$Ni^{2+} + 2H_2O \Leftrightarrow Ni(OH)_2^0 + 2H^+$	-19	
	$Ni^{2+} + 3H_2O \Leftrightarrow Ni(OH)_3^- + 3H^+$	-30	
Cu(II)	$Cu^{2+} + H_2O \Leftrightarrow CuOH^+ + H^+$	< -8	Powell et al. (2007)
	$Cu^{2+} + 2H_2O \Leftrightarrow Cu(OH)_2^0 + 2H^+$	(< -17.3)	
	$Cu^{2+} + 3H_2O \Leftrightarrow Cu(OH)_3^- + 3H^+$	(< -27.8)	
Zn(II)	**$Zn^{2+} + H_2O \Leftrightarrow ZnOH^+ + H^+$**	**-8.96**	Baes & Mesmer (1976)
	$Zn^{2+} + 2H_2O \Leftrightarrow Zn(OH)_2^0 + 2H^+$	-16.9	
	$Zn^{2+} + 3H_2O \Leftrightarrow Zn(OH)_3^- + 3H^+$	-28.4	
Cd(II)	**$Cd^{2+} + H_2O \Leftrightarrow CdOH^+ + H^+$**	**-10.08**	Baes & Mesmer (1976)
	$Cd^{2+} + 2H_2O \Leftrightarrow Cd(OH)_2^0 + 2H^+$	-20.35	
	$Cd^{2+} + 3H_2O \Leftrightarrow Cd(OH)_3^- + 3H^+$	< -33.3	
Pd(II)	$Pd^{2+} + 2H_2O \Leftrightarrow Pd(OH)_2^0 + 2H^+$	-4.0	Hummel et al. (2002)
	$Pd^{2+} + 3H_2O \Leftrightarrow Pd(OH)_3^- + 3H^+$	-15.5	
Be(II)	$Be^{2+} + H_2O \Leftrightarrow BeOH^+ + H^+$	-5.40	Baes & Mesmer (1976)
	$Be^{2+} + 2H_2O \Leftrightarrow Be(OH)_2^0 + 2H^+$	-13.65	
	$Be^{2+} + 3H_2O \Leftrightarrow Be(OH)_3^- + 3H^+$	-23.25	
Eu(III)	**$Eu^{3+} + H_2O \Leftrightarrow EuOH^{2+} + H^+$**	**-7.2**	Guillaumont et al. (2003)
	$Eu^{3+} + 2H_2O \Leftrightarrow Eu(OH)_2^+ + 2H^+$	**-15.1**	(Am hydrolysis data)
	$Eu^{3+} + 3H_2O \Leftrightarrow Eu(OH)_3^0 + 3H^+$	**-26.2**	

Metal	Hydrolysis reactions	log ^{OH}K	Reference
Am(III)	**$Am^{3+} + H_2O \Leftrightarrow AmOH^{2+} + H^+$**	**-7.2**	Guillaumont et al. (2003)
	$Am^{3+} + 2H_2O \Leftrightarrow Am(OH)_2^+ + 2H^+$	**-15.1**	
	$Am^{3+} + 3H_2O \Leftrightarrow Am(OH)_3^0 + 3H^+$	**-26.2**	
Pu(III)	$Pu^{3+} + H_2O \Leftrightarrow PuOH^{2+} + H^+$	-6.9	Guillaumont et al. (2003)
	$Pu^{3+} + 2H_2O \Leftrightarrow Pu(OH)_2^+ + 2H^+$	-14.8	
	$Pu^{3+} + 3H_2O \Leftrightarrow Pu(OH)_3^0 + 3H^+$	-25.9	
Sn(IV)	$Sn^{4+} + H_2O \Leftrightarrow SnOH^{3+} + H^+$	1.18	Baes & Mesmer (1976)
	$Sn^{4+} + 2H_2O \Leftrightarrow Sn(OH)_2^{2+} + 2H^+$	1.65	log Q values converted
	$Sn^{4+} + 3H_2O \Leftrightarrow Sn(OH)_3^+ + 3H^+$	1.55	to log K (I =0) using
	$Sn^{4+} + 4H_2O \Leftrightarrow Sn(OH)_4^0 + 4H^+$	**0.33**	Hummel et al. (2002)
	$Sn^{4+} + 5H_2O \Leftrightarrow Sn(OH)_5^- + 5H^+$	**-7.67**	and Davies (1962)
	$Sn^{4+} + 6H_2O \Leftrightarrow Sn(OH)_6^{2-} + 6H^+$	**-18.07**	
Zr(IV)	$Zr^{4+} + H_2O \Leftrightarrow ZrOH^{3+} + H^+$	0.32	Brown et al. (2005)
	$Zr^{4+} + 2H_2O \Leftrightarrow Zr(OH)_2^{2+} + 2H^+$	0.98	
	$Zr^{4+} + 4H_2O \Leftrightarrow Zr(OH)_4^0 + 4H^+$	-2.19	
	$Zr^{4+} + 6H_2O \Leftrightarrow Zr(OH)_6^{2-} + 6H^+$	-29.0	
Th(IV)	$Th^{4+} + H_2O \Leftrightarrow ThOH^{3+} + H^+$	-2.2	Neck & Kim (2001)
	$Th^{4+} + 2H_2O \Leftrightarrow Th(OH)_2^{2+} + 2H^+$	**-6.0**	
	$Th^{4+} + 3H_2O \Leftrightarrow Th(OH)_3^+ + 3H^+$	**-11.0**	
	$Th^{4+} + 4H_2O \Leftrightarrow Th(OH)_4^0 + 4H^+$	**-17.5**	
U(IV)	$U^{4+} + H_2O \Leftrightarrow UOH^{3+} + H^+$	-0.54	Grenthe et al. (1992)
	$U^{4+} + 2H_2O \Leftrightarrow U(OH)_2^{2+} + 2H^+$	-1.1	Thoenen et al. (2014)
	$U^{4+} + 3H_2O \Leftrightarrow U(OH)_3^+ + 3H^+$	-4.7	Thoenen et al. (2014)
	$U^{4+} + 4H_2O \Leftrightarrow U(OH)_4^0 + 4H^+$	-10	Guillaumont et al. (2003)
Np(IV)	$Np^{4+} + H_2O \Leftrightarrow NpOH^{3+} + H^+$	0.55	Guillaumont et al. (2003)
	$Np^{4+} + 2H_2O \Leftrightarrow Np(OH)_2^{2+} + 2H^+$	0.35	"
	$Np^{4+} + 3H_2O \Leftrightarrow Np(OH)_3^+ + 3H^+$	-2.8	Neck & Kim (2001)
	$Np^{4+} + 4H_2O \Leftrightarrow Np(OH)_4^0 + 4H^+$	-8.3	Guillaumont et al. (2003)
Pu(IV)	$Pu^{4+} + H_2O \Leftrightarrow PuOH^{3+} + H^+$	0.0	Yun et al. (2007)
	$Pu^{4+} + 2H_2O \Leftrightarrow Pu(OH)_2^{2+} + 2H^+$	-1.2	
	$Pu^{4+} + 3H_2O \Leftrightarrow Pu(OH)_3^+ + 3H^+$	-3.1	
	$Pu^{4+} + 4H_2O \Leftrightarrow Pu(OH)_4^0 + 4H^+$	-9.3	
Pa(V)	$PaOOH^{2+} + H_2O \Leftrightarrow PaO(OH)_2^+ + H^+$	-1.24	Trubert et al. (2003)
	$PaOOH^{2+} + 3H_2O \Leftrightarrow Pa(OH)_5^0 + 2H^+$	-8.27	

Metal	**Hydrolysis reactions**	**log ^{OH}K**	**Reference**
Np(V)	$NpO_2^+ + H_2O \Leftrightarrow NpO_2(OH)^0 + H^+$	-11.3	Lemire et al. (2001)
	$NpO_2^+ + 2H_2O \Leftrightarrow NpO_2(OH)_2^- + 2H^+$	-23.6	
U(VI)	$UO_2^{2+} + H_2O \Leftrightarrow UO_2OH^+ + H^+$	-5.25	Guillaumont et al. (2003)
	$UO_2^{2+} + 2H_2O \Leftrightarrow UO_2(OH)_2^0 + 2H^+$	-12.15	"
	$UO_2^{2+} + 3H_2O \Leftrightarrow UO_2(OH)_3^- + 3H^+$	-20.25	"
	$UO_2^{2+} + 4H_2O \Leftrightarrow UO_2(OH)_4^{2-} + 4H^+$	-32.4	"
	$2UO_2^{2+} + H_2O \Leftrightarrow (UO_2)_2OH + H^+$	-2.7	Grenthe et al. (1992)
	$2UO_2^{2+} + 2H_2O \Leftrightarrow (UO_2)_2(OH)_2 + 2H^+$	-5.62	"
	$3UO_2^{2+} + 4H_2O \Leftrightarrow (UO_2)_3(OH)_4 + 4H^+$	-11.9	"
	$3UO_2^{2+} + 5H_2O \Leftrightarrow (UO_2)_3(OH)_5 + 5H^+$	-15.55	"
	$3UO_2^{2+} + 7H_2O \Leftrightarrow (UO_2)_3(OH)_7 + 7H^+$	-32.2	Guillaumont et al. (2003)
	$4UO_2^{2+} + 4H_2O \Leftrightarrow (UO_2)_4(OH)_7 + 7H^+$	-21.9	Grenthe et al. (1992)

Note: Hydrolysis reactions and log K values in bold have been used in the LFERs.

Appendix C: Compilation of strong site surface complexation constants

Tab. C1: Surface complexation data of transition metals on strong sites.

Surface complexation formation reaction	**log K**	**Source of experimental data**
$\equiv S^SOH + Co^{2+} \Leftrightarrow \equiv S^SOCo^+ + H^+$	**1.3**	*This study*
$\equiv S^SOH + Co^{2+} + H_2O \Leftrightarrow \equiv S^SOCoOH^0 + 2H^+$	-8.5	
$\equiv S^SOH + Co^{2+} + 2H_2O \Leftrightarrow \equiv S^SOCo(OH)_2^- + 3H^+$	-18.3	
$\equiv S^SOH + Ni^{2+} \Leftrightarrow \equiv S^SONi^+ + H^+$	**0.7**	Bradbury & Baeyens (2009a)
$\equiv S^SOH + Ni^{2+} + H_2O \Leftrightarrow \equiv S^SONiOH^0 + 2H^+$	-8.2	
$\equiv S^SOH + Ni^{2+} + 2H_2O \Leftrightarrow \equiv S^SONi(OH)_2^- + 3H^+$	-17.3	
$\equiv S^SOH + Zn^{2+} \Leftrightarrow \equiv S^SOZn^+ + H^+$	**2.1**	Montoya et al. (2018)
$\equiv S^SOH + Zn^{2+} + H_2O \Leftrightarrow \equiv S^SOZnOH^0 + 2H^+$	-6.4	
$\equiv S^SOH + Zn^{2+} + 2H_2O \Leftrightarrow \equiv S^{Sv}OZn(OH)_2^- + 3H^+$	-15.0	

Tab. C2: Surface complexation data of trivalent elements on strong sites.

Surface complexation reaction	**log K**	**Source of experimental data**
$\equiv S^SOH + Eu^{3+} \Leftrightarrow \equiv S^SOEu^{2+} + H^+$	**2.8**	Poinssot et al. (1999) and Bradbury & Baeyens (2005a)
$\equiv S^SOH + Eu^{3+} + H_2O \Leftrightarrow \equiv S^SOEuOH^+ + 2H^+$	**-4.4**	
$\equiv S^SOH + Eu^{3+} + 2H_2O \Leftrightarrow \equiv S^SOEu(OH)_2^0 + 3H^+$	**-12.7**	
$\equiv S^SOH + Eu^{3+} + 3H_2O \Leftrightarrow \equiv S^SOEu(OH)_3^- + 4H^+$	**-23.8**	
$\equiv S^SOH + Eu^{3+} \Leftrightarrow \equiv S^SOEu^{2+} + H^+$	**1.9**	Bradbury & Baeyens (2009a)
$\equiv S^SOH + Eu^{3+} + H_2O \Leftrightarrow \equiv S^SOEuOH^+ + 2H^+$	**-4.7**	
$\equiv S^SOH + Eu^{3+} + 2H_2O \Leftrightarrow \equiv S^SOEu(OH)_2^0 + 3H^+$	**-12.7**	
$\equiv S^SOH + Am^{3+} \Leftrightarrow \equiv S^SOAm^{2+} + H^+$	**3.1**	Bradbury & Baeyens (2009b)
$\equiv S^SOH + Am^{3+} + H_2O \Leftrightarrow \equiv S^SOAmOH^+ + 2H^+$	**-4.5**	
$\equiv S^SOH + Am^{3+} + 2H_2O \Leftrightarrow \equiv S^SOAm(OH)_2^0 + 3H^+$	**-13**	
$\equiv ^SSOH + Am^{3+} \Leftrightarrow \equiv S^SOAm^{2+} + H^+$	**1.6**	Gorgeon (1994)
$\equiv ^SSOH + Am^{3+} + H_2O \Leftrightarrow \equiv S^SOAmOH^+ + 2H^+$	**-5.0**	
$\equiv ^SSOH + Am^{3+} + 2H_2O \Leftrightarrow \equiv S^SOAm(OH)_2^0 + 3H^+$	**-13**	
$\equiv S^SOH + Cm^{3+} \Leftrightarrow \equiv S^SOCm^{2+} + H^+$	**2.4**	Rabung et al. (2005)
$\equiv S^SOH + Cm^{3+} + H_2O \Leftrightarrow \equiv S^SOCmOH^+ + 2H^+$	**-3.6**	
$\equiv S^SOH + Cm^{3+} + 2H_2O \Leftrightarrow \equiv S^SOCm(OH)_2^0 + 3H^+$	**-13**	

Tab. C3: Surface complexation data of tetravalent elements on strong sites.

Surface complexation formation reaction	**log K**	**Source of experimental data**
$\equiv^{S}SOH + Sn^{4+} + 2H_2O \Leftrightarrow \equiv^{S}SOSn(OH)_2^{+} + 3H^{+}$	12.5	Bradbury & Baeyens (2009a)
$\equiv^{S}SOH + Sn^{4+} + 3H_2O \Leftrightarrow \equiv^{S}SOSn(OH)_3^{0} + 4H^{+}$	8.5	
$\equiv^{S}SOH + Sn^{4+} + 4H_2O \Leftrightarrow \equiv^{S}SOSn(OH)_4^{-} + 5H^{+}$	2.5	
$\equiv^{S}SOH + Sn^{4+} + 5H_2O \Leftrightarrow \equiv^{S}SOSn(OH)_5^{2-} + 6H^{+}$	-5.7	
$\equiv^{S}SOH + Th^{4+} \Leftrightarrow \equiv^{S}SOTh^{3+} + H^{+}$	7.4	Bradbury & Baeyens (2009b)
$\mathbf{\equiv^{S}SOH + Th^{4+} + H_2O \Leftrightarrow \equiv^{S}SOTh(OH)^{2+} + 2H^{+}}$	2.3	
$\mathbf{\equiv^{S}SOH + Th^{4+} + 2H_2O \Leftrightarrow \equiv^{S}SOTh(OH)_2^{+} + 3H^{+}}$	-2.4	
$\mathbf{\equiv^{S}SOH + Th^{4+} + 3H_2O \Leftrightarrow \equiv^{S}SOTh(OH)_3^{0} + 4H^{+}}$	-8.8	
$\equiv^{S}SOH + Th^{4+} + 4H_2O \Leftrightarrow \equiv^{S}SOTh(OH)_4^{-} + 5H^{+}$	-15.3	

Tab. C4: Surface complexation data of Np(V), Pa(V) and U(VI) on strong sites.

Surface complexation formation reaction	**log K**	**Source of experimental data**
$\equiv^{S}SOH + NpO_2^{+} \Leftrightarrow \equiv^{S}SONpO_2^{0} + H^{+}$	-2.0	Gorgeon (1994)
$\equiv^{S}SOH + NpO_2^{+} + H_2O \Leftrightarrow \equiv^{S}SONpO_2OH^{-} + H^{+}$	-10.3	
$\equiv^{S}SOH + PaOOH^{2+} \Leftrightarrow \equiv^{S}SOPaOOH^{+} + H^{+}$	6.4	Bradbury & Baeyens (2009b)
$\equiv^{S}SOH + PaOOH^{2+} \Leftrightarrow \equiv^{S}SOPaO_2^{0} + 2H^{+}$	0.4	
$\equiv^{S}SOH + PaOOH^{2+} + H_2O \Leftrightarrow \equiv^{S}SOPaO_2OH^{-} + 3H^{+}$	-6.7	
$\equiv^{S}SOH + UO_2^{2+} \Leftrightarrow \equiv^{S}SO\ UO_2^{+} + H^{+}$	2.0	Bradbury & Baeyens (2009b)
$\equiv^{S}SOH + UO_2^{2+} + H_2O \Leftrightarrow \equiv^{S}SOUO_2OH^{0} + 2H^{+}$	-3.9	
$\equiv^{S}SOH + UO_2^{2+} + 2H_2O \Leftrightarrow \equiv^{S}SOUO_2(OH)_2^{-} + 3H^{+}$	-10.8	
$\equiv^{S}SOH + UO_2^{2+} + 3H_2O \Leftrightarrow \equiv^{S}SOUO_2(OH)_3^{2-} + 4H^{+}$	-18..7	

Note: Surface complexation reactions and log K values in bold have been used in the LFERs.

Appendix D: Compilation of weak site surface complexation constants

Surface complexation formation reaction	log K	Source of experimental data
$\equiv S^{W1}OH + Co^{2+} \Leftrightarrow \equiv S^{W1}OCo^{+} + H^{+}$	**-2.0**	Montoya et al. (2018)
$\equiv S^{W1}OH + Ni^{2+} \Leftrightarrow \equiv S^{W1}ONi^{+} + H^{+}$	**-1.8**	Poinssot et al. (1999)
$\equiv S^{W1}OH + Zn^{2+} \Leftrightarrow \equiv S^{W1}OZn^{+} + H^{+}$	**-1.0**	Montoya et al. (2018)
$\equiv S^{W1}OH + Eu^{3+} \Leftrightarrow \equiv S^{W1}OEu^{2+} + H^{+}$	**0.3**	Poinssot et al. (1999)
$\equiv S^{W1}OH + Eu^{3+} + H_2O \Leftrightarrow \equiv S^{W1}OEuOH^{+} + 2H^{+}$	**-6.2**	
$\equiv S^{W1}OH + UO_2^{2+} \Leftrightarrow \equiv S^{W1}OUO_2^{+} + H^{+}$	0.0	Bradbury & Baeyens (2005a) and *this study*
$\equiv S^{W1}OH + UO_2^{2+} + H_2O \Leftrightarrow \equiv S^{W1}OUO_2OH^{0} + 2H^{+}$	-5.8	
$\equiv S^{W1}OH + UO_2^{2+} + 2H_2O \Leftrightarrow \equiv S^{W1}OUO_2(OH)_2^{-} + 3H^{+}$	-12.3	

Note: Surface complexation reactions and log K values in bold have been used in the LFER.

Appendix E: Cation exchange reactions and selectivity coefficients

A-clay + B	**N_B range**	**Background electrolyte**	**K_c**	**Reference**
Na-illite + Ni^{2+}	trace	0.1 M $NaClO_4$	12.6	Bradbury & Baeyens (2009a)
Na-illite + Zn^{2+}	0.1 – 0.9	0.1 M $NaClO_4$	4.0	Montoya et al. (2018)
Na-illite + Co^{2+}	trace	0.1 M $NaClO_4$	12.7	Montoya et al. (2018)
Na-illite + Eu^{3+}	trace	0.1 M $NaClO_4$	76	Bradbury & Baeyens (2009a)
Na-illite + Am^{3+}	trace	0.1 M $NaClO_4$	40	Bradbury & Baeyens (2009b)
Na-illite + NpO_2^+	trace	0.1 M $NaClO_4$	1.0	Bradbury & Baeyens (2009b)
Na-illite + UO_2^{2+}	trace	0.1 M $NaClO_4$	4.5	Bradbury & Baeyens (2009b)

Appendix F: Surface complexation constants for Eu, Am and Cm on illite where the modelling included silicate aqueous species

The sorption edges for Eu (Fig. 3.4), Am (Fig. 3.5) and Cm (Fig. 3.6) have been re-modelled including a Si concentration of 4×10^{-5} M and assuming that the silicate complexes do not sorb. The best fits obtained are shown as red continuous lines in Figs. F1, F2 and F3, for Eu, Am and Cm, respectively. The modified surface complexation constants are given in Tab. F1.

Tab. F1: Surface complexation data of trivalent elements on strong sites including silicates.

Surface complexation reaction	**log K**	**Source of experimental data**
$\equiv S^SOH + Eu^{3+} \Leftrightarrow \equiv S^SOEu^{2+} + H^+$	2.6	Poinssot et al. (1999) and Bradbury & Baeyens (2005a)
$\equiv S^SOH + Eu^{3+} + H_20 \Leftrightarrow \equiv S^SOEuOH^+ + 2H^+$	-3.4	
$\equiv S^SOH + Eu^{3+} + 2H_20 \Leftrightarrow \equiv S^SOEu(OH)_2^0 + 3H^+$	-12.7	
$\equiv S^SOH + Eu^{3+} \Leftrightarrow \equiv S^SOEu^{2+} + H^+$	1.9	Bradbury & Baeyens (2009a)
$\equiv S^SOH + Eu^{3+} + H_20 \Leftrightarrow \equiv S^SOEuOH^+ + 2H^+$	-3.9	
$\equiv S^SOH + Eu^{3+} + 2H_20 \Leftrightarrow \equiv S^SOEu(OH)_2^0 + 3H^+$	-12.8	
$\equiv S^SOH + Am^{3+} \Leftrightarrow \equiv S^SOAm^{2+} + H^+$	3.1	Bradbury & Baeyens (2009b)
$\equiv S^SOH + Am^{3+} + H_20 \Leftrightarrow \equiv S^SOAmOH^+ + 2H^+$	-3.5	
$\equiv S^SOH + Am^{3+} + 2H_20 \Leftrightarrow \equiv S^SOAm(OH)_2^0 + 3H^+$	-13	
$\equiv^SSOH + Am^{3+} \Leftrightarrow \equiv S^SOAm^{2+} + H^+$	1.6	Gorgeon (1994)
$\equiv^SSOH + Am^{3+} + H_20 \Leftrightarrow \equiv S^SOAmOH^+ + 2H^+$	-4.2	
$\equiv^SSOH + Am^{3+} + 2H_20 \Leftrightarrow \equiv S^SOAm(OH)_2^0 + 3H^+$	-13	
$\equiv S^SOH + Cm^{3+} \Leftrightarrow \equiv S^SOCm^{2+} + H^+$	2.4	Rabung et al. (2005)
$\equiv S^SOH + Cm^{3+} + H_20 \Leftrightarrow \equiv S^SOCmOH^+ + 2H^+$	-3.6	
$\equiv S^SOH + Cm^{3+} + 2H_20 \Leftrightarrow \equiv S^SOCm(OH)_2^0 + 3H^+$	-13	

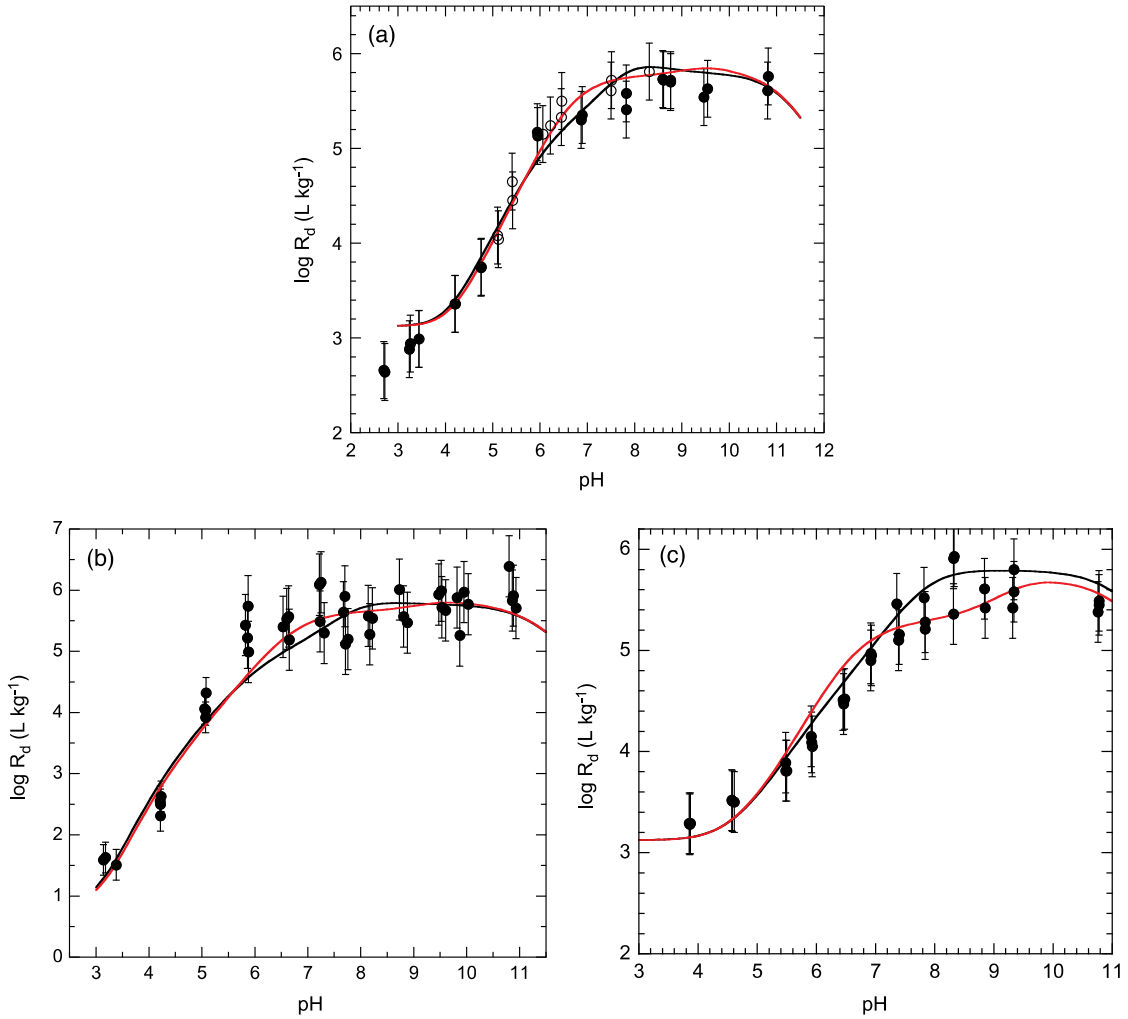

Fig. F1: Sorption edges for Eu(III) on Na-IdP: (a) in 0.1 M $NaClO_4$, (b) in 0.5 M $NaClO_4$ from and (c) in 0.1 M $NaClO_4$.

Experimental data (●): (a) from Poinssot et al. (1999), (b) from Bradbury & Baeyens (2005a) and (c) from Bradbury & Baeyens (2009a). Modelled curves (—) (*this study* and Bradbury & Baeyens 2009a). The red continuous lines are refits of the sorption edges including Eu – Si complexes.

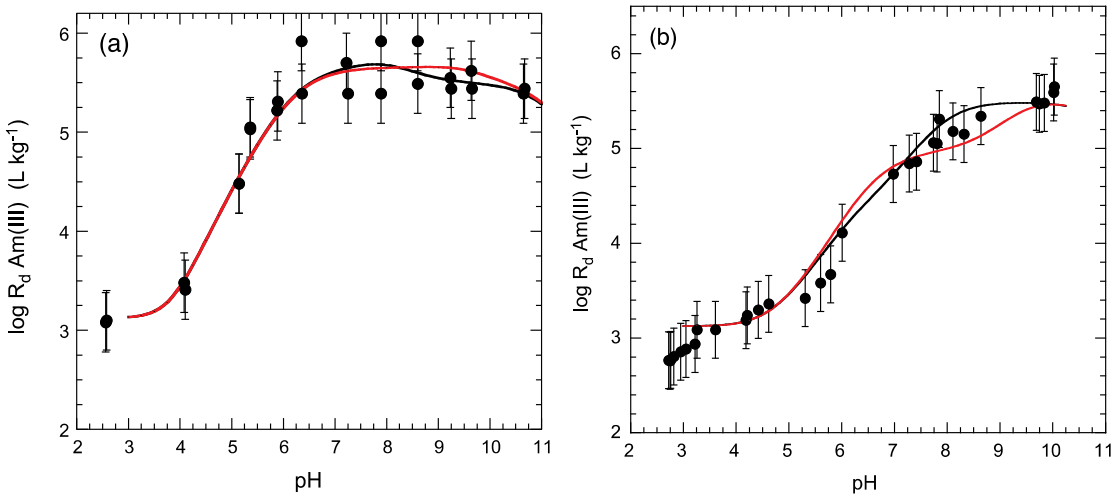

Fig. F2: Sorption edges for Am(III) in 0.1 M $NaClO_4$: (a) on Na-IdP and (b) on Illite du Puy.

Experimental data (●): (a) from Bradbury & Baeyens (2009b) and (b) from Gorgeon (1994). Modelled curves (—) (*this study*). The red continuous lines are refits of the sorption edges including Eu-Si complexes.

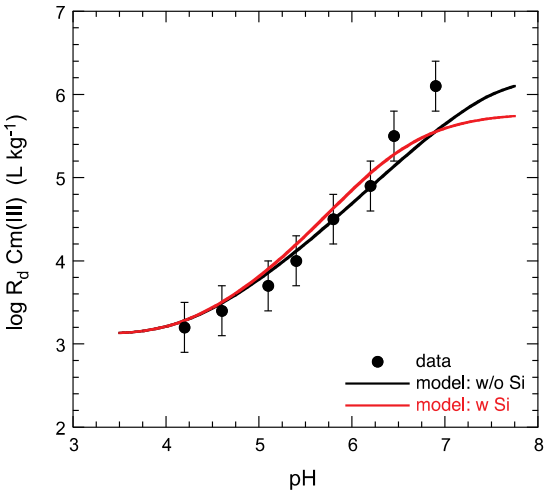

Fig. F3: Sorption edge for Cm(III) in 0.1 M $NaClO_4$.

Experimental data (●) Na-IdP (Rabung et al. 2005) and modelled curve (—) (*this study*). The red continuous line is a refit of the sorption edges including Eu-Si complexes.

Appendix G: Generalised Cs sorption model: Model parameters

Tab. G1: Site types and distributions for illite.

Site types	**Site capacities**
Frayed edge sites	0.25 % of the CEC*
Type II sites	20% of the CEC
Planar sites	~ 80% of the CEC

*CEC = cation exchange capacity in equiv. kg^{-1}.

Tab. G2: Selectivity coefficients for illite with CEC = 0.20 eq. kg^{-1}.

Selectivity coefficients	**Site types**		
	FES	**Type II sites**	**Planar sites**
$\log {}^{Cs}_{K}K_c$	4.6	1.5	0.5
$\log {}^{Rb}_{K}K_c$	2.2	0.5	0.5
$\log {}^{Cs}_{Na}K_c$	7.0	3.6	1.6
$\log {}^{Cs}_{NH_4}K_c$	3.5	-	-
$\log {}^{K}_{Na}K_c$	2.4	2.1	1.1
$\log {}^{NH_4}_{K}K_c$	1.1	-	-

Appendix H: Opalinus Clay mineralogy and water chemistries used in the "bottom up" modelling of the isotherms of Ni(II), Co(II), Eu(III), Th(IV) and U(VI)

Tab. H1: Mineralogical composition of Mont Terri Opalinus Clay (Lauber et al. 2000).

Mineral	[wt.-%]
Clay minerals	
Montmorillonite	-
Illite	22 ±4
Illite/Smectite mixed layers	18 ±4
Kaolinite	20 ±3
Mica	-
Chlorite	10 ±2
Quartz	12 ±2
K-Feldspar/albite	2.3 ±0.7
Calcite	9 ±1
Dolomite/Ankerite	2 ±0.5
Siderite	4 ±1
Pyrite	-

Tab. H2: Synthetic porewater compositions of Opalinus Clay: (a) and (b) Lauber et al. 2000, (c) Van Loon et al. 2005).

	Opalinus clay		
	(a)	**(b)**	**(c)**
pH	6.3 [1)]	8.0 [2)]	7.6 [3)]
p-CO_2(bar)	$10^{-0.3}$	$10^{-3.5}$	$10^{-3.5}$
Ionic strength (M)	0.3	0.39	0.39
Dissolved constituents			
Na	1.9×10^{-1}	2.5×10^{-1}	2.4×10^{-1}
K	4.2×10^{-3}	5.6×10^{-3}	1.6×10^{-3}
Mg	1.4×10^{-2}	2.2×10^{-2}	1.7×10^{-2}
Ca	1.8×10^{-2}	2.9×10^{-2}	2.6×10^{-2}
Sr	2.2×10^{-4}	2.6×10^{-4}	5.1×10^{-4}
Al	$4.2 \times 10^{-}$	4.2×10^{-8}	-
Fe	2.4×10^{-5}	4.0×10^{-6}	-
F	1.4×10^{-4}	1.2×10^{-4}	-
Cl	1.9×10^{-1}	3.0×10^{-1}	3.0×10^{-1}
SO_4	2.8×10^{-2}	2.8×10^{-2}	1.4×10^{-2}
$C_{inorg.}$	1.7×10^{-2}	1.8×10^{-4}	4.76×10^{-4}
Si	2.8×10^{-4}	1.8×10^{-4}	-

[1)] The Ni(II) sorption isotherm was measured in the porewater at pH 6.3.

[2)] The Eu(III), Th(IV) and U(VI) sorption isotherms were measured in porewater at pH 8.

[3)] The Co(II) sorption isotherm was measured in the porewater at pH 7.6.

Appendix J: Mineralogy and water chemistries used in the modelling of the Cs isotherms given in Chapter 9

Tab. J1: Mineralogies of Boom Clay (Griffault et al. 1996), Oxford Clay (McKinley & West 1982), Palfris Marl (Aksoyoglu et al. 1991) and Opalinus Clay (Lauber et al. 2000).

	Boom Clay [wt.-%]	**Oxford Clay** [wt.-%]	**Palfris Marl** [wt.-%]	**Opalinus Clay** [wt.-%]
Quartz	20	9 – 30	12 – 18	10 – 14
K-Feldspar	5 – 10	Trace	< 1	1.5 – 3
Carbonates	1 – 5	2 – 40	30 – 47	10 – 13
Siderite	-	-	-	3 – 5
Pyrite	1 – 5	1 – 5	0.3	b.d.l.
Clay minerals				
Illite	20 – 30	16 – 36	11 – 1	18 – 26
Smectite	10 – 20	4 – 48	-	-
Chlorite	5 – 20	trace	6 – 14	8 – 12
Kaolinite	20 – 30	trace	2 – 23	17 – 23
Illite/smectite mixed layer	5 – 10	-	5 – 7	14 – 22
Chlorite/smectite mixed layer	5 – 10	-	-	-

b.d.l.: below detection limit.

Tab. J2: Water compositions for Boom Clay (Baeyens 1982), Oxford Clay (McKinley & West 1982), Palfris Marl (Aksoyoglu et al. 1991) and Opalinus Clay (Lauber et al. 1999).

	Boom Clay	**Oxford Clay**	**Palfris Marl**	**Opalinus Clay**
Na [M]	2.9×10^{-2}	1.6×10^{-1}	8.0×10^{-2}	2.5×10^{-1}
K [M]	1.0×10^{-3}	1.1×10^{-5}	1.1×10^{-3}	5.8×10^{-3}
NH_4 [M]	-	2.4×10^{-4}	-	-
Ca [M]	-	6.0×10^{-3}	3.4×10^{-3}	2.8×10^{-2}
Mg [M]	5.0×10^{-4}	-	2.8×10^{-3}	2.1×10^{-2}
Sr [M]	-	1.2×10^{-4}	-	2.6×10^{-4}
Cs [M]	-	-	2.5×10^{-8}	4.8×10^{-8}
Cl (M)	2.0×10^{-3}	1.7×10^{-1}	8.0×10^{-3}	3.0×10^{-1}
$C_{inorg.}$ [M]	1.5×10^{-2}	1.0×10^{-4}	4.5×10^{-3}	1.8×10^{-4}
SO_4 [M]	-	4.6×10^{-3}	4.5×10^{-3}	2.7×10^{-2}
F [M]	1.5×10^{-3}	4.2×10^{-5}	-	1.2×10^{-4}
pH	8.8	7 – 7.5	7.3	7.9

Appendix K: Thermodynamic data used in the modelling of natural Opalinus Clay/groundwater systems

Tab. K1: Summary of the aqueous complexation constants (log K values) for Ni(II), Eu(III), Th(IV) and U(VI) with chloro, sulphato and carbonato species used in the calculations (Thoenen et al. 2014).

Metal complex	**Co(II)**	**Ni(II)**	**Eu(III)**	**Th(IV)**	**U(VI)**
$MeCl$	0.57	0.08	1.1	1.70	0.17
$MeCl_2$	0.02	-	1.5	-	-1.1
$MeSO_4$	2.30	2.35	3.95	6.17	3.15
$Me(SO_4)_2$	-	-	5.7	9.69	4.14
$Me(SO_4)_3$	-	-	-	10.75	3.02
$MeCO_3$	4.23	4.2	8.1	-	9.94
$Me(CO_3)_2$	6.0	6.2	12.1	-	16.61
$Me(CO_3)_3$	-	-	-	-	21.84
$MeHCO_3$	12.22	11.72	-	-	-
$Me(CO_3)_4$	-	-	-	-	-
$Me(CO_3)_5$	-	-	-	31.0	-
$Me(OH)_3CO_3$	-	-	-	-3.1 *	-
$Me(OH)_2(CO_3)_2$	-	-	-	8.80	-
$Me(OH)(CO_3)_4$	-	-	-	21.6	-
$Me(OH)_4CO_3$	-	-	-	-15.6	-
$MeMg(CO_3)_3$	-	-	-	-	26.11
$MeCa(CO_3)_3$	-	-	-	-	27.18
$MeCa_2(CO_3)_3$	-	-	-	-	29.22
$Me_2(OH)_3CO_3$	-	-	-	-	-0.86

* Hummel et al. (2002).